NASA
TP
1596
c.1

NASA Technical Paper 1596

Loading Tests of a Wing Structure for a Hypersonic Aircraft

Roger A. Fields, Lawrence F. Reardon,
and William H. Siegel

JANUARY 1980

NASA

NASA Technical Paper 1596

Loading Tests of a Wing Structure for a Hypersonic Aircraft

Roger A. Fields, Lawrence F. Reardon,
and William H. Siegel
Dryden Flight Research Center
Edwards, California

LOADING TESTS OF A WING STRUCTURE FOR A HYPERSONIC AIRCRAFT

Roger A. Fields, Lawrence F. Reardon,
and William H. Siegel
Dryden Flight Research Center

INTRODUCTION

Various structural concepts have been evaluated analytically and experimentally for application to hypersonic aircraft wings in recent years (refs. 1 to 5). The structural concepts that have been considered can be classified, in general, as hot or cold structures. Hot structures are those in which the primary load-carrying structural members are required to function at the elevated temperatures that approach the practical operating limits of the particular material used. Most commonly, the suggested material is a high-temperature metal alloy with a nickel or cobalt base such as René 41 or Haynes 25. In contrast, cold structures are those in which the primary load-carrying structural members function at relatively low temperatures because of active cooling or an ablative or insulative covering. Active cooling may involve, for instance, a liquid such as hydrogen fuel, which is circulated through structural skin panels to absorb and carry away the surface heat load.

Reference 1 reports on an analytical and experimental investigation that was conducted to study various combinations of promising hot structural concepts for a hypersonic vehicle. It was specified that the vehicle was to cruise at Mach 8 at a maximum dynamic pressure of 1053 hN/m^2 for a 10,000 hour lifespan. It is a requirement for a vehicle of this type to have a minimum weight structure that can operate in a high-temperature environment. The structural concepts, which included primary wing structure, the heat shield, and leading edge, were evaluated with respect to weight, cost, performance, and reliability. The concept found to provide the lowest weight and total-system cost was a semimonocoque wing structure with single sheet spanwise-stiffened beaded panels made of René 41, heat shields on the external surfaces made of corrugated René 41 and TD NiCr, and segmented leading edges of TD NiCr.

The next logical step in the development of structural concepts is to progress through a realistic design exercise and produce a full-scale component for a comprehensive test program. A 7.9 square meter planform portion of a wing was designed and fabricated (ref. 5) using the structural concept from the preceding investigation and a NASA-specified Mach 8 hypersonic research airplane. This wing portion, or hypersonic wing test structure (HWTS), is currently being tested in the Dryden Flight Research Center flight loads research facility (ref. 6) to evaluate (1) the

structural concept itself and the final structural design, and (2) the flight loads instrumentation, high-temperature calibration methods, and temperature simulation techniques.

This report covers only the first evaluations mentioned above and only with respect to the room-temperature aspects of the experimental program.

The HWTS was subjected to a series of room-temperature loading tests, which were designed to establish the ability of the wing structure to withstand the design loads and to determine the strength interaction curve for the beaded panels. Test results from strain gages and deflection transducers are presented and compared with design data and with calculated data from a finite-element structural analysis.

Physical quantities in this report are given in the International System of Units (SI). The measurements were taken and the calculations were made in U.S. Customary Units. Factors relating the two systems are presented in reference 7.

VEHICLE AND MISSION

The design of the HWTS was based on the mission loads and temperatures calculated for the wing portion of a hypersonic research airplane concept as shown by the shaded area in figure 1. The hypersonic research airplane configuration is a single-place design with horizontal takeoff and landing capability and an estimated gross weight of 3,228 hectonewtons. The configuration is 30.78 meters long, has a wingspan of 11.58 meters, and consists of a discrete wing-body with a single vertical tail. The fuselage cross section is circular, with two lower corner areas added to permit wing attachment and to provide a flat lower surface, additional fuselage volume, and a longitudinal carry-through area. All fuel tanks are of nonintegral design; the large forward tank is for liquid hydrogen and the aft tank is for hydrocarbon fuel. The fuselage primary structure is of insulated, semimonocoque design. The main landing gear is attached and stowed below the wing plane and outboard of the inlet/ramjet components.

The propulsion system consists of separate turbofanjets and ramjets with a common two-dimensional inlet design. The two turbofanjets, located in the aft fuselage bay, operate on hydrocarbon fuel at Mach numbers up to 2.8. The two hydrogen-burning ramjets, located beneath the aft fuselage operate at Mach numbers from 0.8 to 8.0. The inlet is a mixed-compression fixed-capture-area design with variable ramp geometry. Actuators for the variable ramps and inlet ducting for the turbofanjets extend into or through the center-wing section.

The wing and vertical tail are hot radiating structures. The wing is a low-mounted, clipped double-delta design with leading-edge sweep angles of 85° and 70°. The wing design does not include any twist, angle of incidence, or dihedral. The basic delta wing has a symmetrical 30/70 Hex (modified) airfoil section which is 4 percent thick and has a leading-edge radius of 1.91 centimeters. The total wing planform area is 145.6 square meters. Wing loading at takeoff is estimated to be 22.17 hN/m^2.

A nominal research mission profile for the hypersonic research airplane, shown in figure 2, consists of horizontal takeoff at 103 meters per second, subsonic climb to a 7.32 kilometer altitude, and acceleration at a dynamic pressure of 47.88 kN/m^2 to Mach 8 at an altitude of 30.8 kilometers. A 5-minute cruise flight is performed at Mach 8 at altitudes between 30.8 and 35.8 kilometers. Descent follows a constant 23.94 kN/m^2 dynamic pressure profile.

A major design consideration was the pushover-pullup loads maneuver shown by the dashed line profile in figure 2. This maneuver is to be initiated at Mach 8 at an altitude of 27.4 kilometers, and consists of a -0.5 g pushover, a 2.5 g pullup, and a return to the nominal research mission descent profile. A more specific time history for this loads maneuver is shown in figure 3. Preloads and postloads maneuvers precede and follow the actual loads maneuver to provide transitions to and from the nominal flight profile. The entire loads maneuver encompasses 42 seconds, and the maximum dynamic pressure obtained during the maneuver is 83.78 kN/m^2.

TEST ARTICLE

The HWTS was designed for a service life of 100 flight hours assuming, in total, 150 flights. It was further assumed that the 150 flights included (1) 60 flights with a 5-minute cruise at Mach 8, (2) 30 flights with a pushover-pullup loads maneuver at Mach 8, and (3) 10 flights with a Mach 8 launch maneuver. The design limit load factors were (1) 2.5 g and -1.0 g for normal accelerations, (2) 1.0 g and -2.0 g for longitudinal accelerations, and (3) ±0.5 g for lateral accelerations. The maximum design dynamic pressure was 83.78 kN/m^2.

The primary load-carrying members of the HWTS are the René 41 beaded panels. The bending loads normally carried by the spars of conventional aircraft wing structures are carried by the beaded panels in the hypersonic research airplane. The panels are also subject to shear loads resulting from wing torsion and to pressure loads normal to the surface resulting from internal pressure lag. A typical panel is shown in figure 4. The panel was formed from a single sheet of René 41 with the seven alternating up-and-down circular arc beads parallel to the span of the wing. Doublers were spotwelded to the ends of the panel to prevent local end failure and to reduce excessive deformation due to shear. The overall panel dimensions are 48.8 centimeters by 109.0 centimeters. The beads are 0.066 centimeter thick and have a radius of 2.654 centimeters with an included angle of 155°. The flat sections between the beads are 1.113 centimeters wide and 0.091 centimeter thick. Figure 4 shows four channel sections which are spotwelded to the beaded panel to provide attachment points for metallic heat shields. The beaded panels are attached to the caps of orthogonal spars and ribs by screws.

Figure 5 shows the general dimensions and shape of the HWTS and a transition section. The wing is cantilevered from wing station (W.S.) 1.067. The wing was tested inverted, so that the compressively loaded surface of the actual vehicle would be on the lower surface of the test structure. (In the remainder of this report, "upper surface" refers to that nearest the sky and "lower surface" to that

nearest the ground.) The transition section was included in the tests to provide a buffer between the support structure and the test portion of the wing. (It is not a part of the aircraft design.) The five most critically compression-loaded panels are the lower root panels, which are shaded in figure 5 and numbered 1 to 5 from fore to aft.

Figure 6(a) shows the HWTS mounted in a support fixture with the heat shields removed. The Z-shaped clips are used to connect the heat shields to the structure. The HWTS has six spars, which are perpendicular to the aircraft centerline and produce five chordwise bays. The outboard portion of the structure is covered by an insulation packet; the insulation is intended to keep maximum structural temperatures below 1005 K and to keep spanwise temperature gradients constant.

Both the spar and rib webs have sine wave corrugations (figs. 6(a) and 6(b)) to allow for thermal expansion. Figure 6(b) shows the HWTS with the heat shields installed. The heat shields are slightly corrugated in the chordwise direction. In general, two heat shields cover each full size beaded panel. Heat shield extensions were also provided around the boundaries of the test structure to improve the simulation of the heating of the HWTS outer spar and rib webs in subsequent elevated temperature testing.

Figure 7 shows a closeup view of the room-temperature loading setup of the HWTS. Two-point whiffletrees can be seen in the lower portion of the figure with load cells and hydraulic actuators attached to them. Horizontal loading jacks are visible on the right. An independent structure, which is evident above the HWTS, supports position transducers.

In order to apply pressure loads normal to the beaded panel surfaces, pressure pans were constructed and added to the test structure. Figure 8 shows the top view of a pressure pan that was exposed by removing an upper beaded panel. Two lines are attached to the pan; the larger one is a pressure feedline and the other is a pressure monitor line. Each of the five lower surface root panels (panels 1 to 5 in fig. 5) is backed by a pressure pan so that an internal pressure of 5.2 kN/m^2 could be applied to the panels during testing. The pans were constructed from 0.0076 centimeter thick stainless steel. Doublers were spot welded to the center of the pans to facilitate pressure feedline and pressure monitor line attachment. The total thickness at the center of the pans is 0.1600 centimeter.

TEST EQUIPMENT AND INSTRUMENTATION

Strain Gage Instrumentation

Strain gages were located as shown in figures 9(a) and 9(b). The two strain gages on the spar caps are single-gage axial gages in a T-configuration and are of a foil type. The strain gages on the spar web centerlines and on the panel flats are of the delta-rosette foil type. The strain gages on the panel up and down beads are single-gage axial strain gages of two types: foil and capacitance. Two of these strain gages, one of each type, were mounted end to end at each location shown by the circular symbols in figure 9(b). Only the capacitance gages are capable of

operating at high temperatures. Figure 10 shows typical strain gage installations on the beaded panels and on the wing spars. The delta-rosette strain gages were used to make measurements at three angular orientations (A, B, and C) spaced 120° apart starting in the direction parallel to the wing spars and rotating clockwise (when looking down on the HWTS beaded panels and forward at the spar webs).

The accuracy of the data acquisition system for strain gage measurements was ±4.88 microstrain, which represents 0.3 percent of the strain gage calibrate output. This provided accurate recorded data; in fact, it represents a 3 percent or less error for 93.5 percent of the recorded data.

Hydraulic Loading System and Deflection Instrumentation

Twenty channels of closed-loop electrohydraulic equipment (ref. 6) were used to apply loads to the test structure at the locations shown in figure 11. Ten hydraulic jacks applied vertical loads to the structure. Eight of those jacks applied loads through two-point whiffletrees. Horizontal (fore and aft) loads were applied by the remaining 10 hydraulic jacks at single points.

Load transducers of various capacities were used to measure the forces applied to the structure. The accuracy of the loading data was governed primarily by the accuracy of these transducers. Inaccuracies from all other sources (for example, positioning and the data acquisition system) were considered to be negligible. The estimated accuracy of the load transducers was as follows:

Load transducer capacity, N	Accuracy, N
88,960	±222
44,480	±111
22,240	±56

Position transducers were used to measure wing structural deflection during loading. The estimated accuracy of the position transducers was as follows:

Position transducer range, cm	Accuracy, cm
2.54	±0.0254
7.62	±0.0508

The location of the position transducers is shown in figure 12. The position transducer range used at each location is shown in the table below. Transducers attached to the lower HWTS surface were mounted on the floor and are marked with an A. Those attached to the upper surface to measure vertical displacement were mounted on an overhead frame; those attached to the upper surface to measure horizontal displacement were mounted to an independent frame and are marked with parentheses. Transducers 40 to 47 were mounted to measure wing structural motion at the

Transducer number	Range, cm
1A, 2	2.54
3, 4	7.62
5A, 6	2.54
7, 8	7.62
9A	2.54
10, 11, 12	7.62
13A	2.54
14, 15, 16	7.62
17A	2.54
18, 19, 20	7.62
21A	2.54
22, 23, 24	7.62
(25), 26, (27), 28, (29), 30, (31), 32, (33), 34	2.54
(35)	7.62
36	2.54
(37)	7.62
38A, 39A, (40), 41, (42), 43, (44), 45, (46), 47	2.54

root. Transducers 25 to 37 were mounted to measure fore and aft (horizontal) movement. Portions of the loading system and deflection-measuring system are shown in figure 7.

TEST PROCEDURE

Six tests were performed at room temperature. The magnitude and direction of the loads and the size of the load cell at each load point are listed in table 1. Figure 13 illustrates the applied load distribution during the six tests. The vectors in the figure indicate the direction and magnitude of the applied loads.

The loads applied during tests 1 to 3 are the structural loads that would be experienced by this wing section during a 2.5 g load maneuver at Mach 8. These loads were applied using a load-versus-time profile which simulated the 2.5 g load maneuver shown in figure 3. In test 1, only vertical loads were applied to the structure. In test 2, the structure was loaded vertically and horizontally. The horizontal loads simulated loads predicted to be introduced into the HWTS area by the wing portions forward and aft of the HWTS area (fig. 1). In test 3, three types of loads were applied to the structure: horizontal loads, vertical loads, and internal pressure loads on the lower five inboard panels (fig. 5). The loads applied in test 3 are the predicted design ultimate loads for the wing portion represented by the HWTS. In this test, the five lower panels were first pressurized to 5.2 kN/m^2 by individually controlled valves, and then loaded using the time-versus-load profile shown in figure 3.

Tests 4 to 6 were designed to establish the failure envelope of the panels. The envelope defines the combinations of the in-plane shear and compression which produce panel failure. In tests 4 to 6 internal pressure loads of 5.2 kN/m^2

6

were applied first, and then the structural loads were applied in small increments to establish the failure envelope. Test 4 applied vertical loads to introduce almost pure compressive loading into the wing panels. Test 5 utilized a combination of vertical and horizontal loads so that the ratio of the resulting compressive load to shear load on the panels was 2.5:1. Test 6 used vertical loads and horizontal loads to produce a ratio of compressive loading to shear load of 1:1.

ANALYSIS

Before the results of the computer analysis could be compared with the results of the tests performed on the HWTS, the data had to be processed by a number of computer programs. The flow chart in figure 14 displays the sequence of the programs required. As many as six programs were necessary, depending on the nature of the loads applied. Briefly, these programs are:

NWML—A NASTRAN finite-element computer model (ref. 8) of the hypersonic wing test structure.

EQULD—A FORTRAN program written to generate load data cards for input to the NASTR model. Data for EQULD were derived from the NWML NASTRAN computer model.

NASTR—A NASTRAN finite-element computer model of one-fourth of a beaded panel.

NEWGD—A FORTRAN program which generated a new grid point network for NASTR.

TWOBD—A NASTRAN finite-element computer model of two full length panel beads.

ROSETTE—A FORTRAN program which converted stresses generated by the finite-element computer models to strains so that direct comparisons with experimental results could be made.

A more complete description of each program follows.

HWTS Program

The finite-element computer model which represented the entire hypersonic wing test structure (fig. 15) was named NWML. The model was used in the design of the hypersonic wing test structure. The model consisted of 481 elements and 106 grid points. The spar and rib caps were modeled as rods, the spar and rib webs as shear panels, and the beaded panels as four overlapping triangular membrane elements. Using a finer element size for the beaded panels to more closely represent their actual geometry was impractical because the additional grid points, elements, and degrees of freedom would have made the model too large. The support structure, which is also shown in figure 15, was modeled by using bar elements.

Mechanical loads were applied at the grid points in the NWML model that corresponded to the load points on the HWTS. Direct comparisons between test data for

7

the beaded panels and the data for the NWML model could not be made because of the large size of the elements representing the beaded panels in the NWML model. The panel stresses derived from the NWML model represented average stresses for the entire panel. Thus, comparisons between the results of a strain gage mounted at a specific location on a beaded panel and the NWML model results would not necessarily be accurate. It was, therefore, necessary to develop the EQULD and NASTR programs.

Internal pressure loads applied to the beaded panels of the HWTS also could not be adequately modeled by the NWML model. Therefore, the effects of internal pressure were accounted for by using the NASTR finite-element panel model discussed below.

EQULD Program

The EQULD program was written to generate NASTRAN load cards specifically for the NASTR beaded panel model. The input data to the EQULD program were derived from the NWML NASTRAN model analyses. Average stresses computed by the NWML program for the beaded panels were multiplied by the nominal thickness of a panel. The results, loads per unit length of the panels, were then input to the EQULD program. The EQULD program divided up the loads per unit length and distributed them to the grid points of the NASTR model corresponding to the edges of the beaded panel. The same procedure was used to determine and distribute shear forces.

NASTR and NEWGD Programs

The NASTR program consisted of a finite-element model of one-fourth of a beaded panel with 392 elements and 418 grid points (fig. 16). The model closely approximated the actual geometry of one-fourth of a beaded panel. The elements were small enough in size so that accurate comparisons could be made between the element stresses and the beaded panel stresses.

In cases where internal pressure was not applied to the beaded panels, only one run of NASTR utilizing the shear and compression loads computed with the EQULD program was necessary. The stresses output by NASTR were input directly into the ROSETTE program for conversion to strains and finally used for comparison with experimental results.

In cases where internal pressure was applied to the beaded panels, two executions of NASTR were required. The first execution of the NASTR program was done with internal pressure loads data only. Deflections due to internal pressure loads were output on computer cards for subsequent use in the NEWGD (new grid) program. The NEWGD program added the deflections (translations in the X, Y, and Z directions) to the original undeflected grid network. This produced a grid network which was deflected by pressure. The NASTR program was executed again using this deflected grid combined with in-plane compression and shear loads data from the EQULD program. The output of this execution was element stresses.

TWOBD and ROSETTE Programs

The NASTR program failed to yield satisfactory stresses from an internal pressure load case, although the deflections did appear reasonable. Therefore, the TWOBD NASTRAN model was formulated. It was assumed that the beaded panels had zero stiffness in the direction perpendicular to the beads and in the plane of the panel. In addition, it was assumed that the beads carried the internal pressure load as a beam in bending. TWOBD was a finite-element model of two full length panel beads, as shown in figure 17. The model consisted of 478 elements and 516 grid points. The model was loaded with the same internal pressures as the test structure, and the resulting panel stresses were combined with the element stresses output from the second execution of the NASTR program. The combined panel stresses were then input into the ROSETTE program (fig. 14) for reduction to strains. The strains were compared with the experimental results of the HWTS loading tests.

RESULTS AND DISCUSSION

Force-Stiffness Measurements

Data for the beaded panel strength interaction curve (fig. 18) were calculated in the HWTS design study (ref. 5) using an optimization computer program (OPTBEAD). The curve was calculated for the beaded panels for a temperature of 1005 K and with a uniform internal pressure load of 5.2 kN/m^2; thus, the curve is basically the failure envelope for the panels subjected to Mach 8 temperatures. For instance, any combination of compression and shear loads below the curve that are applied to the panel should not cause a structural failure. Conversely, any combination of loads above the curve should cause a panel failure. As noted in the figure, the panels are stress critical in one portion of the curve and buckling critical in the remainder of the curve. The symbols in the figure, also from reference 5, show the load levels the five compressively loaded panels would be subjected to at the design ultimate load condition (a 2.5 g maneuver at Mach 8 temperatures). As can be seen, the final panel design was conservative due to manufacturing restraints, geometric restrictions, and so forth, which caused the panels to be nonoptimum.

The OPTBEAD optimization computer program, which established the elevated temperature strength interaction curve in figure 18, was utilized to calculate a similar curve for a room temperature case with an internal pressure load (fig. 19, solid line). The elevated temperature curve from figure 18 is repeated in figure 19 (the dashed line). The panel failure loads at room temperature are obviously much higher because the material modulus of elasticity is higher than at elevated temperature.

Figure 19 shows the loads imposed on the five compressively loaded root panels in loading tests 4 to 6. As these loads were applied in increasing increments real-time force-stiffness (ref. 9) plots were created and observed to determine the onset of panel buckling. None of the real-time plots nor any of the additional post-test force-stiffness plots predicted buckling failure.

Figure 20 compares the axial stresses calculated by OPTBEAD (dashed line) and the corresponding stress measurements without bending effects. For these measure-

ments the five delta-rosette strain measurements in the direction parallel to the beads on each root panel (fig. 9(b)) at the maximum load for tests 4, 5, and 6 were averaged. Stresses were then calculated from the average strain measurements and plotted (fig. 20, open symbols) for each panel and test condition as a function of panel compression load. Since the measurements for these stresses were made on the panel flats and hence on the neutral axis, they do not include the effects of panel bending. The dashed line in the figure shows the corresponding calculated stress from the OPTBEAD program. The correlation between the measured and calculated stresses is good.

Figure 20 also compares the calculated axial stresses with bending effects (solid line) and the corresponding stresses (solid symbols) from strain measurements on the panel beads. These stresses, which were measured using axial strain gages, include components of both in-plane load and bending because the strain gages are off the neutral axes (panel flats). In this case, the measured stresses are about 60 percent of the calculated values. This indicates that the assumptions made to determine panel out-of-plane eccentricities were too liberal. Hence, the calculated effects of panel bending were too large. The discrepancy also suggests that the upper or nearly flat portions of the strength interaction curves in figures 18 and 19 should be higher.

Data from another investigation of the compression of beaded panels (ref. 10) showed an elastic buckling failure to occur at a compression load of 3055 newtons per centimeter with no shear. The strength interaction curve for that test case (room temperature and no pressure) showed a failure load of 2520 newtons per centimeter with no shear. This corroborates the finding that the upper or flat portion of the calculated strength interaction curves in figures 18 and 19 is conservative.

Furthermore, the beaded panel design was conservative, as noted in figure 18, resulting in a minimum design margin of safety for the beaded panels of 0.24. The corresponding design margin of safety for crippling of the HWTS spar caps is 0.03 (ref. 5). The spar caps, therefore, would fail well before any panel failure predictions could be made in loading tests 4 to 6.

Principal Stress Data

To calculate principal stress magnitudes and directions, data from the delta-rosette strain gages on the HWTS were input into the ROSETTE computer program. Figures 21(a) to 21(f) show the resulting maximum stresses and their directions for the five compressively loaded lower root panels for all six load tests. The figures also show the corresponding calculated data. The data are shown for each delta-rosette strain gage on each panel. All delta-rosette strain gages were located on the flats between panel beads, as mentioned previously. The solid and dashed lines (fig. 21) show the directions of the calculated and measured maximum stresses, respectively. Except for a few cases in which the directions are very close to 0° (vertical), all experimental and analytical stress directions are rotated from zero in the same way (either clockwise or counterclockwise). The best comparisons of the stress and direction data were on panel 3, which, of course, is the farthest from the free edges of the HWTS. In general, more shear was measured than calculated, as indicated by the larger angles of the experimental data than the analytical data (fig. 21).

10

No trend is apparent in the stress comparisons in figure 21 due to variations in load: Any differences in comparison appear to be random as opposed to increasing with increased compression panel load. The mean differences between the experimental strains and the analytical strains in the three delta-rosette strain gage directions (A, B, and C; see Strain Gage Instrumentation) are as follows: 118 microstrain in the A direction, 132 microstrain in the B direction, and 149 microstrain in the C direction. These strains translate into a difference in stress of 4.1 kN/cm^2, which can be seen in the data of figure 21.

Since the overall strain and stress levels are relatively low, the differences between the analytical and experimental data represent a high percentage of the total strain and stress values. However, both the strain and stress levels and the differences between the experimental and analytical data are small compared with either the yield strain/stress of René 41 or to the predicted critical buckling values of strain or stress for the beaded panels. In view of the foregoing factors, the performance of the analytical procedures used to predict strains and stresses at the beaded panel delta-rosette strain gage locations is considered to be good.

Cross Section Stresses From Spar Caps and Panel Neutral Axes

Spanwise stress data from two span stations (W.S. 1.926 and W.S. 3.034) are presented in figure 22. The analytical data were obtained from the NWML and NASTR NASTRAN programs. The experimental data represent (1) the strains measured on the spar caps, and (2) the strains measured on the panels by using the spanwise-oriented gages from the delta-rosette configurations. The strain gages were located as shown in figures 9 and 10. Stresses were then calculated using these measured strains. The measured data are shown with open symbols (fig. 22). The analytical data have been connected with a solid line.

At the inboard span station (W.S. 1.926) data are presented for the spar caps and three flats across the midspan of the five panels. Data for the outboard span station are presented for the spar caps and one flat near the center of each panel. The gages for the outboard station (W.S. 3.034), like those for the inboard station, are located on the midspan of each corresponding row of panels (fig. 9(b)).

Figure 22 shows agreement between the analytical and measured data at both span stations, indicating the ability of the analytical programs to predict panel and spar stresses from relatively simple structural models. The few discrepancies that appear were felt to be due primarily to three factors. First, the wing was attached to the support structure at 12 points, using turnbuckles to react the loads from the spars. Since it was not feasible to preload the turnbuckles equally, nonuniform loads were introduced into the test structure, even though a short buffer bay existed between the attachment points and the root panels.

Second, the analytical model considered neither the increase in spar stiffness due to the pressure pan flanges that were sealed on the lower spar caps nor that due to the nut plate strips on the upper and lower spar caps of both the inboard and outboard panels. Figures 22(a) to 22(f) show that there is closer agreement between the analytical and measured data at the ouboard section. This indicates that the farther the stress measurements are from the attachment points, the smaller the effects of the nonuniform attachment reactions. The figures also show that the

predicted stresses in the spar caps are higher than the measured stresses in almost all cases, indicating that the spar stiffness was underestimated in the analytical model. At the outboard panels, the discrepancy was smaller because there were no pressure pan flanges to consider for these panels.

The third source of error was experimental error. This error was determined by using the differences in data from the axial strain gages mounted end to end on the panel beads at six locations per panel (fig. 9). The average of the differences between the gages, or estimated experimental error, was 1.5 kN/cm^2. The differences between the analytical and measured stress data at the outboard section (fig. 22) were consistent with this estimated error.

Panel Bead Stresses

Figure 23 shows the stresses that were measured at cross sections of one-quarter ($l/4$), one-third ($l/3$), and one-half ($l/2$) the length of the lower surface root panels (open symbols, fig. 9(b)). Data are shown for each of the three cross sections for tests 1 to 6. The corresponding analytical data are also shown in figure 23 (solid symbols).

The measured and analytical stress data in figure 23(a) show essentially the same stresses at each spanwise cross section. The stresses at $l/2$ (W.S. 1.926) compare well with the corresponding spanwise stresses in figure 22(a). In a like manner, the average stresses from the up and down beads from figures 23(b) to 23(f) also compare well with the corresponding spanwise data in figures 22(b) to 22(f).

The measured data in figure 23(b) should be similar to those in figure 23(a). However, stresses indicated by the open symbols at $l/3$ in figure 23(b) exhibit a bending component (that is, the stresses for the up and down beads are different). The bending is due to the shear of the horizontal loads that were applied during test 2. In this case, the up bead has an additional tension component and the down bead has an additional compression component.

The bending due to the pressure on the panels is even more apparent in figures 23(c) to 23(f). In these cases the bending causes an added compression component on the up bead and a tension component on the down bead.

The bending components are apparently a result of shear deformations that occur in beaded panels of this type. Irregular shear deformations of beaded panels were noted in previous tests on beaded panels (ref. 3). The bending in the measured stress data in figures 23(c), 23(e), and 23(f) should increase from the values at the $l/4$ cross section to a maximum at the $l/2$ cross section, as it does in figure 23(d). In figure 23(c), however, the measured bending is actually at a minimum at the $l/3$ cross section. In figures 23(e) and 23(f), the measured bending is at a maximum at the $l/3$ cross section. The direction of the applied shear load is opposite in test 4 from that in tests 5 and 6, so it is consistent for the direction of the panel bending anomaly due to shear in those tests to be opposite. The applied shear load is practically zero in test 4. Consequently, the stress data from that test (fig. 23(d)) show no unusual bending at the $l/3$ cross section. It appears definite, then, that shear loading on the beaded panels produced a significant change in the measured bending stresses at the $l/3$ cross section. A similar, but less significant, change is apparent at the $l/4$ cross section.

12

The analytical stress data (solid symbols) generally agree well with the measured stress data (open symbols), with the major exception of the data affected by the shear anomaly discussed above ($l/4$ and $l/3$ cross sections in figures 23(b), 23(c), 23(e), and 23(f)). The measured and analytical data compared well at the $l/2$ cross section in all cases. The panel 3 stress comparisons at the $l/2$ cross section are particularly good for all test conditions, because that panel was influenced least by structural boundary conditions.

Deflections

Deflections were measured at the HWTS locations shown in figure 12 in all tests. Figure 24 shows the deflection measurements (circular symbols) made at the maximum test 3 loading condition as a function of location along individual spars. The triangular symbols represent the corresponding analytical deflection data. As can be seen, the difference between the experimental and analytical data at F.S. 23.114 is large, and it becomes even larger at each succeeding spar going aft (figs. 24(b) to 24(f)). The primary reason for this discrepancy is that the structural model used in the analysis did not account for the loose fit of the wing attachment fittings. As a result, small errors in calculated deflections at the wing root produced large errors in the calculated deflections at the outboard wing stations.

In order to establish the wing root (W.S. 1.372, fig. 5) as a reference (that is, zero displacement and rotation) for comparing experimental and analytical deflections, the vertical and rotational displacements must be known. However, too few measurements were made at the wing root to define those displacements adequately. Therefore, an assessment of the analytical deflection data for the wing structure, exclusive of the support structure, was made by establishing W.S. 2.479 as a reference for deflections. It was assumed that the spar deflections between W.S. 1.372 and W.S. 2.479 were linear. All of the deflections (analytical and experimental) outboard of W.S. 1.372 were then corrected by simple rotations and translations to provide a fixed end condition at W.S. 2.479. These data are shown by the solid and dashed lines in figure 24. These data, which typify data for all tests, in general show very good agreement between the analytical and experimental wing deflections. One anomaly is apparent in figure 24(c). This is caused by a probable error of the experimental measurement at W.S. 3.586; this error produces a discontinuity in the measurements along that spar which is unrealistic and inconsistent with the applied loads.

CONCLUDING REMARKS

Room-temperature loading tests were conducted on a wing section that was designed using a hot structural concept for a Mach 8 cruise hypersonic airplane. The 7.9 square meter planform semimonocoque wing test structure consists of spanwise-stiffened beaded panels attached to orthogonal spars and ribs. Metallic heat shields with shallow chordwise corrugations cover the beaded panels and constitute the external surface.

The experimental program evaluated the structural concept and the final structural design. Strain, stress, and deflection measurements were made during the test series. These data were compared to data calculated from three finite-element structural analysis programs.

In general, the measured stresses and deflections compared well with the calculated values. Measured delta-rosette strain gage data on the beaded panels showed slightly more shear stress than was predicted. The differences between axial stress measurements and calculated values at an outboard wing station were consistent with the estimated experimental error of 1.5 kN/cm^2. Differences between measured and calculated stresses were higher near the wing root because of (1) local stresses due to nonuniform reaction loads from the support structure and (2) inadequacies of the structural model used in the analysis program.

Stress measurements on the root panel beads showed an anomaly at cross sections which were one-third of the panel lengths. The bending stresses at these cross sections varied from predicted values depending upon the magnitude and direction of the shear load.

A force-stiffness method was used in conjunction with various combinations of panel shear and compression loads to determine the panel failure envelope. Since no predictions of failure were obtained and the stress levels were lower than predicted by analysis, it was concluded that the beaded panels were designed conservatively. This was a result of design constraints and liberal assumptions of panel eccentricities.

In conclusion, the relatively simple finite-element structural analysis programs were considered to have calculated strains and stresses well, and the hypersonic wing test structure in this test program was believed to have provided a positive demonstration of the beaded panel concept.

Dryden Flight Research Center
National Aeronautics and Space Administration
Edwards, Calif., February 7, 1979

14

REFERENCES

1. Plank, P. P.; Sakata, I. F.; Davis, G. W.; and Richie, C. C.: Hypersonic Cruise Vehicle Wing Structure Evaluation. NASA CR-1568, 1970.

2. Shideler, John L.; and Bohon, Herman L.: Evaluation of Bead-Stiffened Metal Panels. AIAA Paper 75-815, 1975.

3. Musgrove, Max D.; and Greene, Bruce E.: Advanced Beaded and Tubular Structural Panels. NASA CR-2514, 1975.

4. Greene, Bruce E.; and Northrup, Russell F.: Design and Fabrication of René 41 Advanced Structural Panels. NASA CR-132646 [1975].

5. Plank, P. P.; and Penning, F. A.: Hypersonic Wing Test Structure Design, Analysis, and Fabrication. NASA CR-127490, 1973.

6. Sefic, Walter J.; and Anderson, Karl F.: NASA High Temperature Loads Calibration Laboratory. NASA TM X-1868, 1969.

7. Mechtly, E. A.: The International System of Units—Physical Constants and Conversion Factors. Second Rev. NASA SP-7012, 1973.

8. NASTRAN User's Guide. NASA CR-2504, 1975.

9. Jones, Robert E.; and Greene, Bruce E.: The Force/Stiffness Technique for Nondestructive Buckling Testing. AIAA Paper 74-351, 1974.

10. Siegel, William H.: Experimental and Finite Element Investigation of the Buckling Characteristics of a Beaded Skin Panel for a Hypersonic Aircraft. NASA CR-144863, 1978.

TABLE 1.—HWTS MAXIMUM APPLIED LOADS

[Load points attached to whiffletrees are noted by connected lines]

Load point number	Load cell size, N	Load direction	Test number					
			1	2	3[c]	4[c]	5[c]	6[c]
			Maximum applied load[b], N					
1[a]	88960	Horizontal	-------	-49,610	-49,610	-------	27,470	26,020
2	44480	Horizontal	-------	-29,250	-29,250	-------	27,470	26,020
3[a]	44480	Horizontal	-------	-12,900	-12,900	-------	-27,470	-26,020
4	44480	Horizontal	-------	17,790	17,790	-------	-27,470	-26,020
4	22240	Vertical	-8,400	-8,400	-8,400	-4,180	-5,920	-5,600
5	22240	Vertical	11,010	11,010	11,010	-4,180	-10,140	-9,610
6	22240	Vertical	-11,830	-11,830	-11,830	-4,180	-5,920	-5,600
7	22240	Vertical	-5,690	-5,690	-5,690	-10,450	-5,920	-5,600
8	22240	Vertical	9,520	9,520	9,520	-10,450	-10,140	-9,610
9	22240	Vertical	-7,740	-7,740	-7,740	-7,530	-5,920	-5,600
10	44480	Vertical	-4,940	-4,940	-4,940	-12,540	-5,920	-4,000
11	44480	Vertical	-2,820	-2,820	-2,820	-12,540	-5,920	-4,000
12	22240	Vertical	-6,030	-6,030	-6,030	-7,530	-5,920	-4,800
13	44480	Vertical	-4,720	-4,720	-4,720	-12,540	-5,920	-4,000
14	44480	Vertical	-4,110	-4,110	-4,110	-12,540	-5,920	-4,000
15	22240	Vertical	1,060	1,060	1,060	-7,530	-5,920	-4,800
16	22240	Vertical	-3,830	-3,830	-3,830	-10,450	-5,920	-2,400
17	22240	Vertical	-2,720	-2,720	-2,720	-10,450	-5,920	5,600
18	44480	Vertical	-7,720	-7,720	-7,720	-8,360	-1,690	1,600
19[a]	22240	Horizontal	-------	-12,230	-12,230	-------	21,130	20,020
20	44480	Horizontal	-------	-31,580	-31,580	-------	27,470	26,020
21[a]	44480	Horizontal	-------	29,870	29,870	-------	-27,470	-26,020
22	44480	Horizontal	-------	9,140	9,140	-------	-27,470	-26,020
22	22240	Vertical	-14,860	-14,860	-14,860	-4,180	-5,920	-2,400
23[a]	44480	Horizontal	-------	28,250	28,250	-------	-25,350	-24,020
24	44480	Horizontal	-------	-5,470	-5,470	-------	-25,350	-24,020
24	22240	Vertical	-6,870	-6,870	-6,870	-4,180	-5,920	5,600
25	44480	Vertical	-17,470	-17,470	-17,470	-4,180	-1,690	1,600

[a]Denotes upper surface; all others are lower surface.

[b]Positive up and forward.

[c]Panel pressure loads of 5.2 kN/m^2 were applied during these tests.

F.S. 0

F.S. 29.57

11.58

85°

Hypersonic wing test structure

70°

30.78

F.S. 6.10   F.S. 12.19   F.S. 17.68   F.S. 24.38

2.74
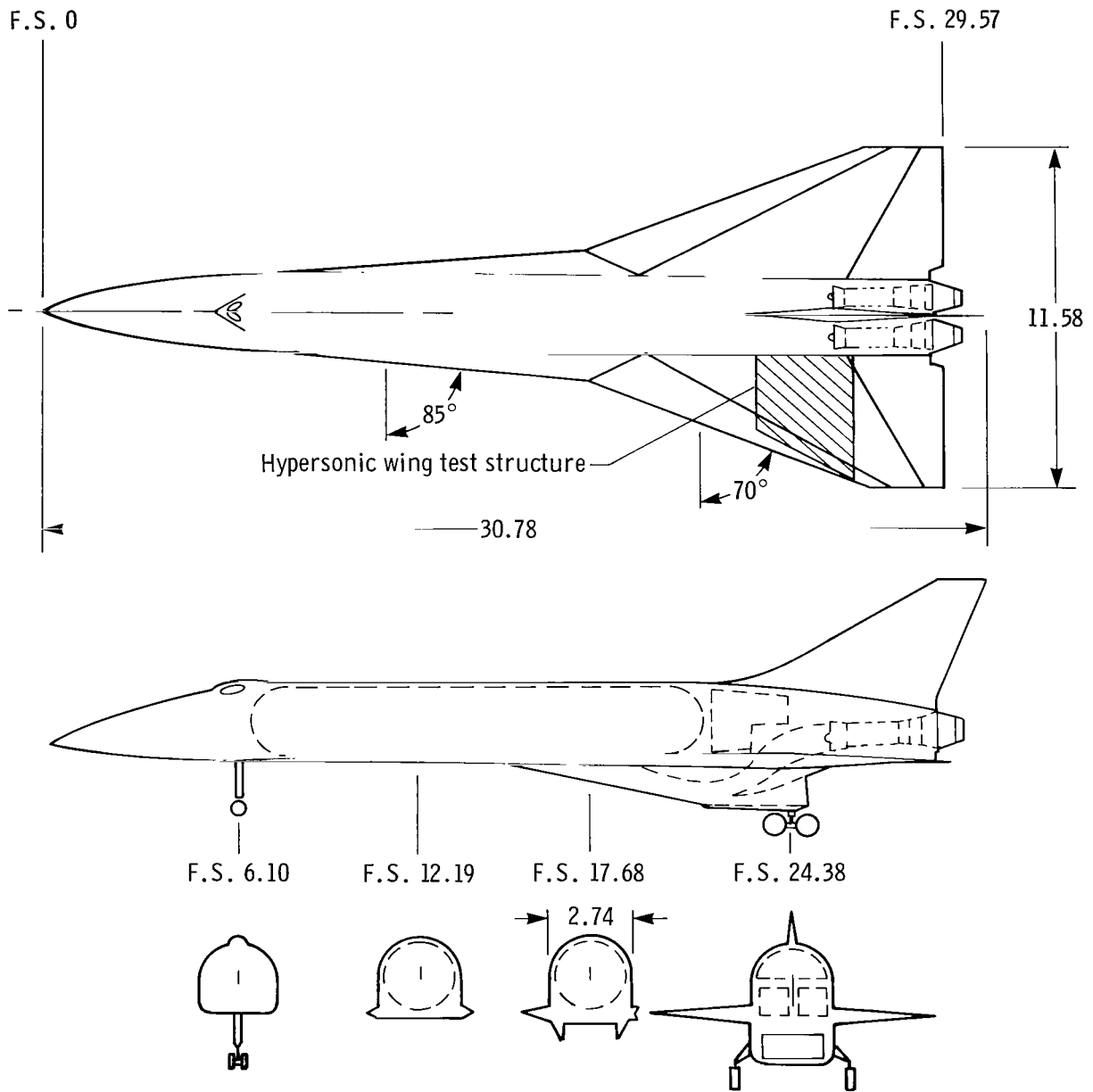
Figure 1. Hypersonic research airplane configuration. Fuselage stations (F.S.) and dimensions in meters.

17
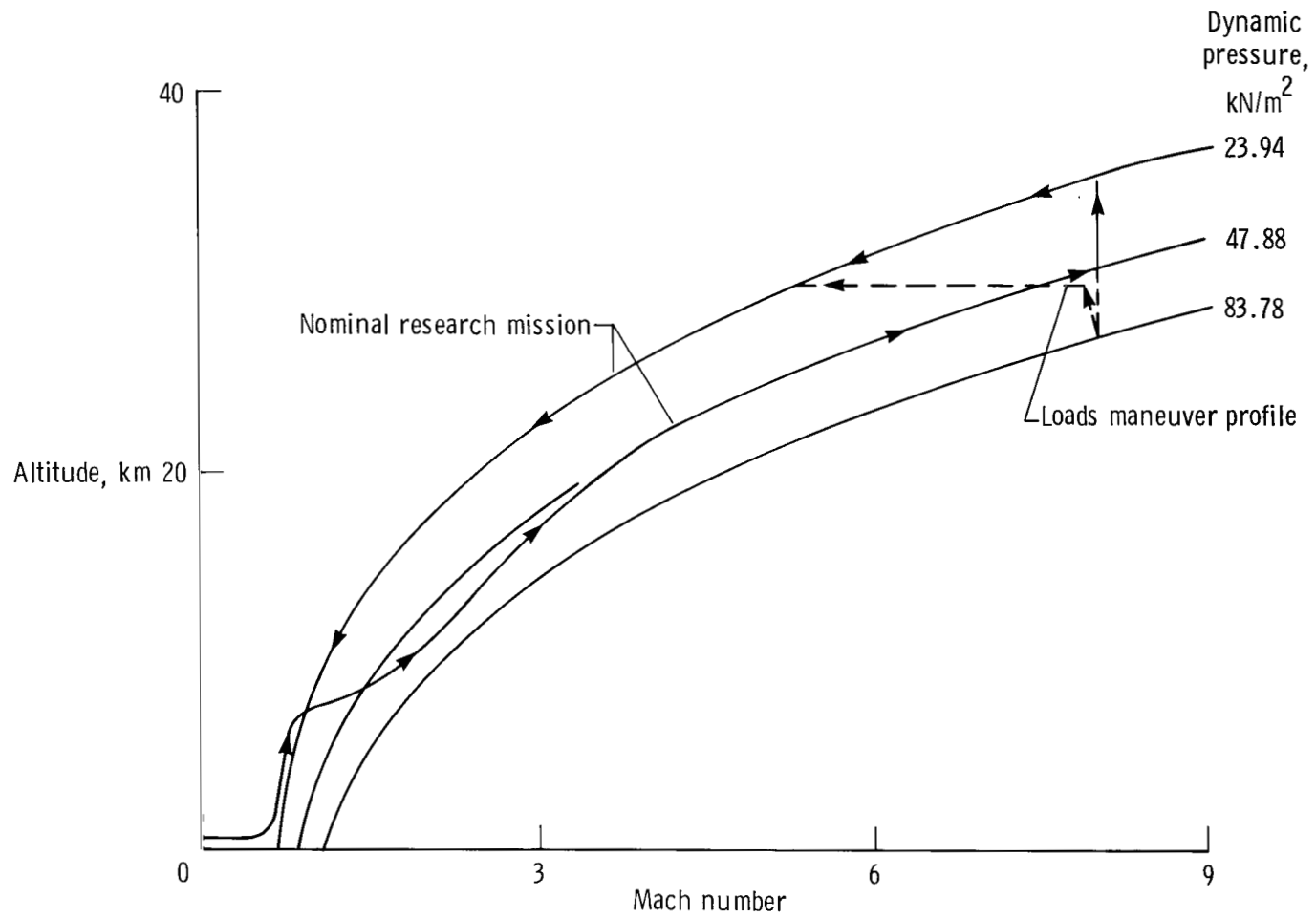
Figure 2. Hypersonic research airplane research-mission profile.
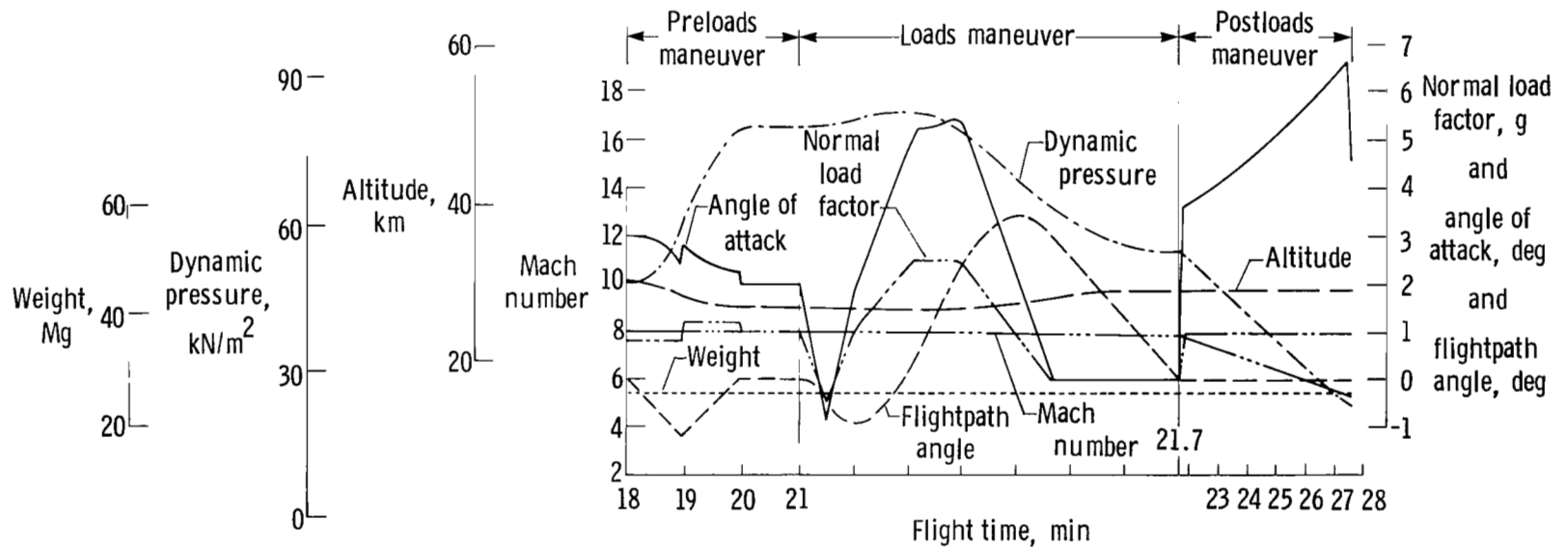
Figure 3. *Time history for a loads maneuver of the hypersonic research airplane.*

Doubler

Heat shield support

C   C

Up bead

Down bead

Panel flat

E 36158

48.8

155°

0.091

1.113

0.066

2.654

Section C-C
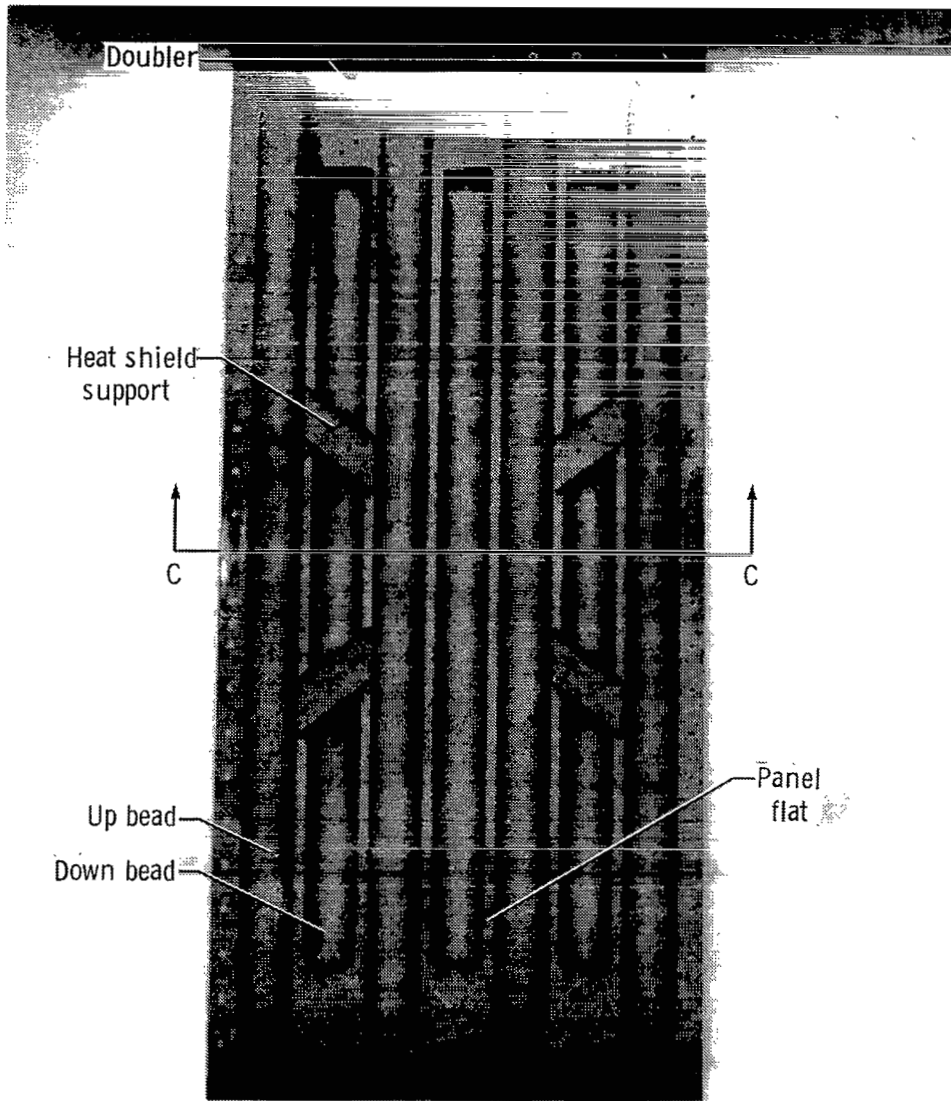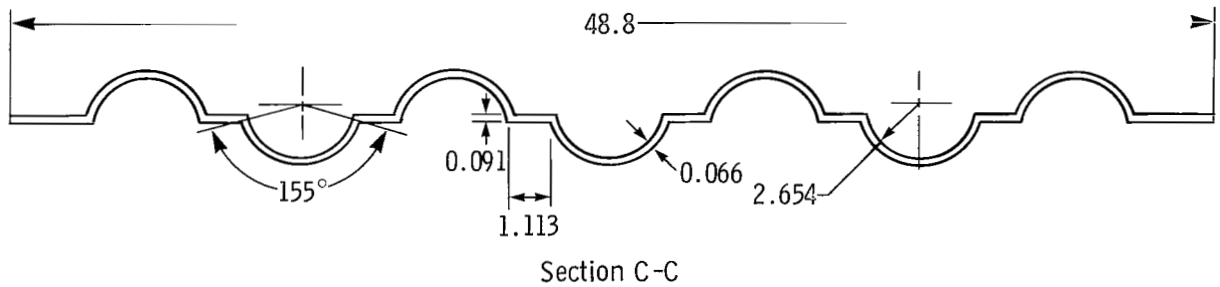
Figure 4. Beaded panel for HWTS. Dimensions in centimeters.
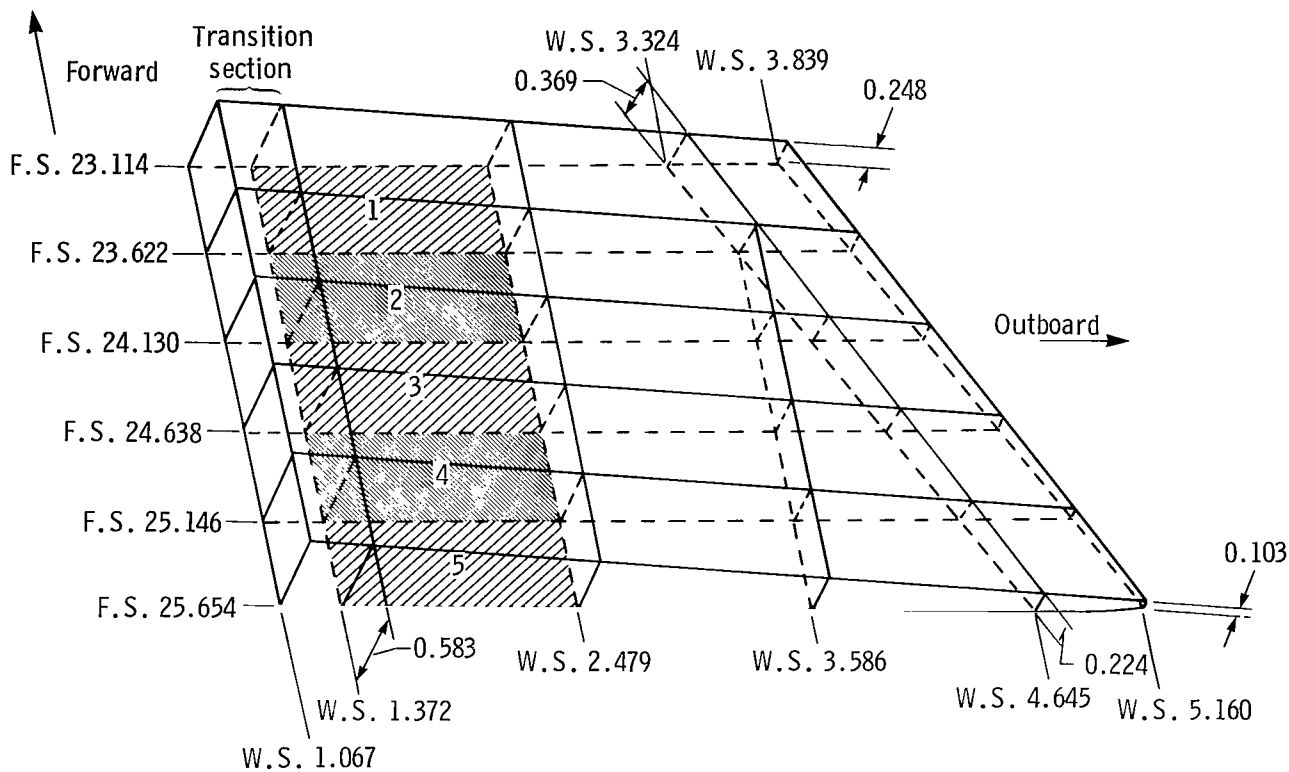
Figure 5. Hypersonic wing test structure dimensions. The most critically loaded panels are shaded and numbered 1 to 5 going aft. Fuselage stations, wing stations (W.S.), and dimensions in meters.

(a) Heat shields removed.

E 27650
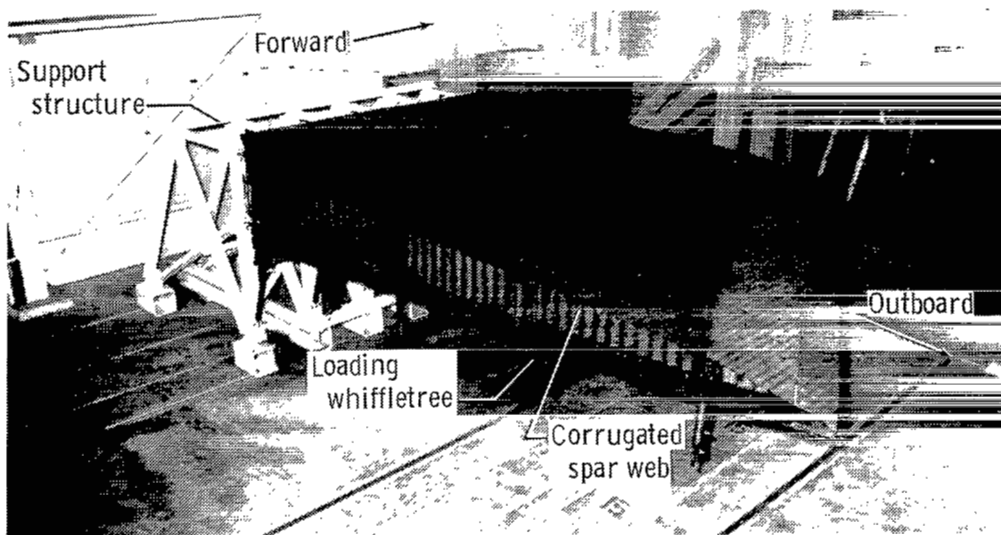
(b) Heat shields installed.

E 26145

Figure 6. Hypersonic wing test structure.

22
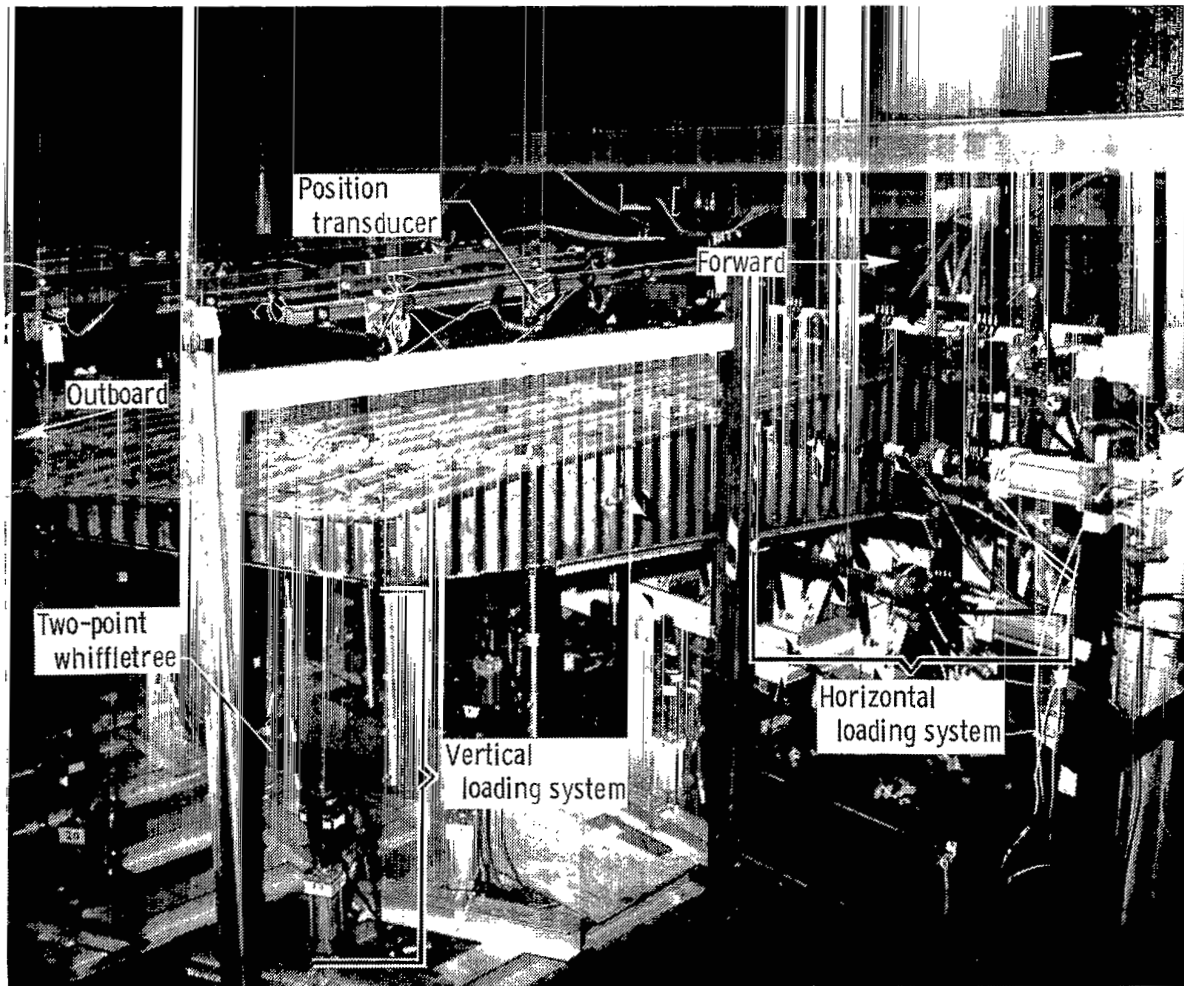
Figure 7. HWTS loading test setup.

E 30865
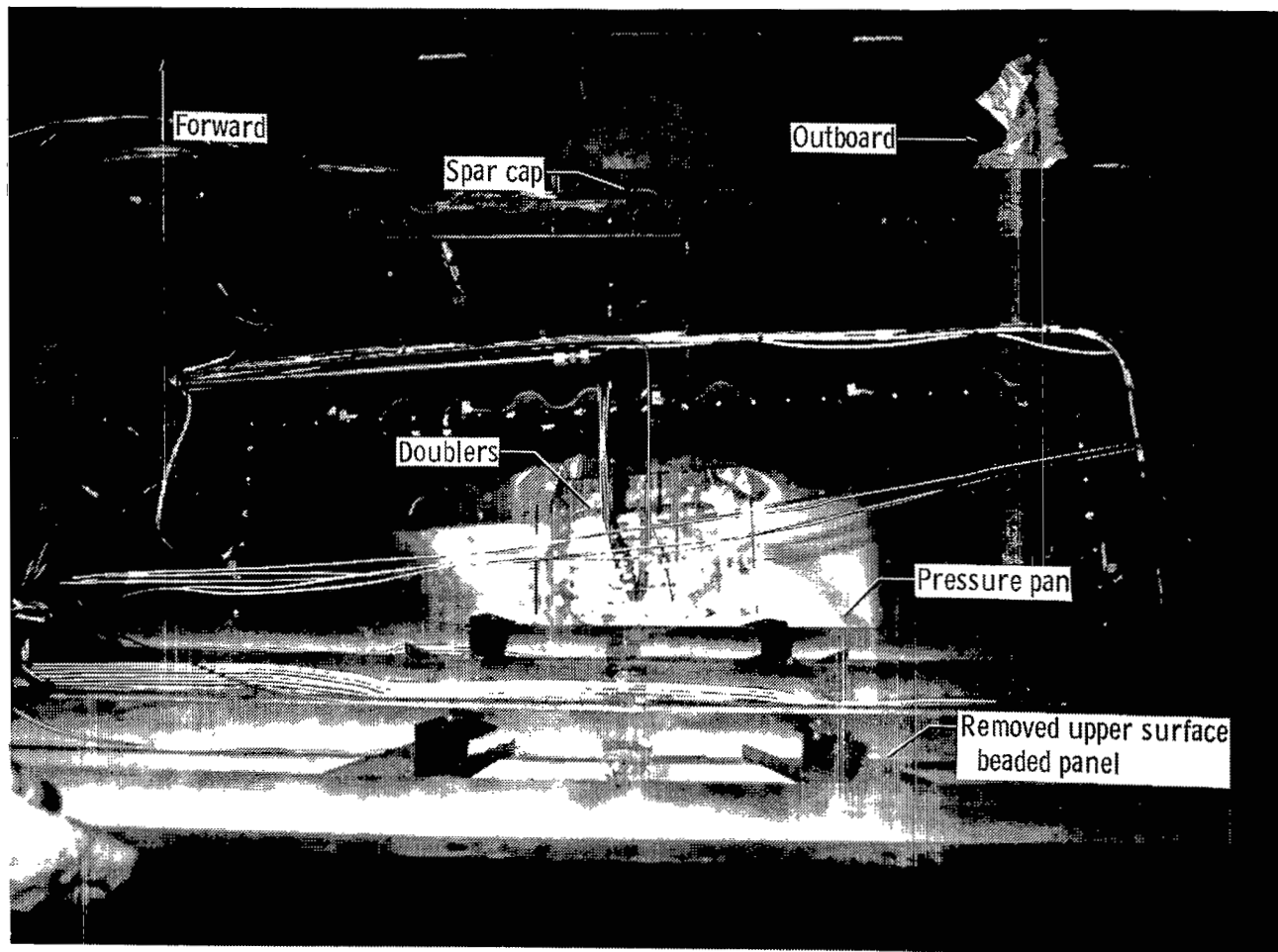
Figure 8.   Interior of HWTS bay showing pressure pan.   E 28432
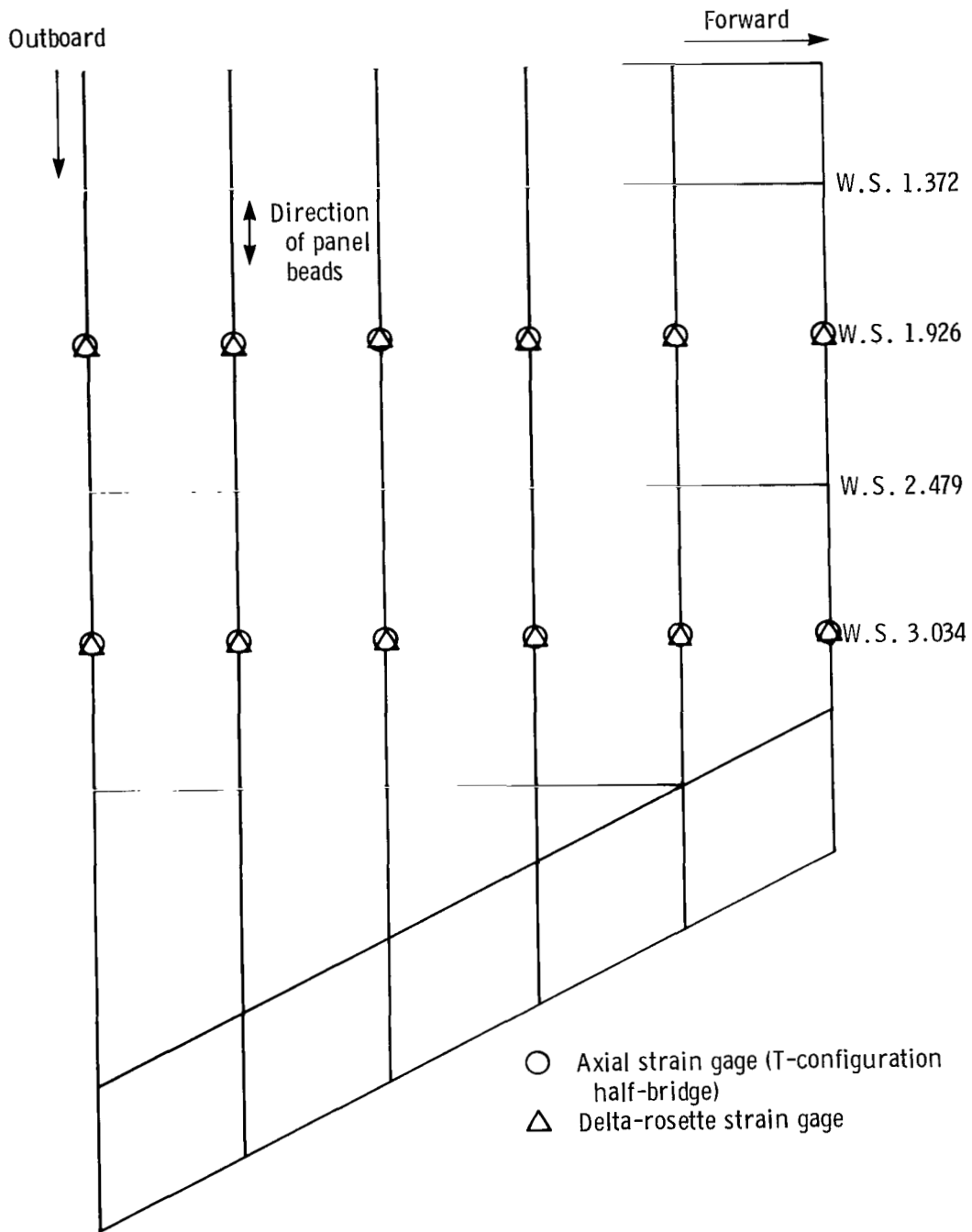
(a) *Strain gage locations on spar caps and web (view looking down). Axial strain gages were installed on upper and lower spar caps, and delta-rosette strain gages were used on spar web centerlines.*

Figure 9. Strain gage locations. Wing stations are in meters.

O Axial strain gage
△ Delta-rosette strain gage
l panel length

Forward ⟶

W.S. 1.372

$l/3$ $l/4$

$l/2$

A

B

W.S. 1.926

C

$l/4$

D

l

W.S. 2.479

Outboard

33°

Section A-A

Up bead

Down bead

Section B-B

W.S. 1.926

Section C-C
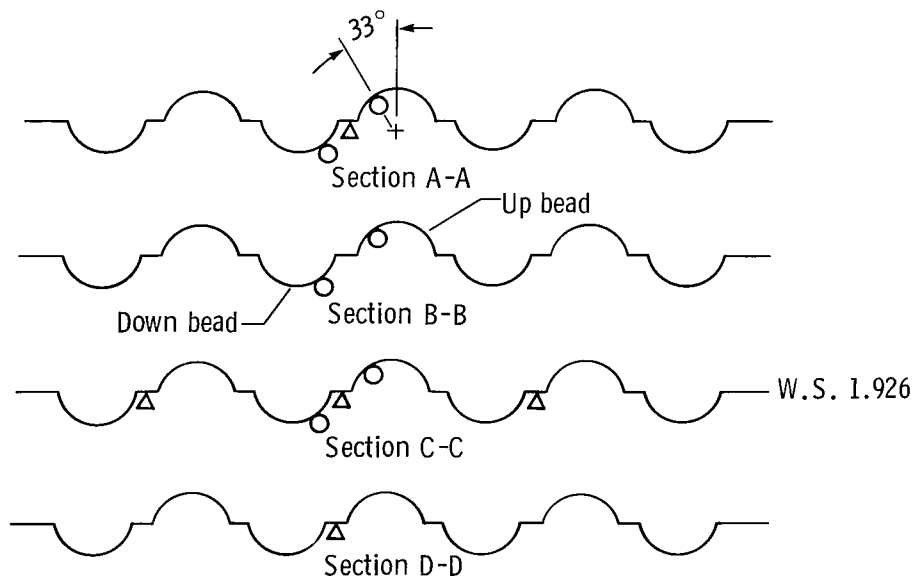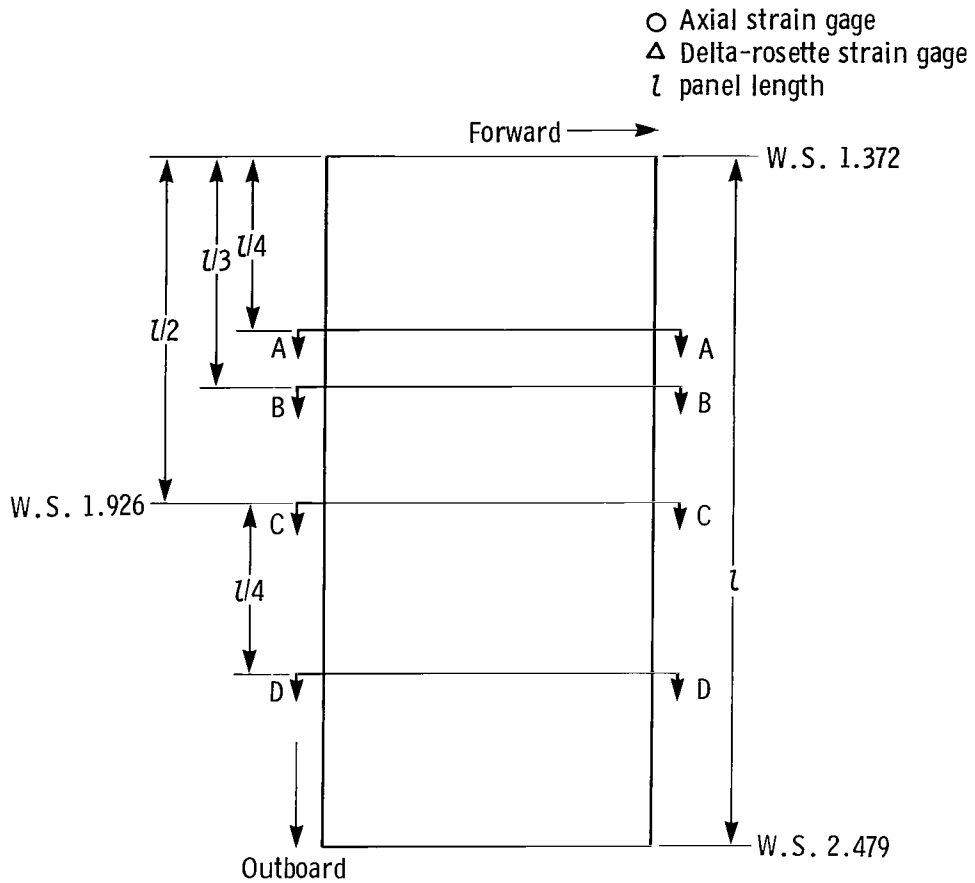
Section D-D

(b) Strain gage locations on lower root panels between W.S. 1.372 and 2.479. Instrumentation was identical for each root panel.

Figure 9. Concluded.
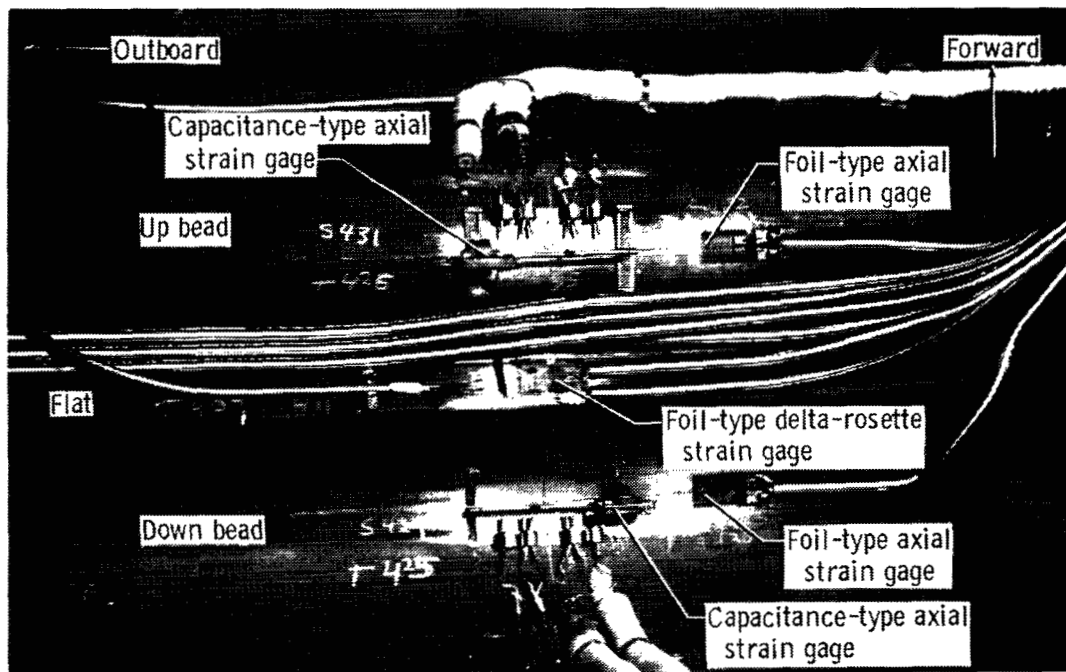
(a) External instrumentation on center section of root panel 4.
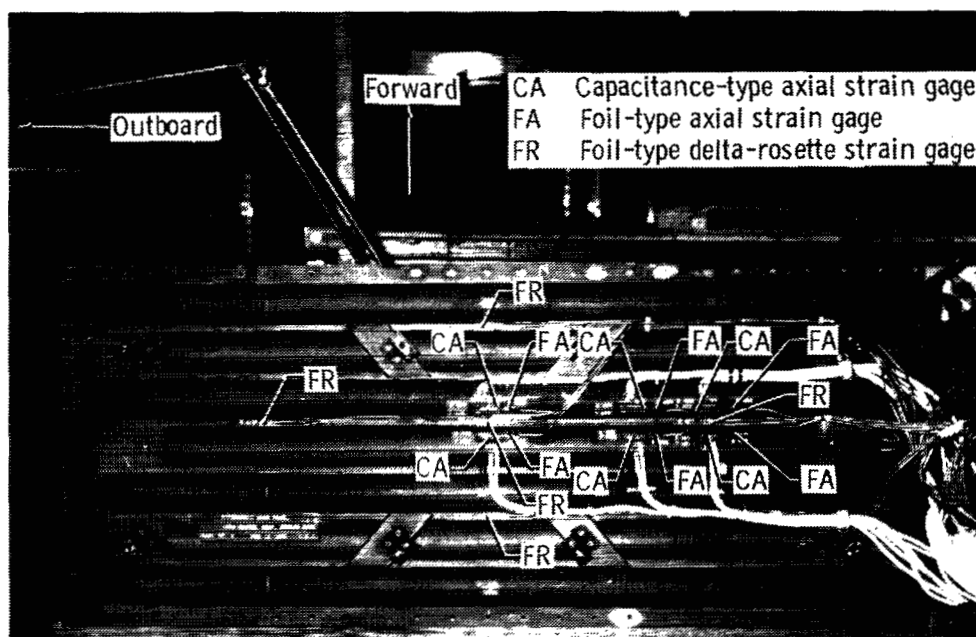
(b) External instrumentation on root panel 4.

Figure 10.   Strain gage instrumentation.

27
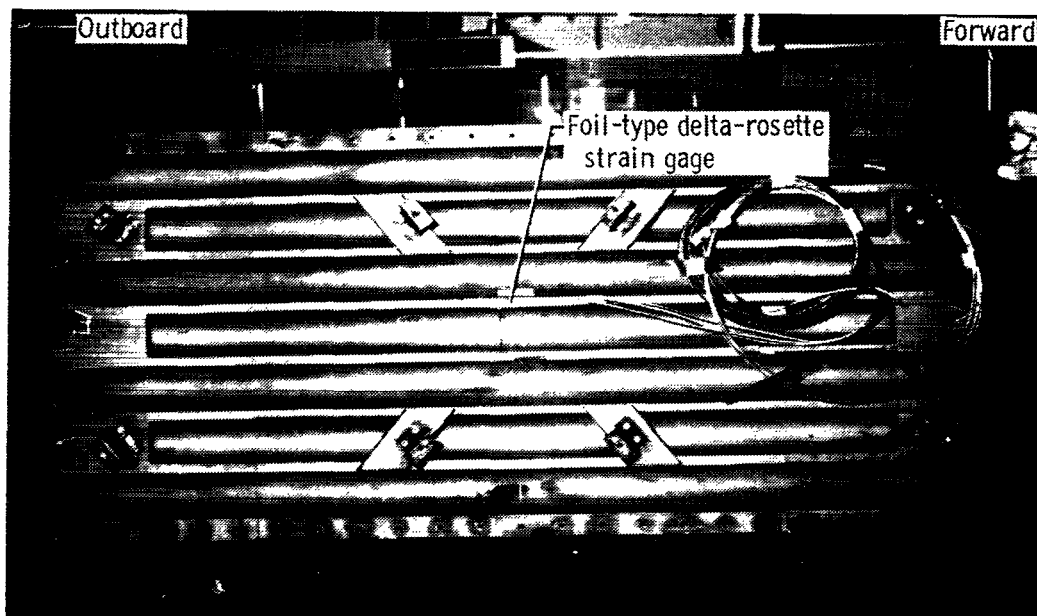
(c) External instrumentation on an outboard panel.　E 28111
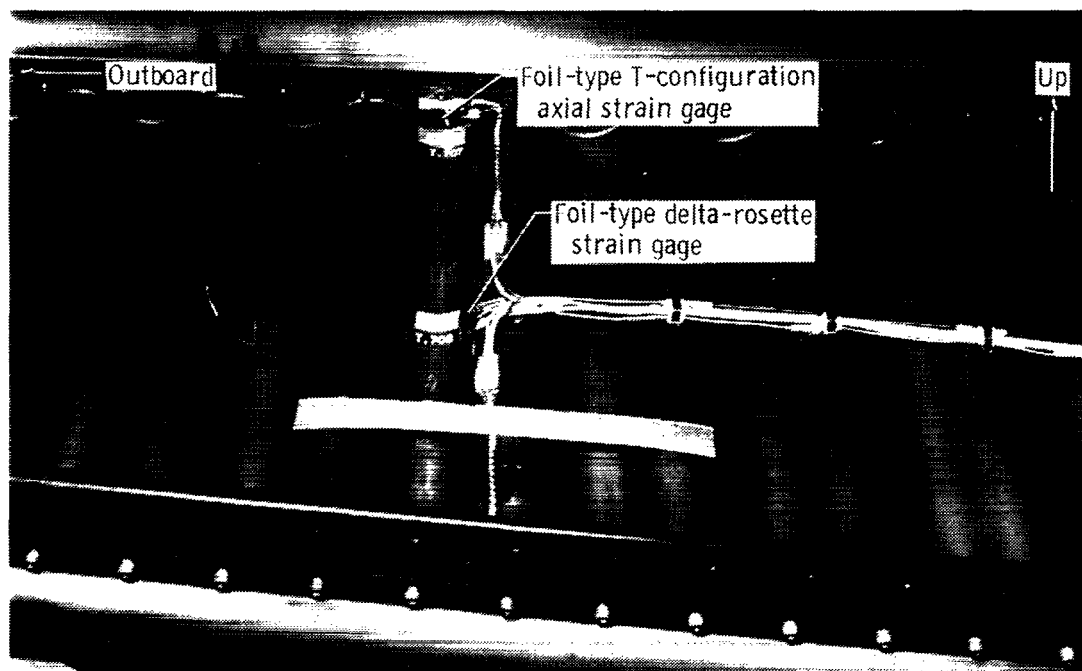
(d) Typical spar cap and web instrumentation.　E 28159

Figure 10.　Concluded.
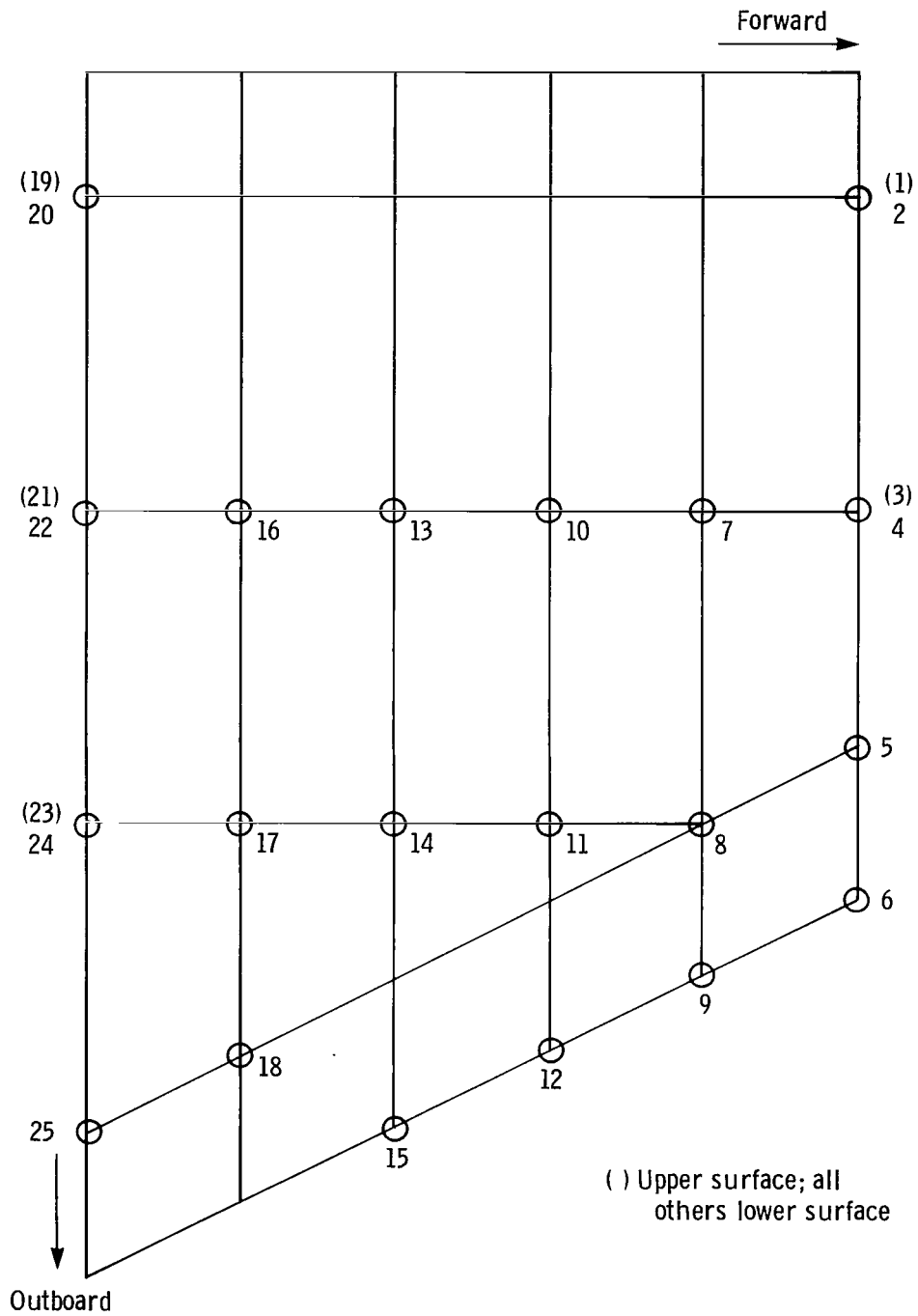
Figure 11. HWTS load points.
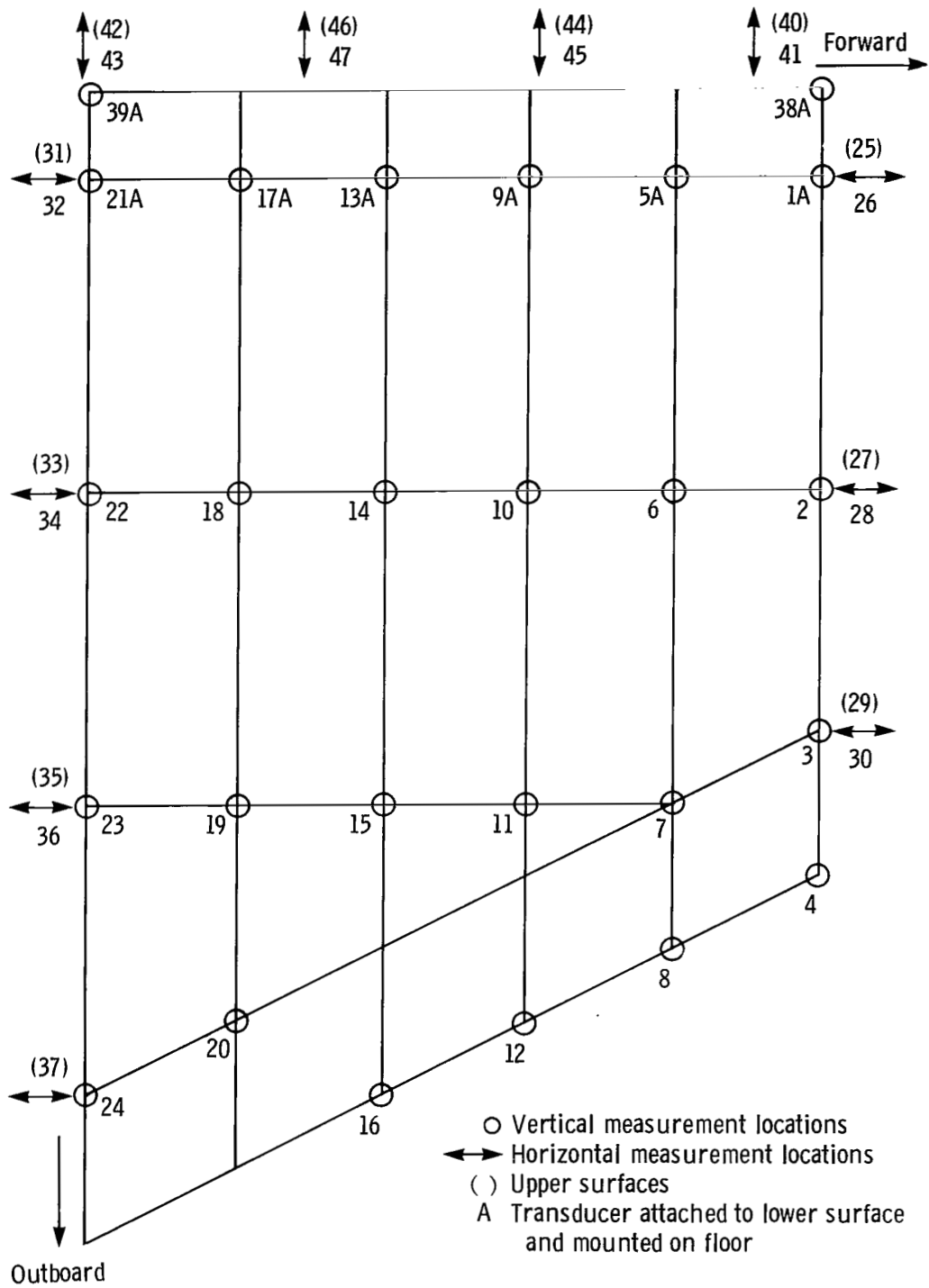
Figure 12. HWTS deflection measurement locations.

Forward   Up

Outboard
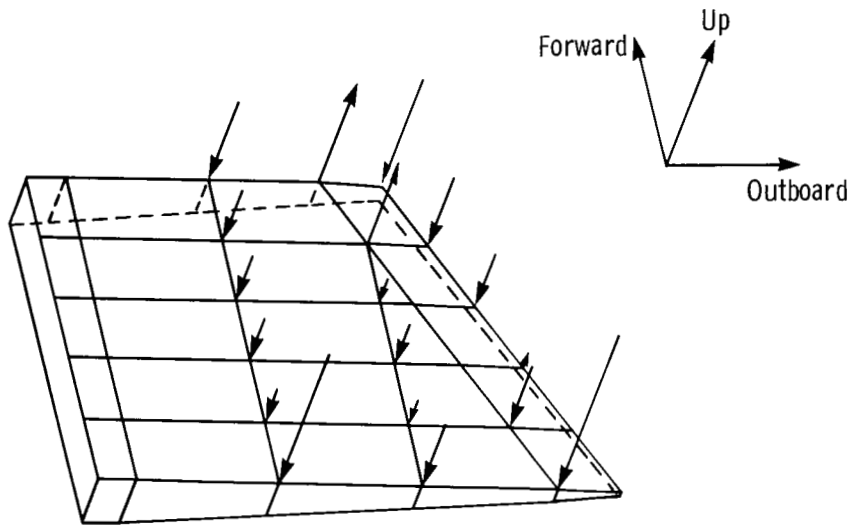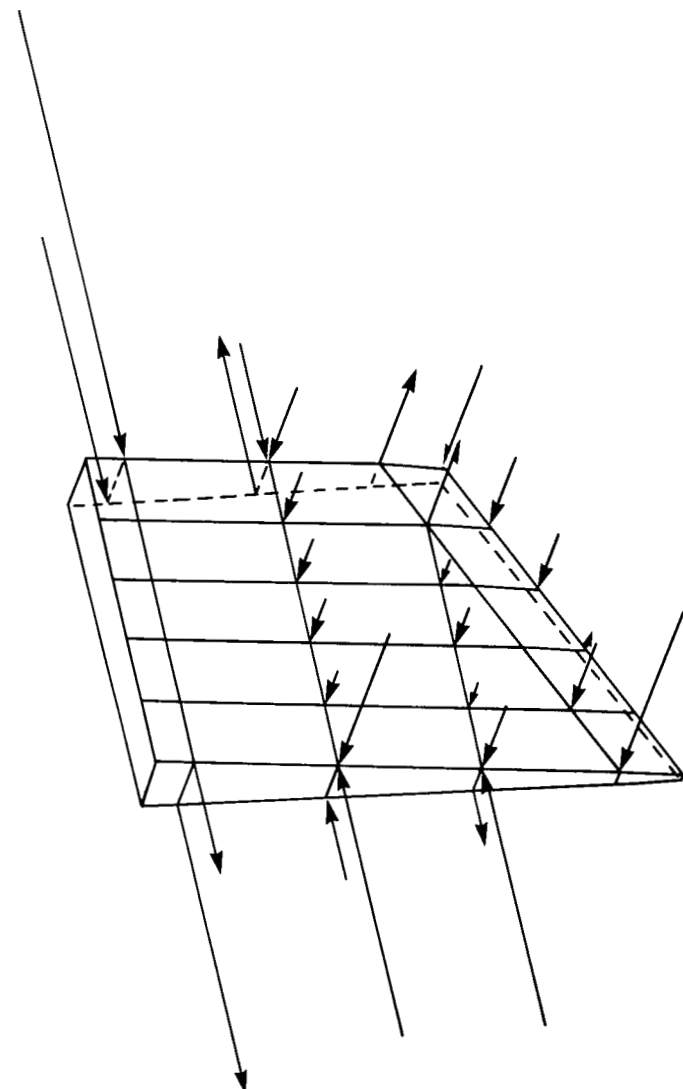
(a) Test 1.   (b) Tests 2 and 3.

Figure 13. Applied load distribution on HWTS.

Up

Forward

Outboard
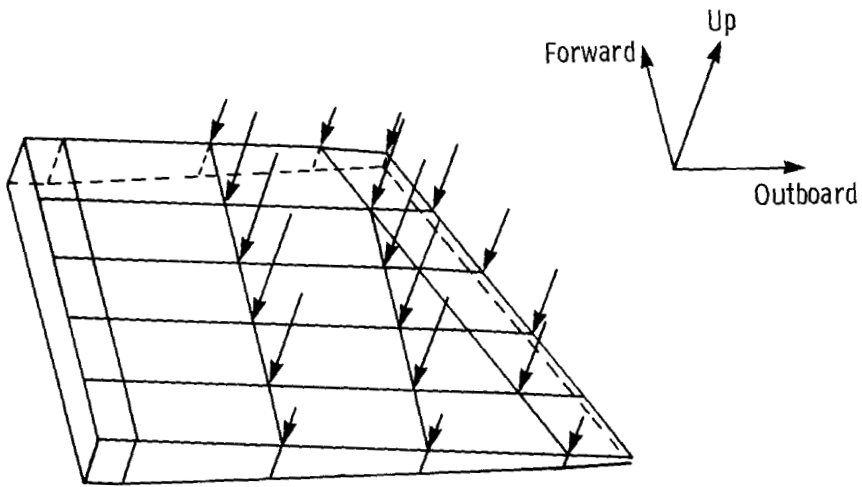
(c) Test 4.
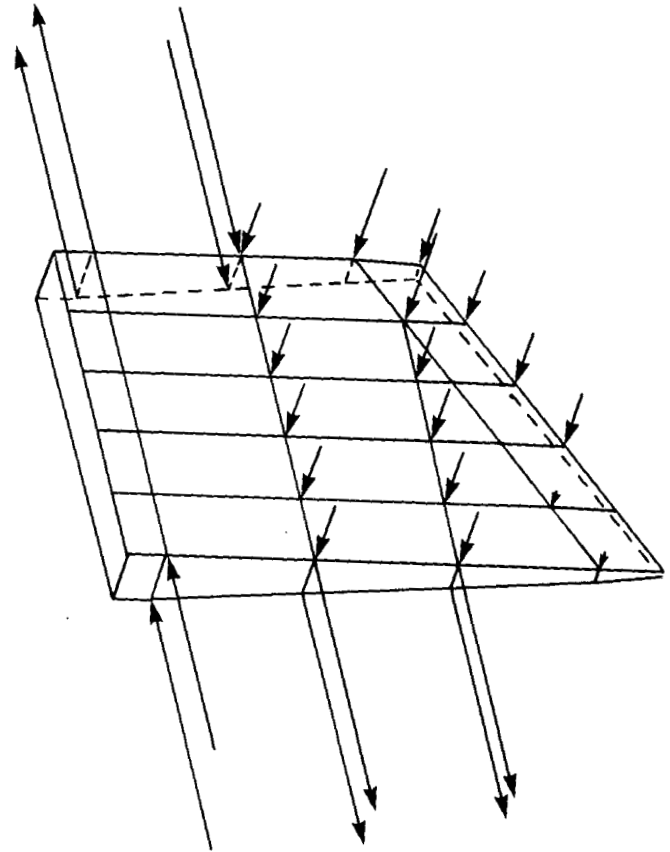
(d) Test 5.

Figure 13. Continued.
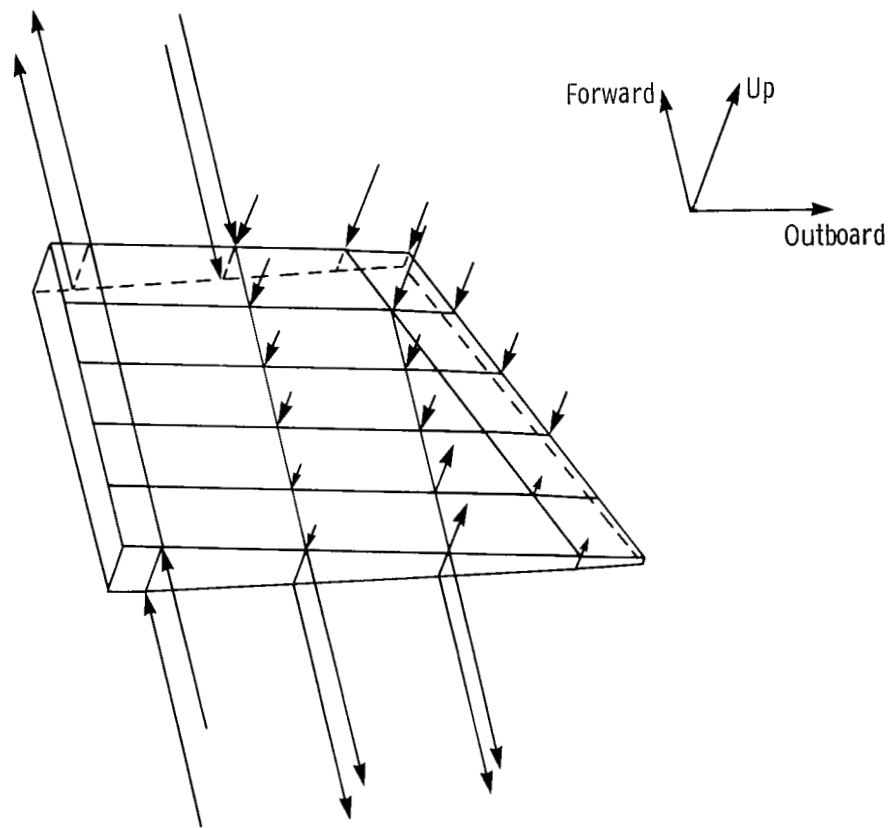
(e) Test 6.

Figure 13. Concluded.
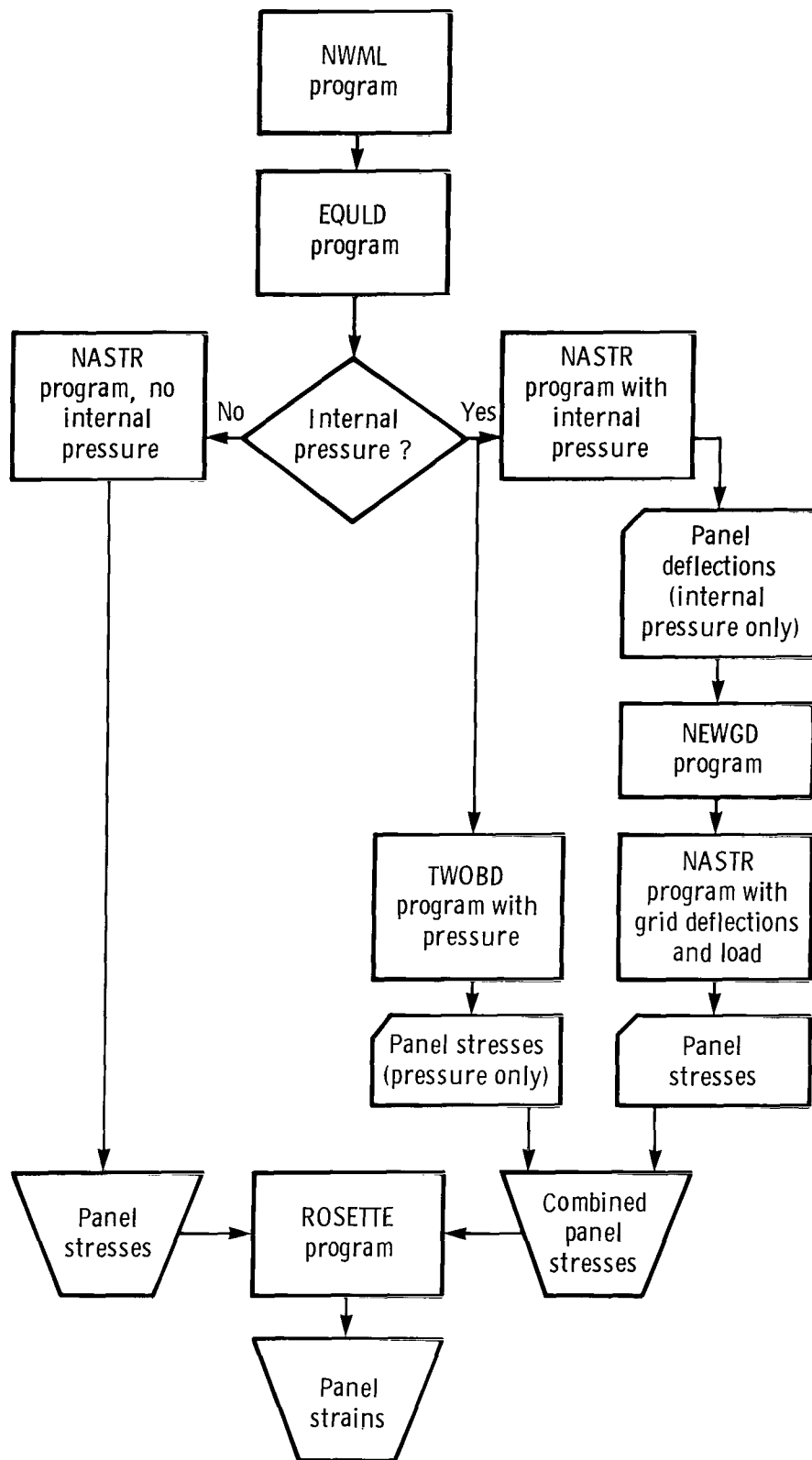
Figure 14. Analysis flow chart.
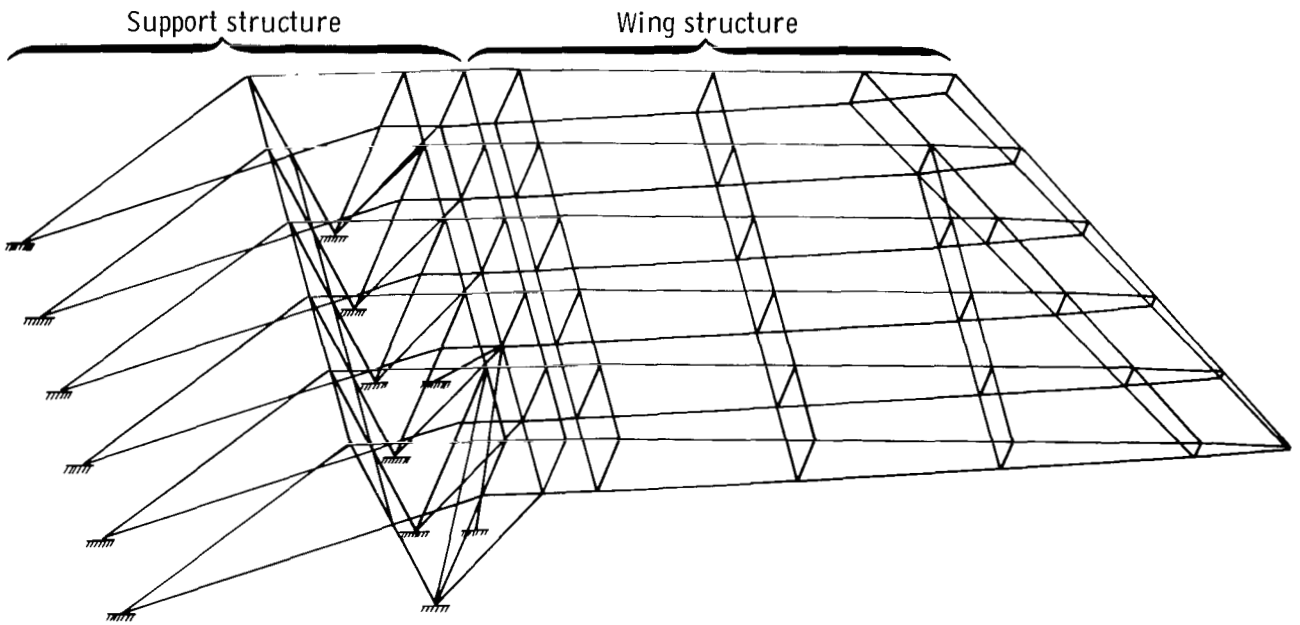
Figure 15. NASTRAN NWML model.
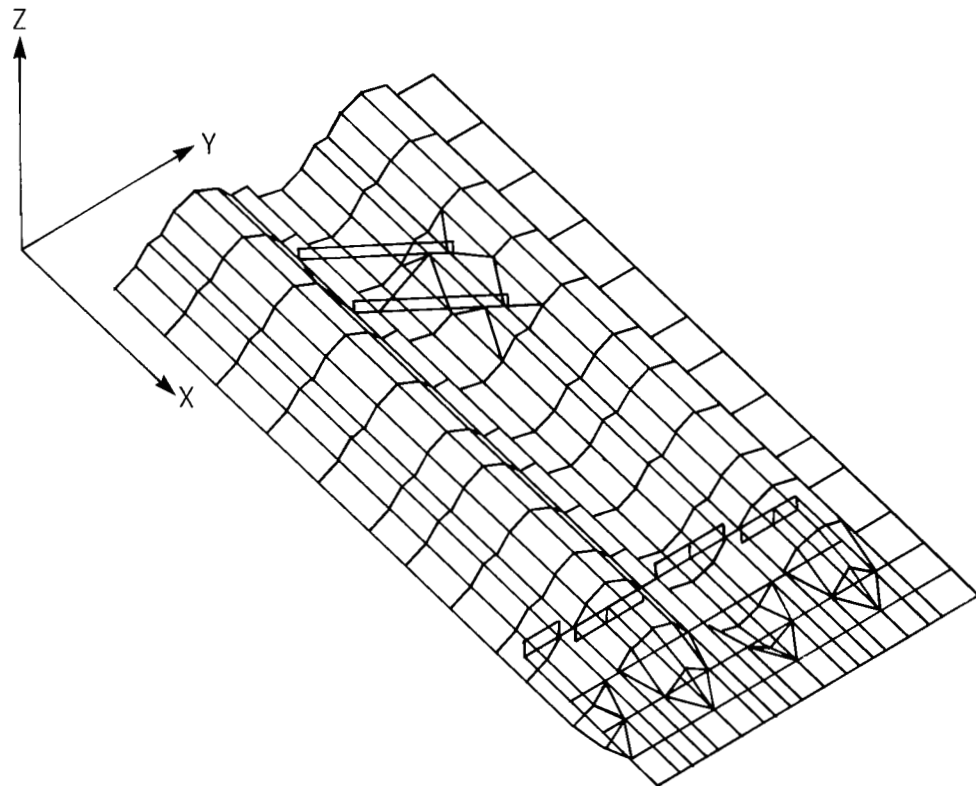
Figure 16. NASTR NASTRAN finite-element computer model.
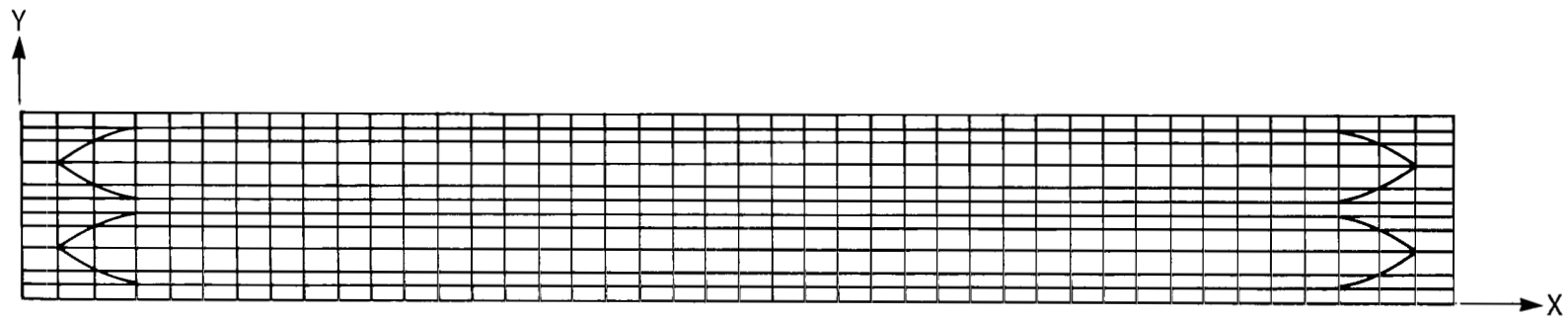
Figure 17. TWOBD NASTRAN finite-element computer model.

Panel number	Ultimate load, N/cm		Margin of safety
	Axial	Shear	
1	-930	-194	0.77
2	-981	-205	0.67
3	-1070	-240	0.50
4	-1166	-301	0.30
5	-1208	-322	0.24
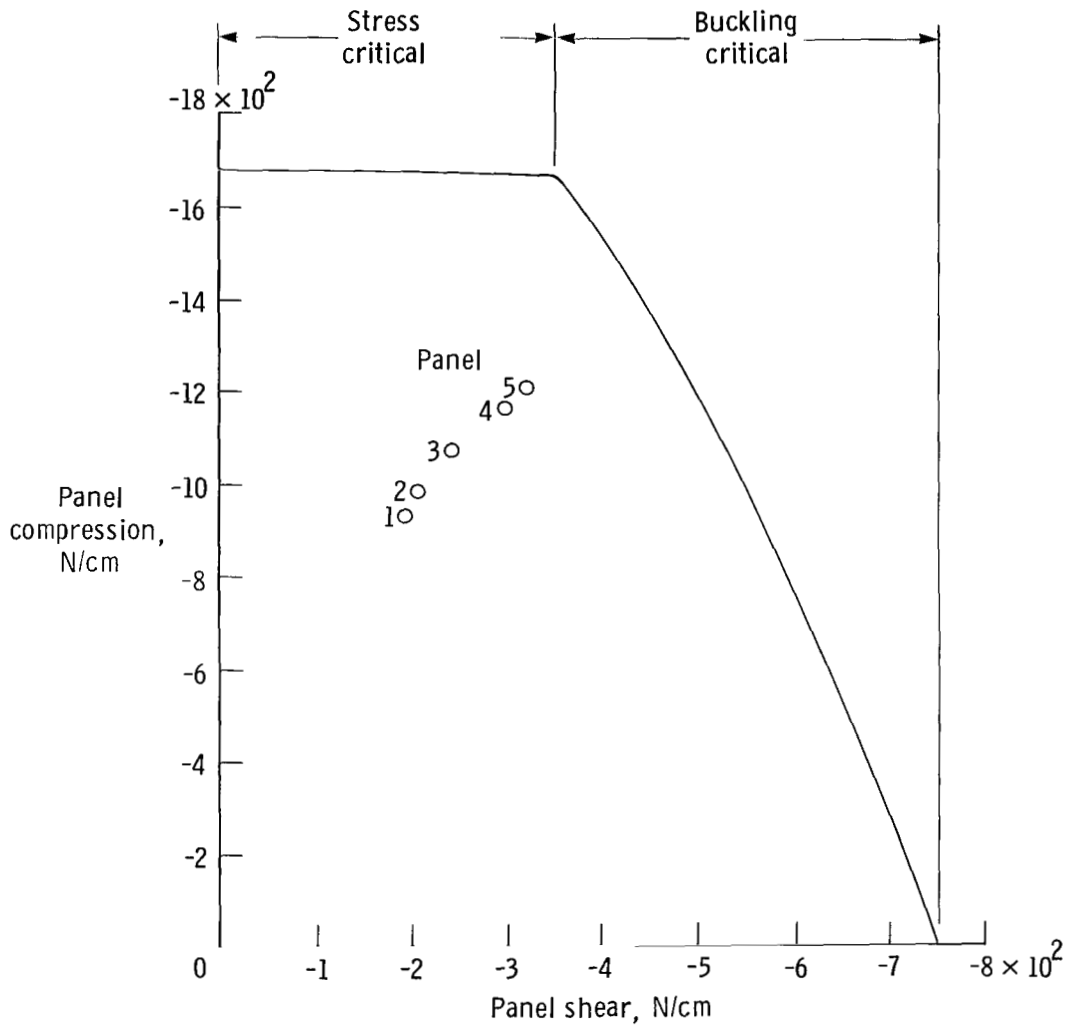
Figure 18. Beaded panel strength interaction curve at 1005 K and 5.2 kN/m² from OPTBEAD program (ref. 5).
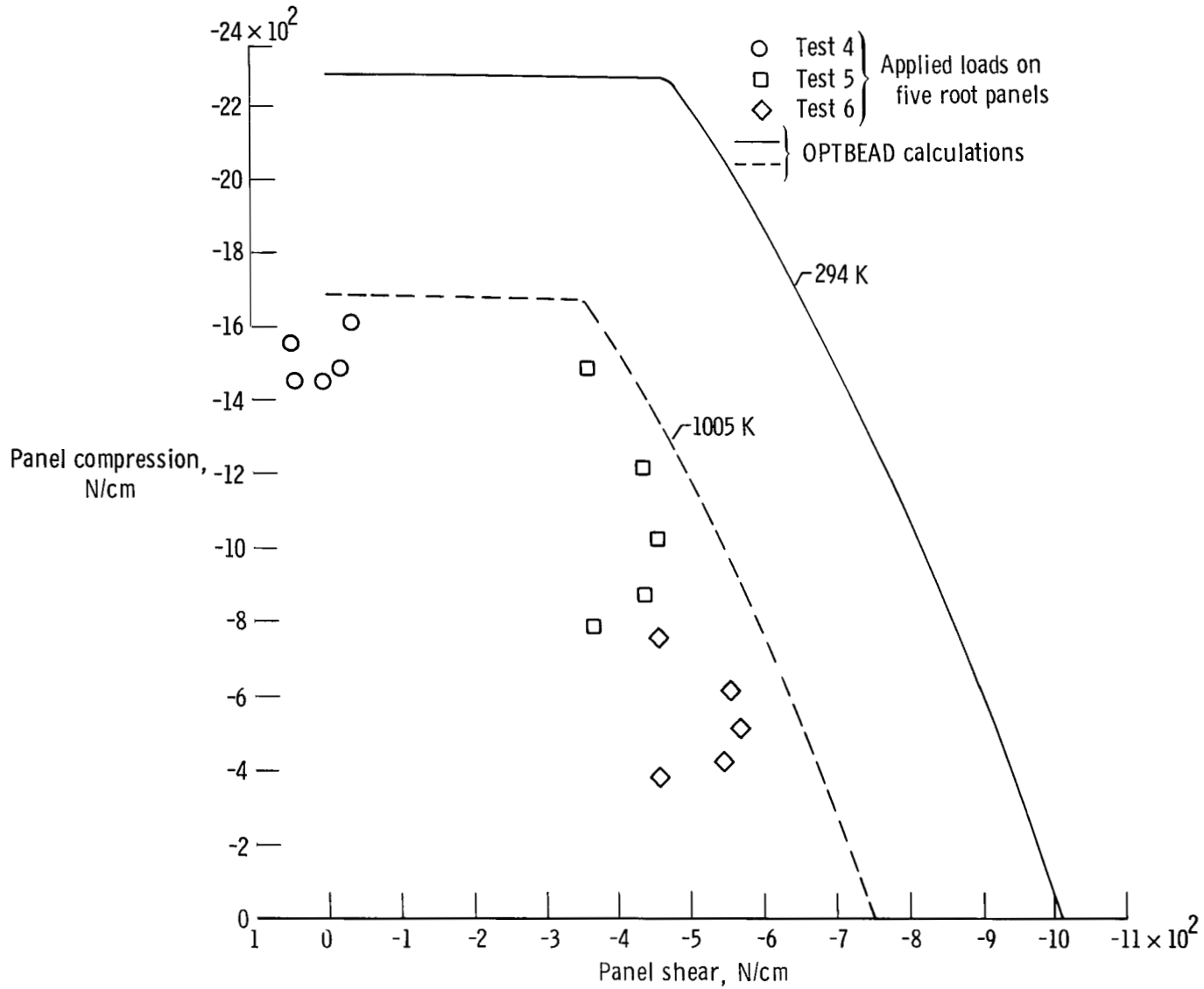
Figure 19. Beaded panel strength interaction curves at 1005 K and 294 K, and room temperature applied panel loads. Data taken at a panel pressure of 5.2 kN/m^2.
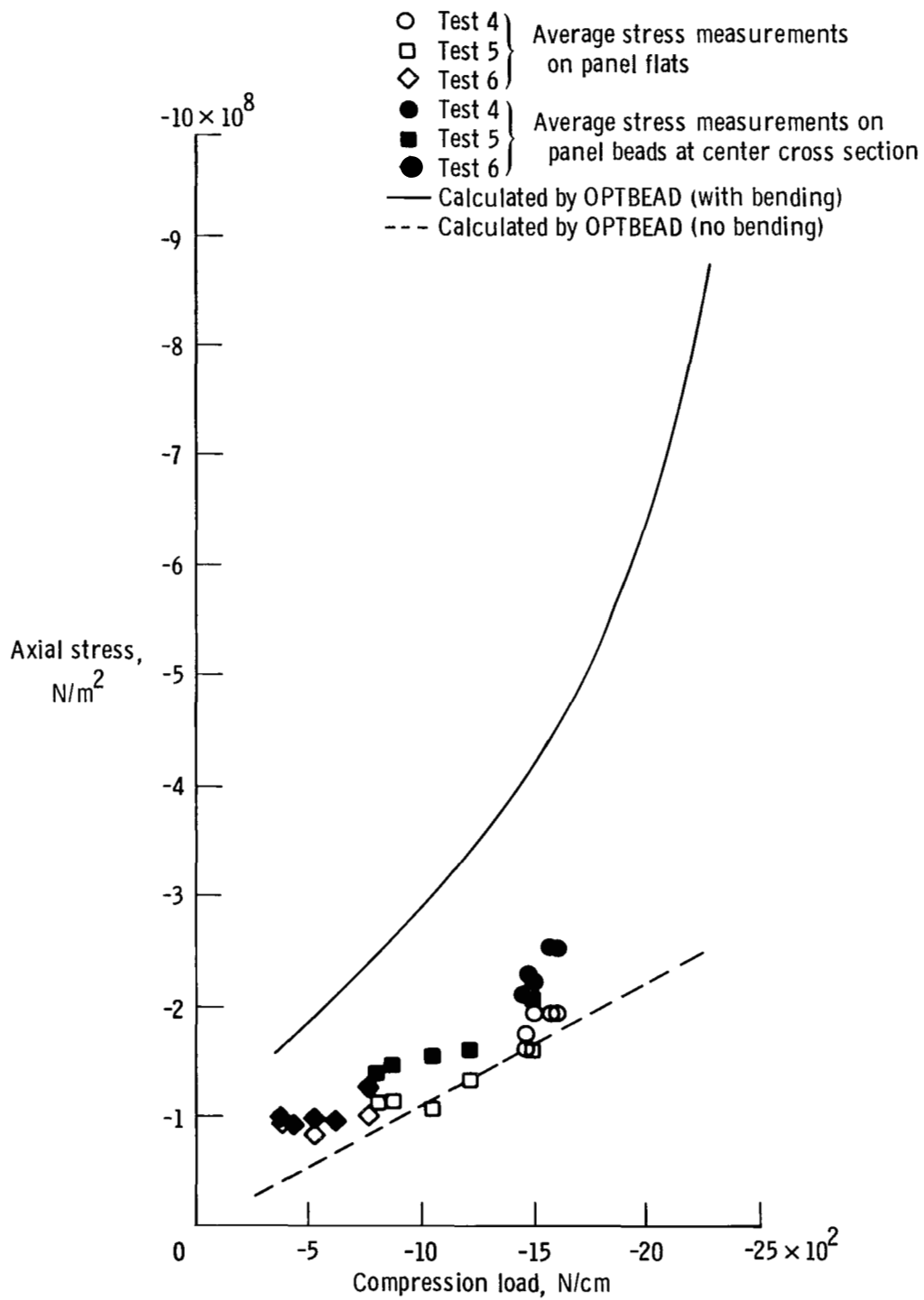
Figure 20. Beaded panel axial stresses as a function of compression load.

40
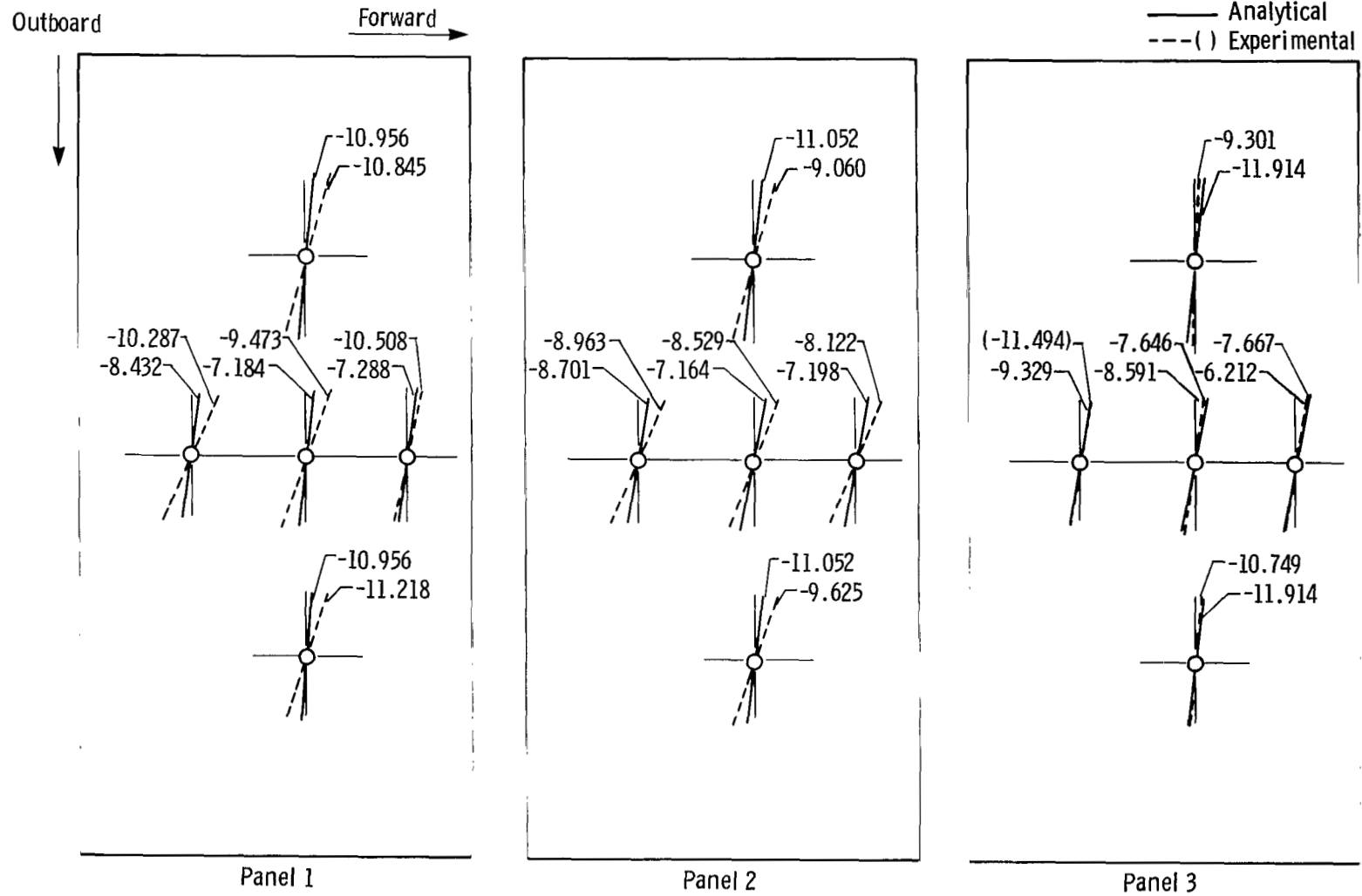
(a) Test 1.

Figure 21. Beaded panel maximum stresses and directions. All units in kN/cm^2

-13.328
-14.224

-12.817
-10.356
-12.873
-8.591
(-13.279)
-8.598

-13.328
-15.017

Panel 4

-16.871
-15.368

-11.756
-16.830
(-14.513)
-10.328
(-13.362)
-10.321
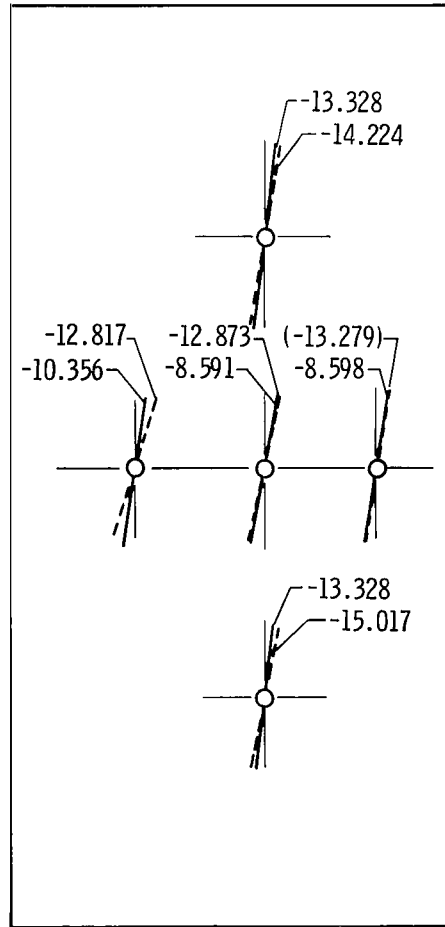
-15.368
-18.064
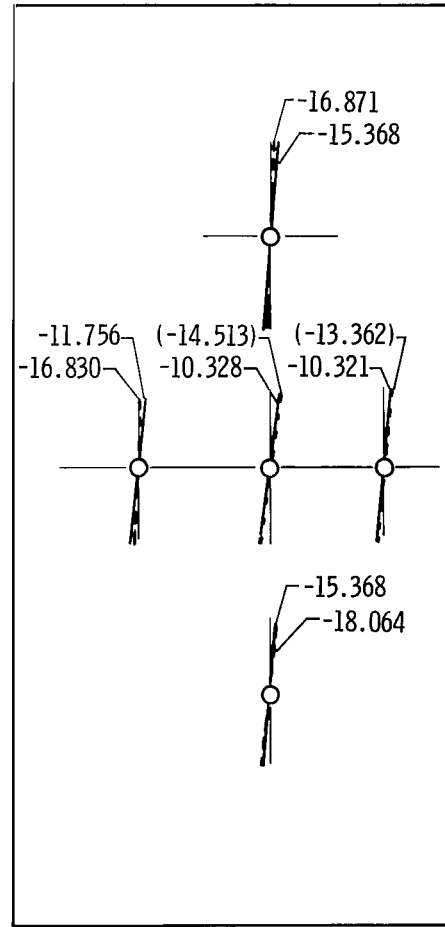
Panel 5

(a) Concluded.

Figure 21.   Continued.

Outboard

Forward

——— Analytical

––– ( ) Experimental

-13.665
-12.666

-12.528
-11.080

-11.563
-8.301

-14.058
-8.287

-13.665
-13.900

Panel 1

-12.224
-10.583

-11.128
-10.066

-10.397
-7.267

-10.246
-7.246

-12.224
-11.363

Panel 2

-9.577
-12.093

-12.314
-10.046

-7.226
-9.432

-7.260
(-8.170)

-12.093
-12.286
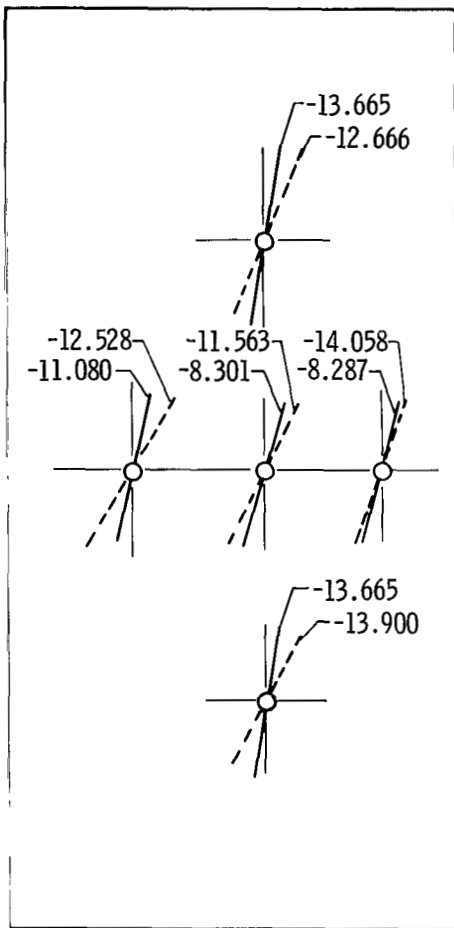
Panel 3

(b) Test 2.

Figure 21. Continued.
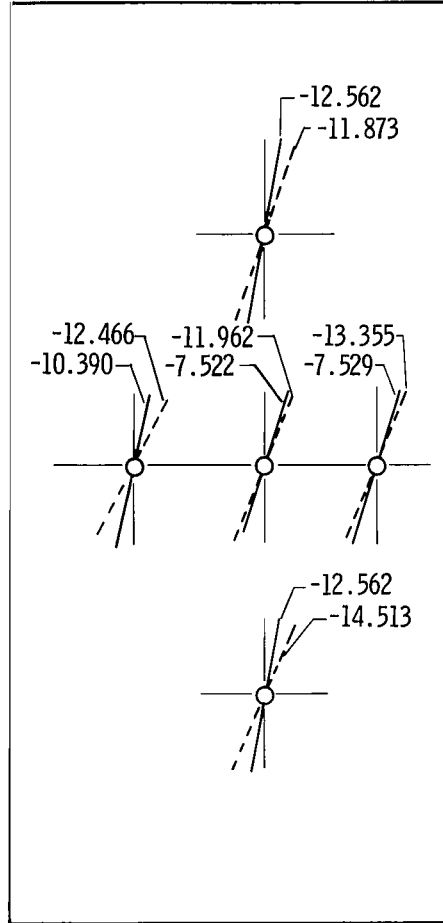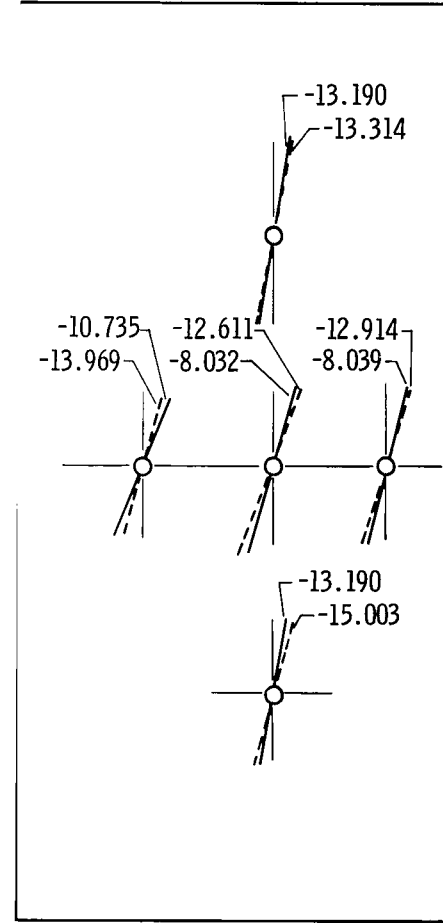
Panel 4

Panel 5

(b) Concluded.

Figure 21. Continued.

Outboard

Forward →

—— Analytical
---( ) Experimental

-13.679
-12.369

-10.983- -11.218- -7.419-
-11.466- -8.301- -15.644-

-13.679
-12.767

Panel 1

-12.252
-9.349

-8.536- -9.653- -12.038-
-10.418- -7.295- -6.447-

-12.252
-10.004

Panel 2

-8.667
-12.135

-10.535- -7.253- -6.460-
-10.397- -8.749- -8.639-

-12.135
-10.928
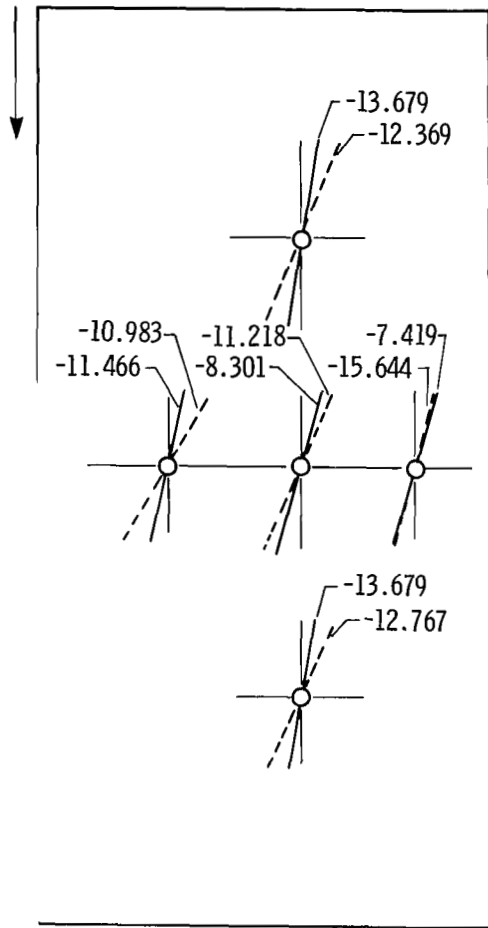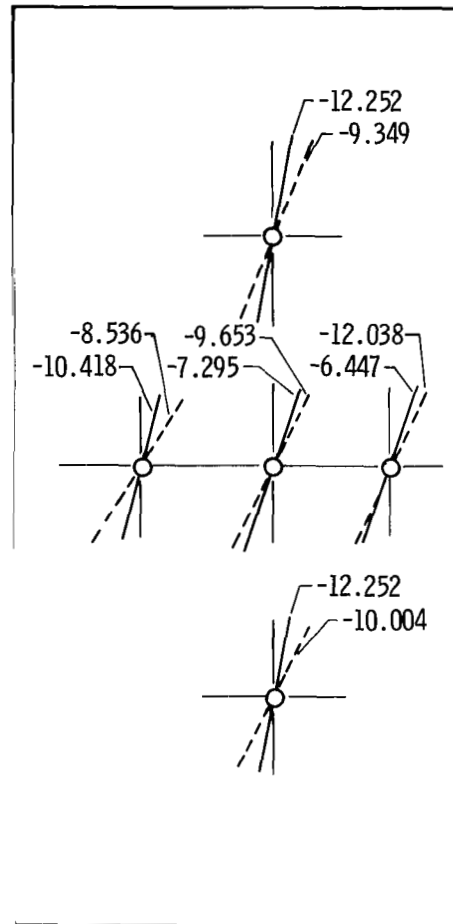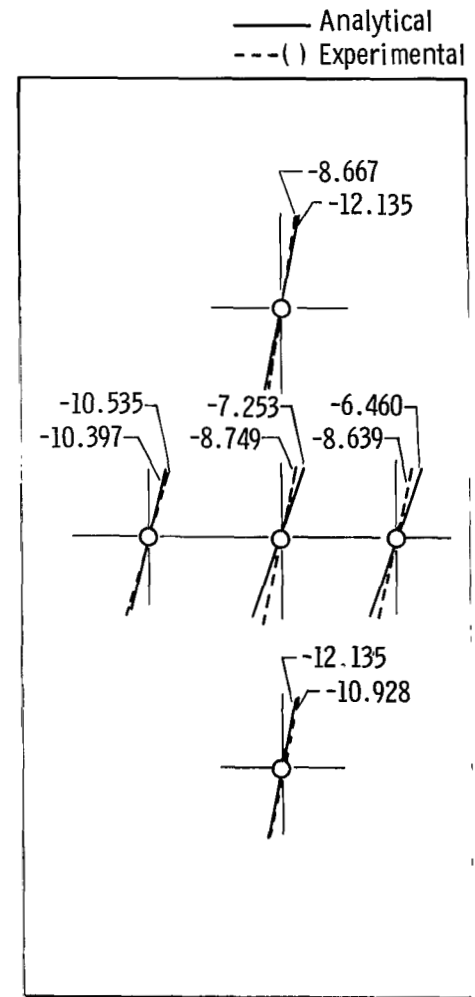
Panel 3

(c) Test 3.

Figure 21. Continued.
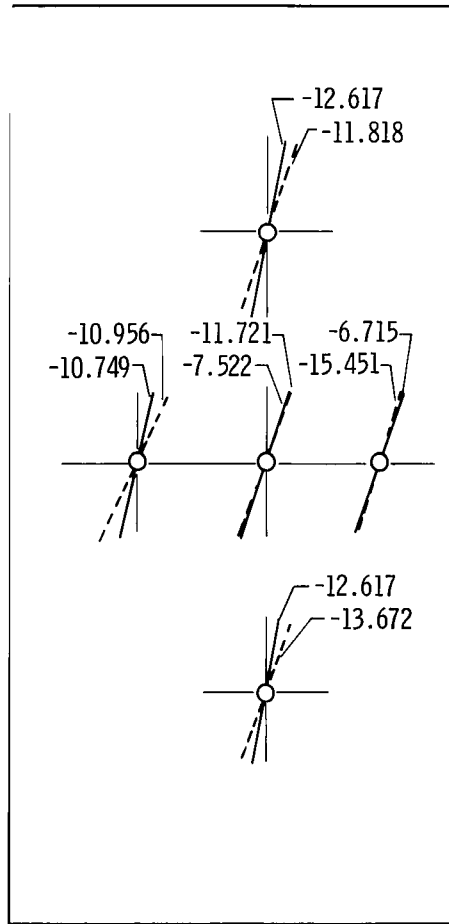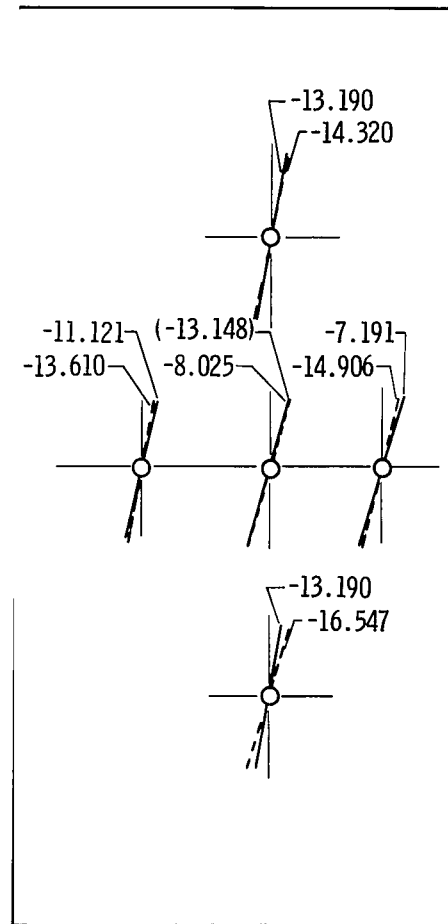
Panel 4

Panel 5

(c) Concluded.

Figure 21. Continued.

Outboard

Forward

—— Analytical
- - -( ) Experimental

-19.402
-21.643

-15.120┐ -17.133┐ -13.245┐
-15.320┐ -14.341┐ -24.621┐

(-18.244)
-19.402

Panel 1

-18.064
-19.953

-16.189┐ -13.417┐ (-17.533)┐
-14.320┐ (-17.016)┐ -12.383┐

-18.064
-17.582

Panel 2

-17.444
-18.009

-14.155┐ -13.652┐ -12.562┐
(-16.416)┐ -15.203┐ -14.969┐

-16.272
-18.009
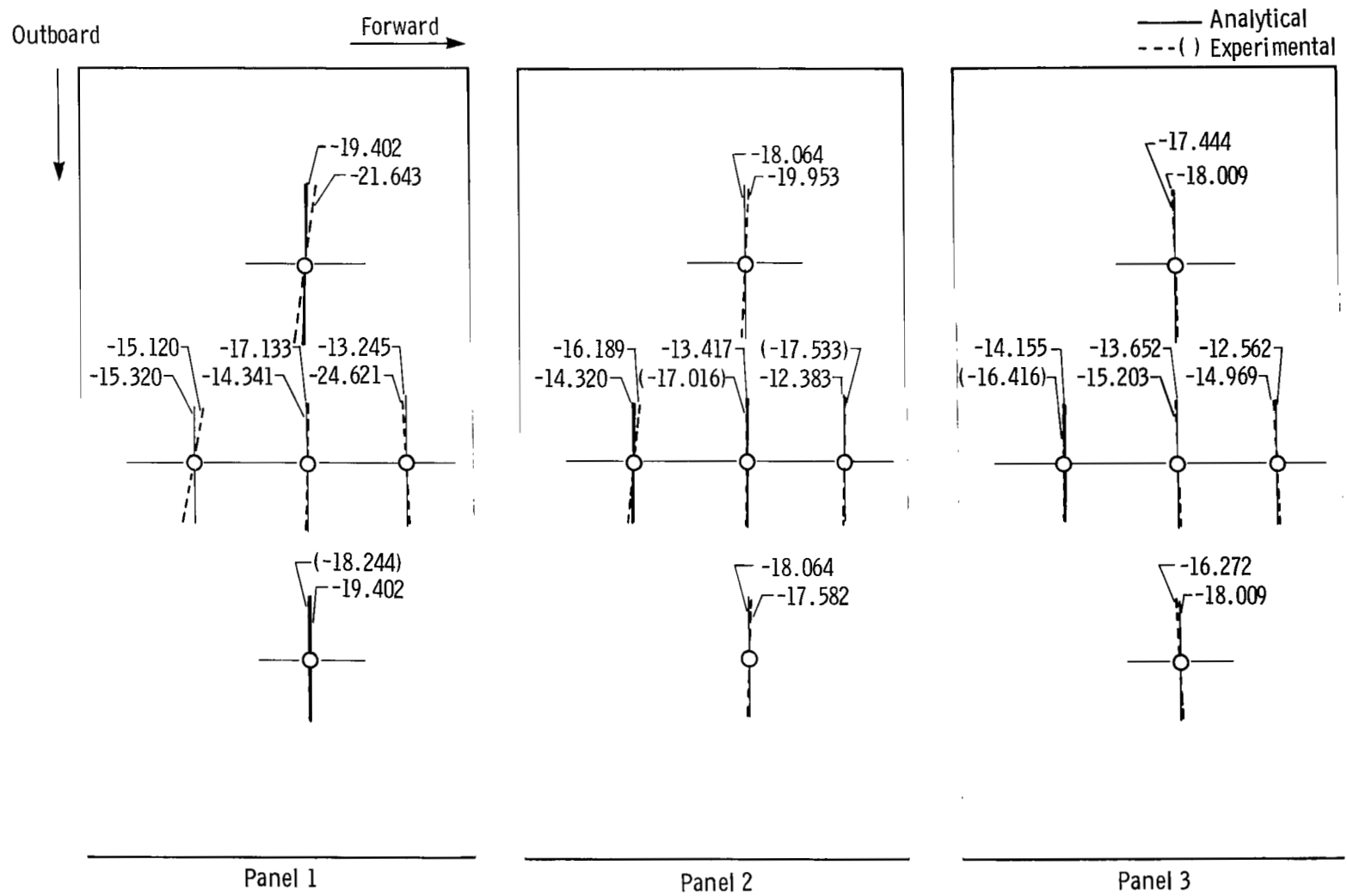
Panel 3

(d) Test 4.

Figure 21. Continued.
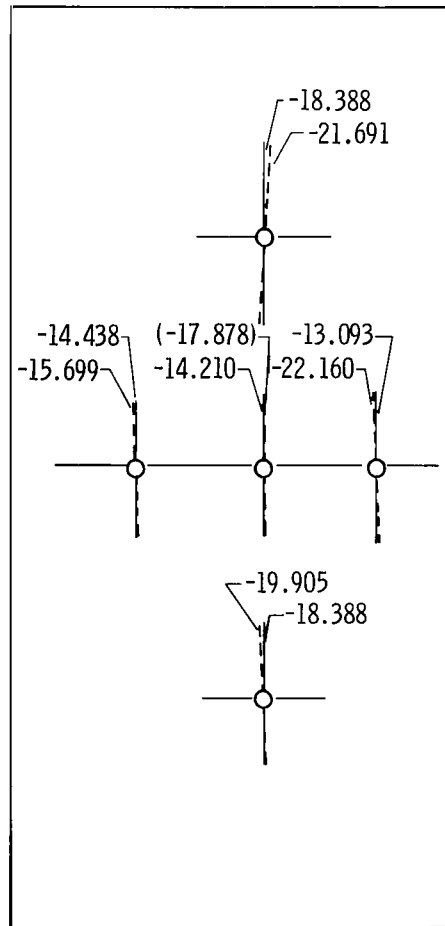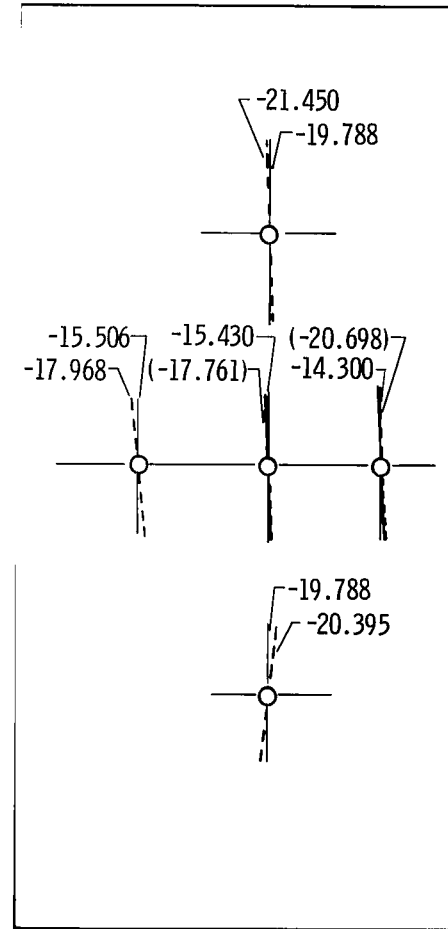
Panel 4   Panel 5

(d) Concluded.

Figure 21. Continued.

Outboard

Forward →

—— Analytical
———— Experimental

-12.611
-9.618

-10.742
-9.584
-11.390
-10.128
-8.749
-15.155

-7.888
-9.618

Panel 1

-12.900
-11.121

-9.377
-10.570
-12.948
-11.225
-11.769
-13.004

-8.901
-11.121

Panel 2

-13.417
-13.004

-11.080
-10.680
-14.314
-10.632
-13.217
-11.714

-6.791
-13.004
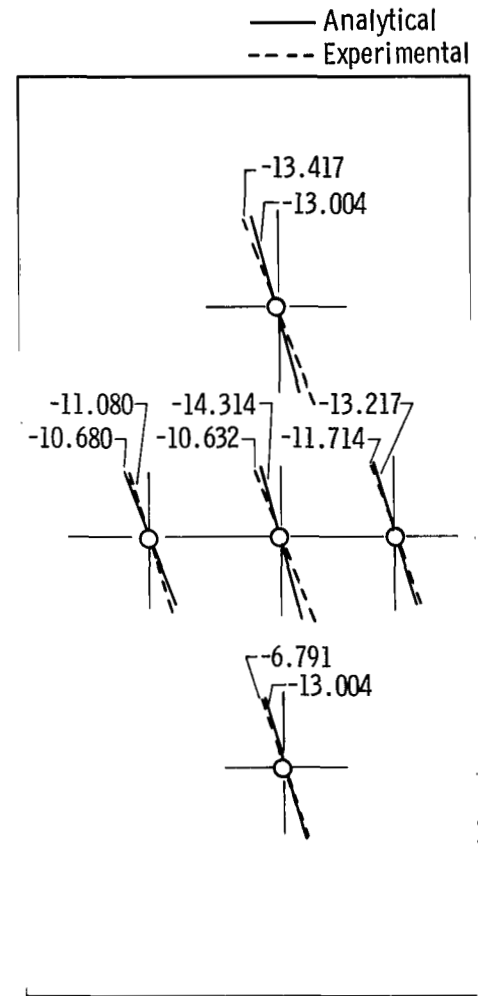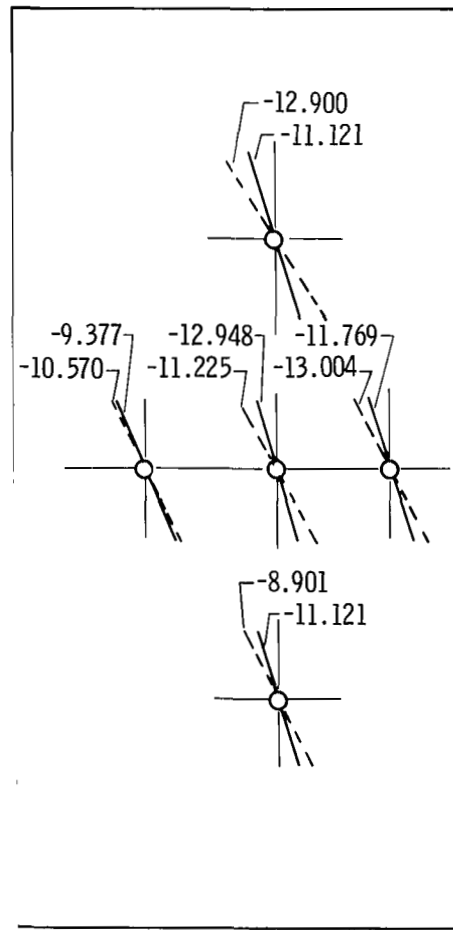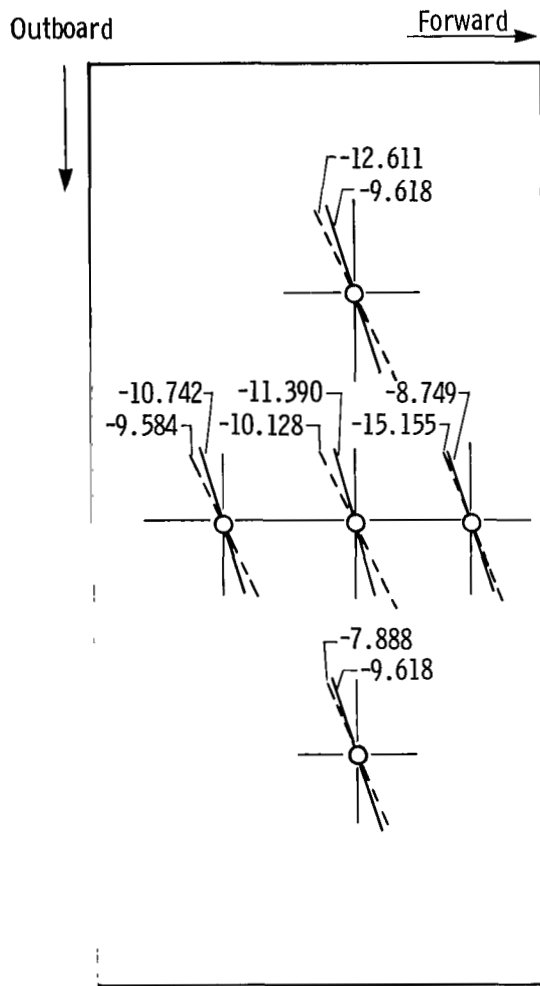
Panel 3

(e) Test 5.

Figure 21. Continued.
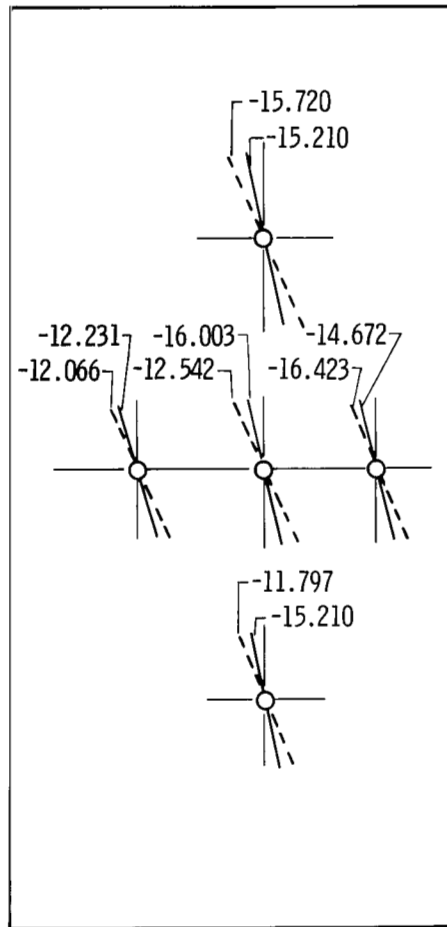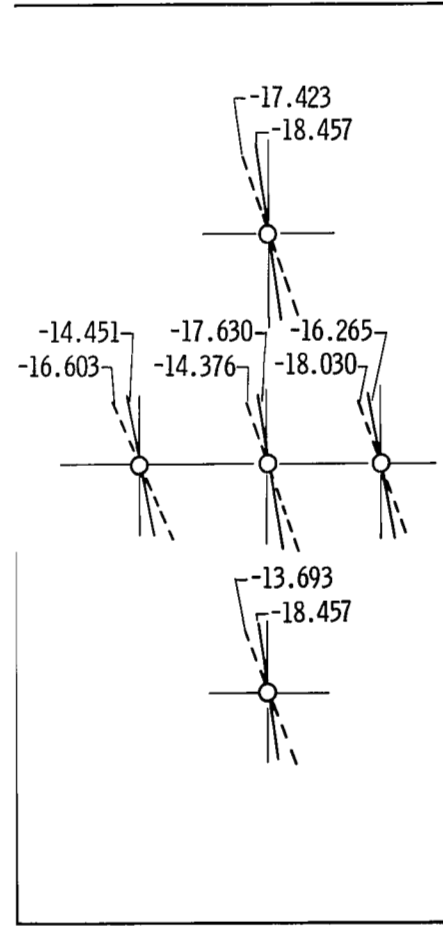
Panel 4

Panel 5

(e) Concluded.

Figure 21. Continued.

Outboard

Forward →

—— Analytical
---( ) Experimental

Panel 1

-10.783
-5.805

(-8.315)⌐   -8.922⌐   -7.963⌐
-5.950⌐   -9.053⌐   -13.479⌐

-5.805
(-5.240)

Panel 2

-11.211
-6.943

-7.019⌐   -10.611⌐   -9.480⌐
(-8.722)⌐   -9.342⌐   -12.197⌐

-5.736
-6.943

Panel 3

-11.762
-7.963

-8.412⌐   -11.673⌐   -10.521⌐
-7.791⌐   -8.729⌐   -10.384⌐

-7.963
-2.903
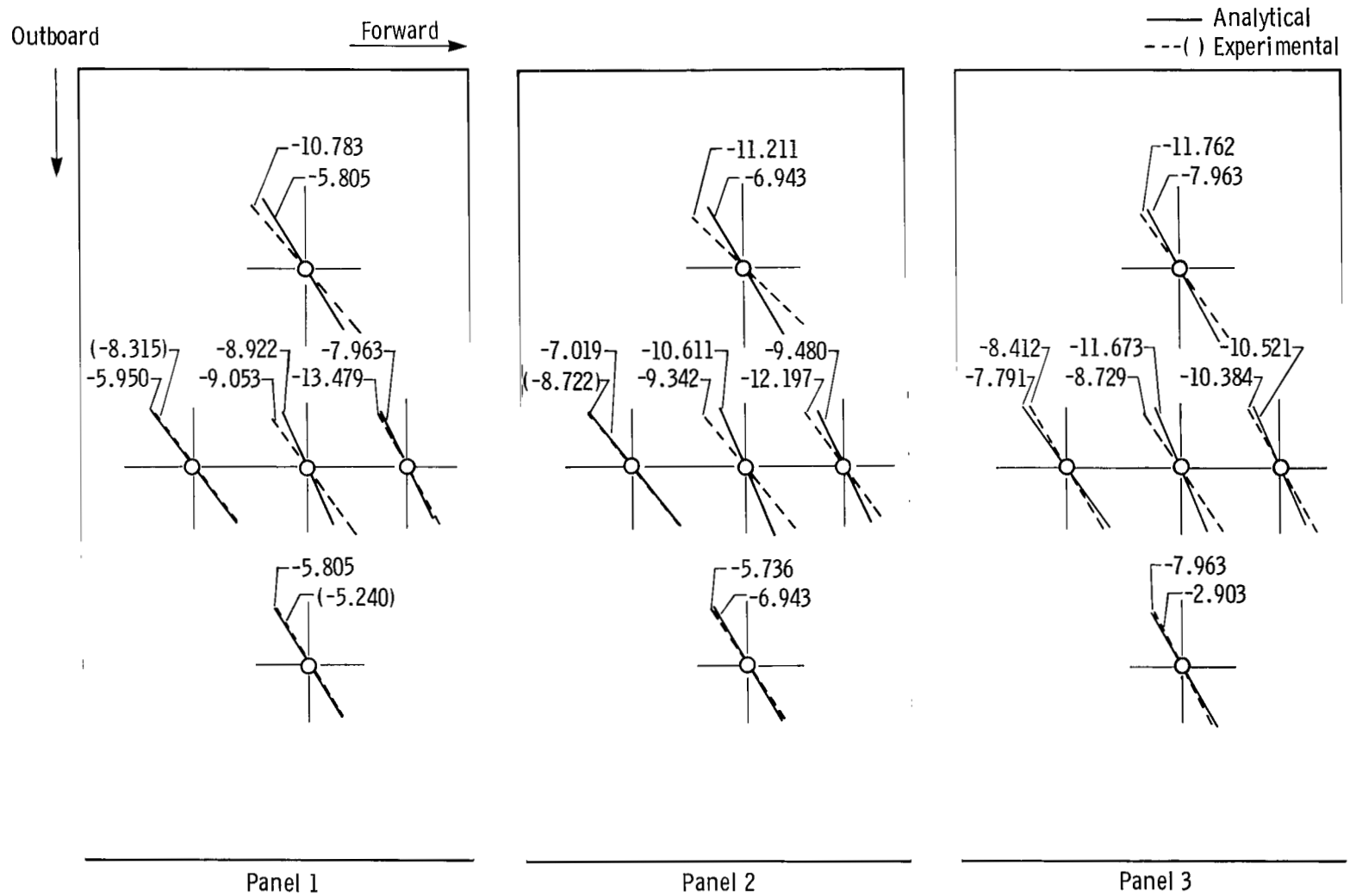
(f) Test 6.

Figure 21. Continued.
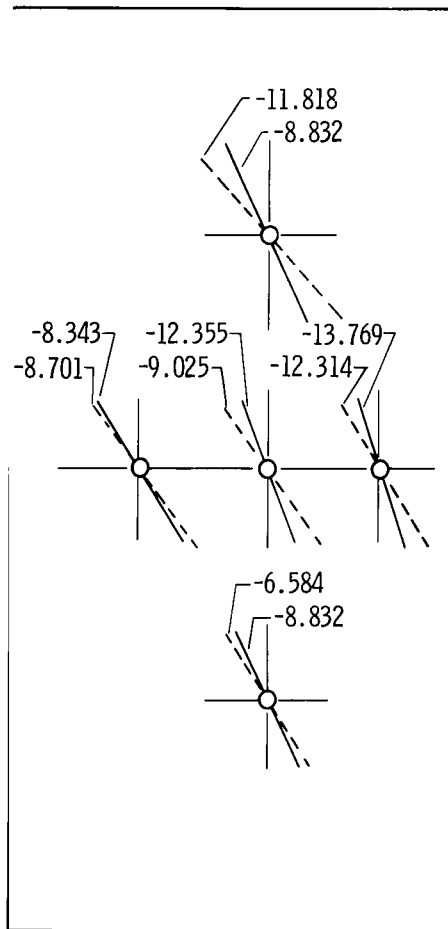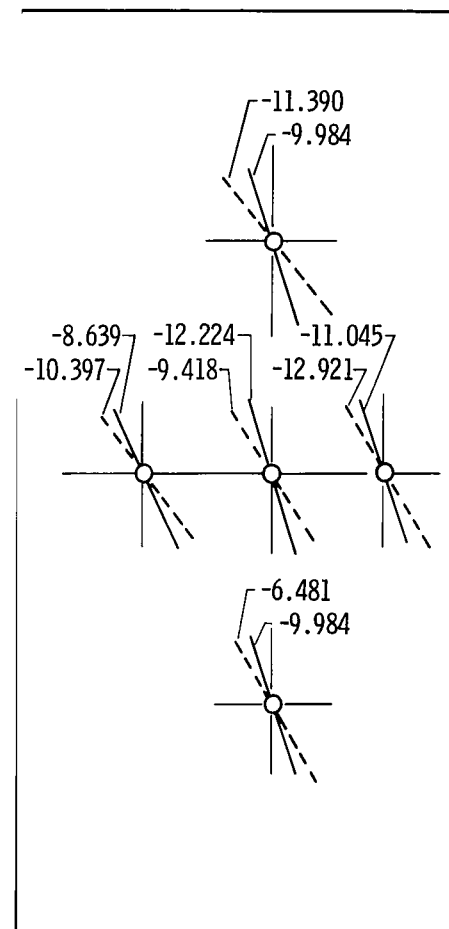
Panel 4   Panel 5

(f) Concluded.

Figure 21. Concluded.
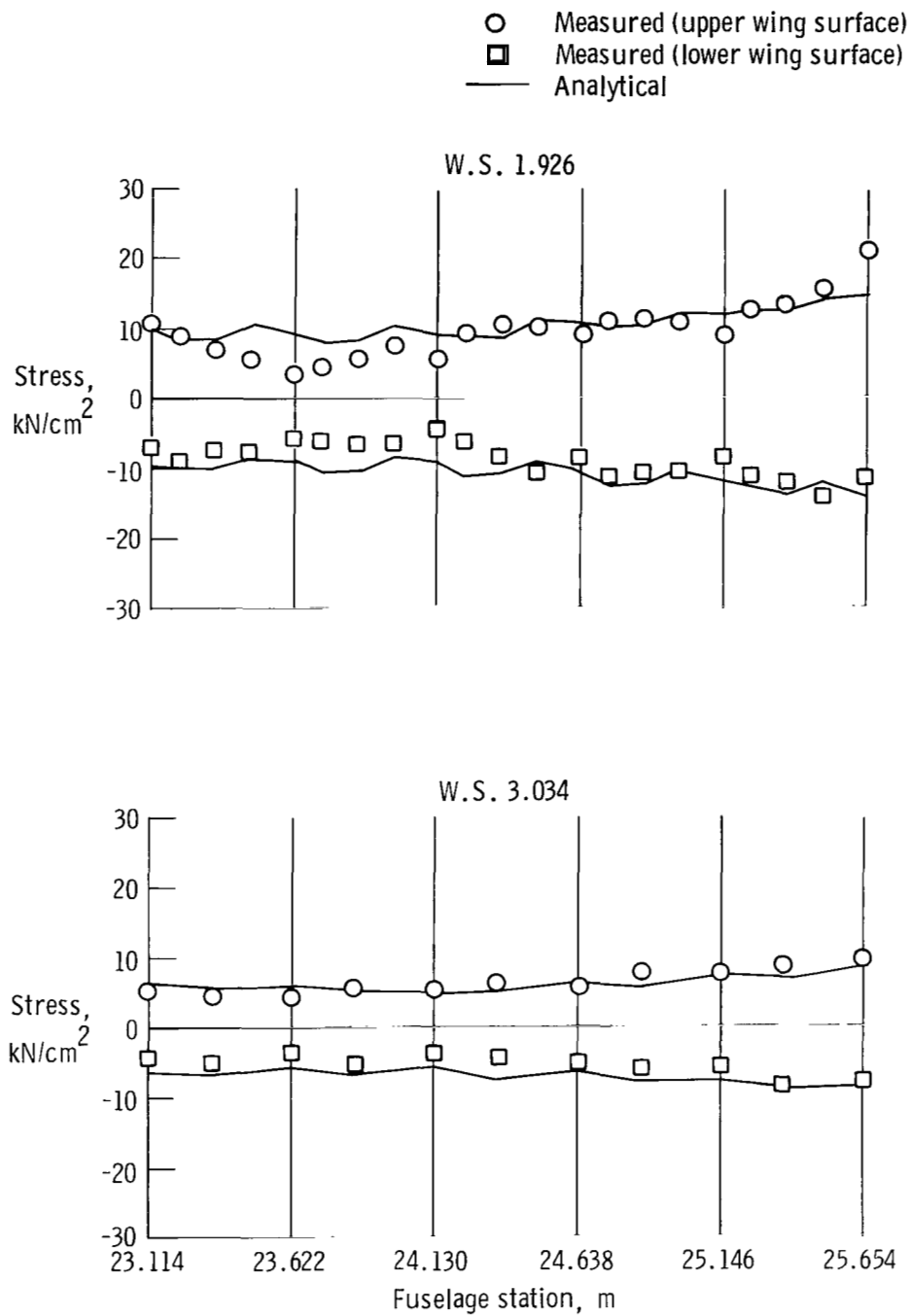
*Figure 22. Measured and analytical stresses at
W.S. 1.926 and W.S. 3.034 due to various load
conditions at room temperature; all vertical lines
(including Y-axis) denote spar locations.*
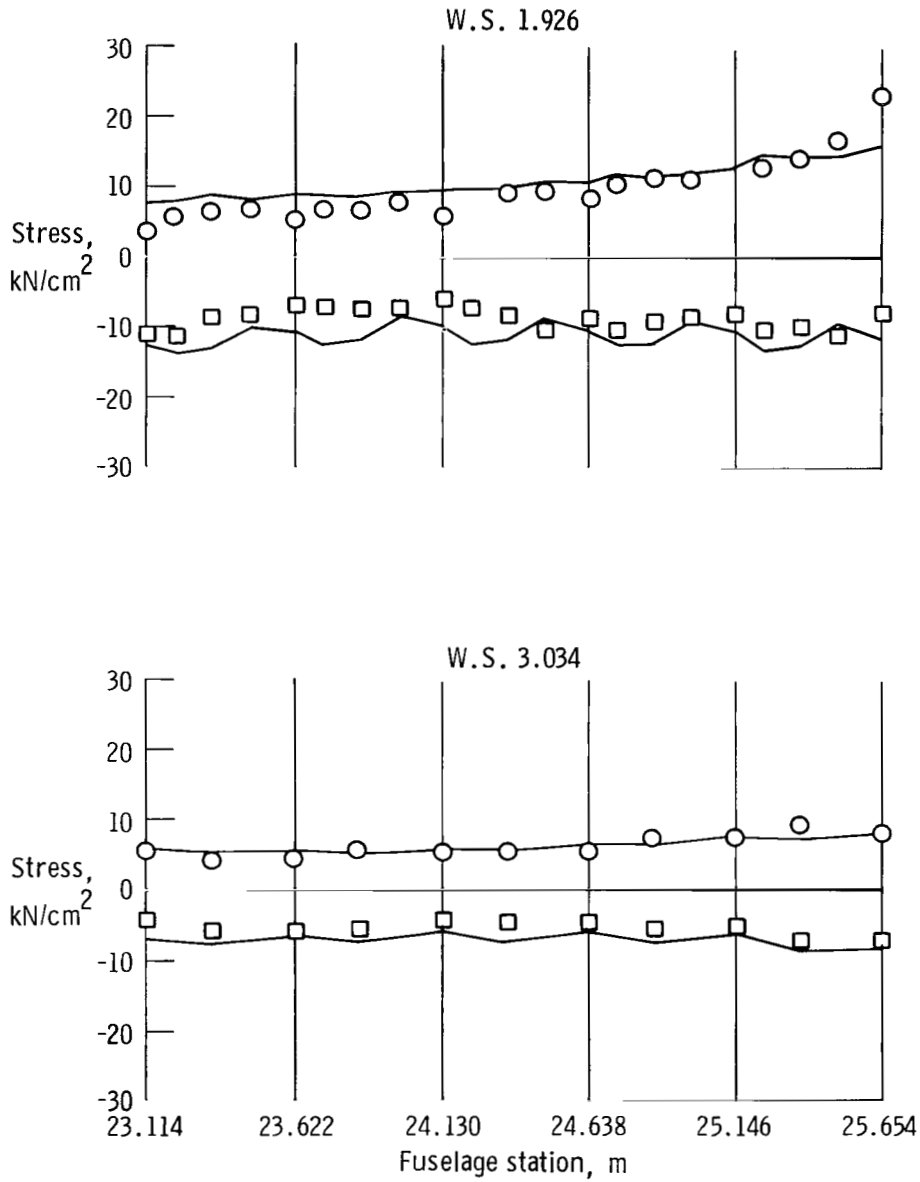
Figure 22. Continued.

(b) Test 2.
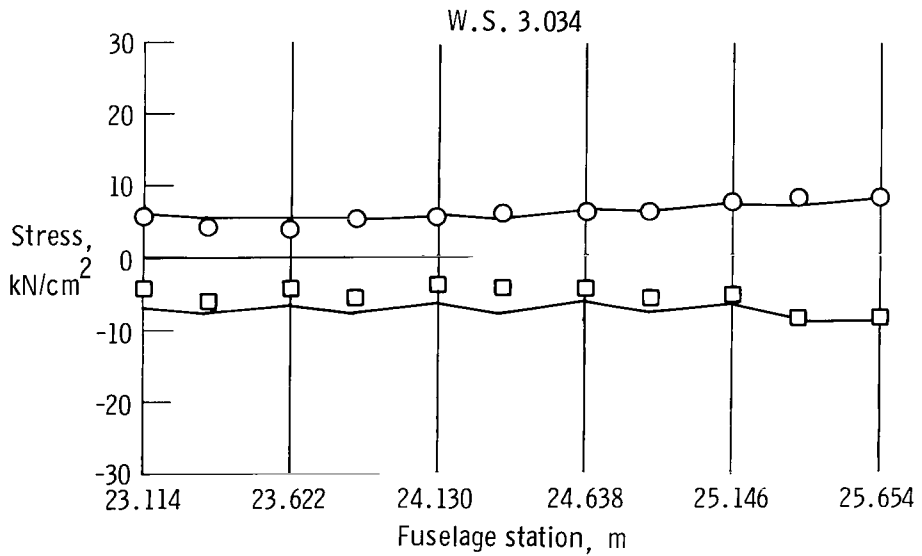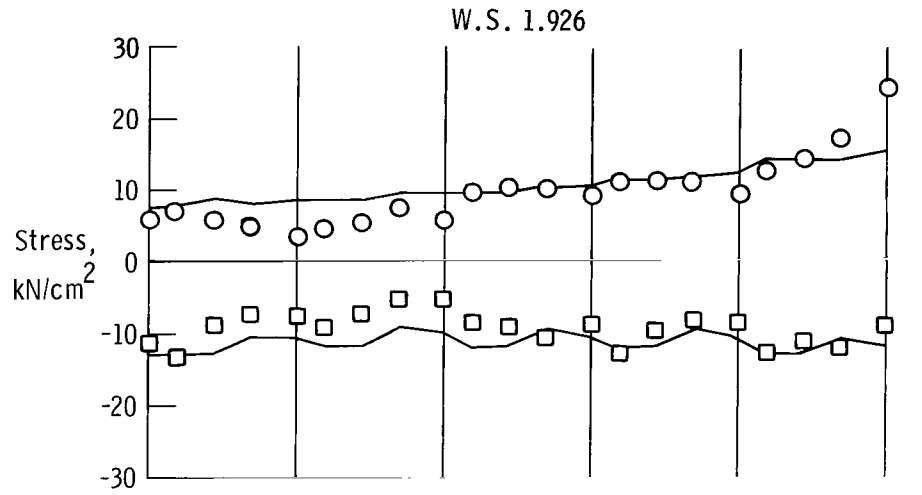
(c) Test 3.

Figure 22. Continued.
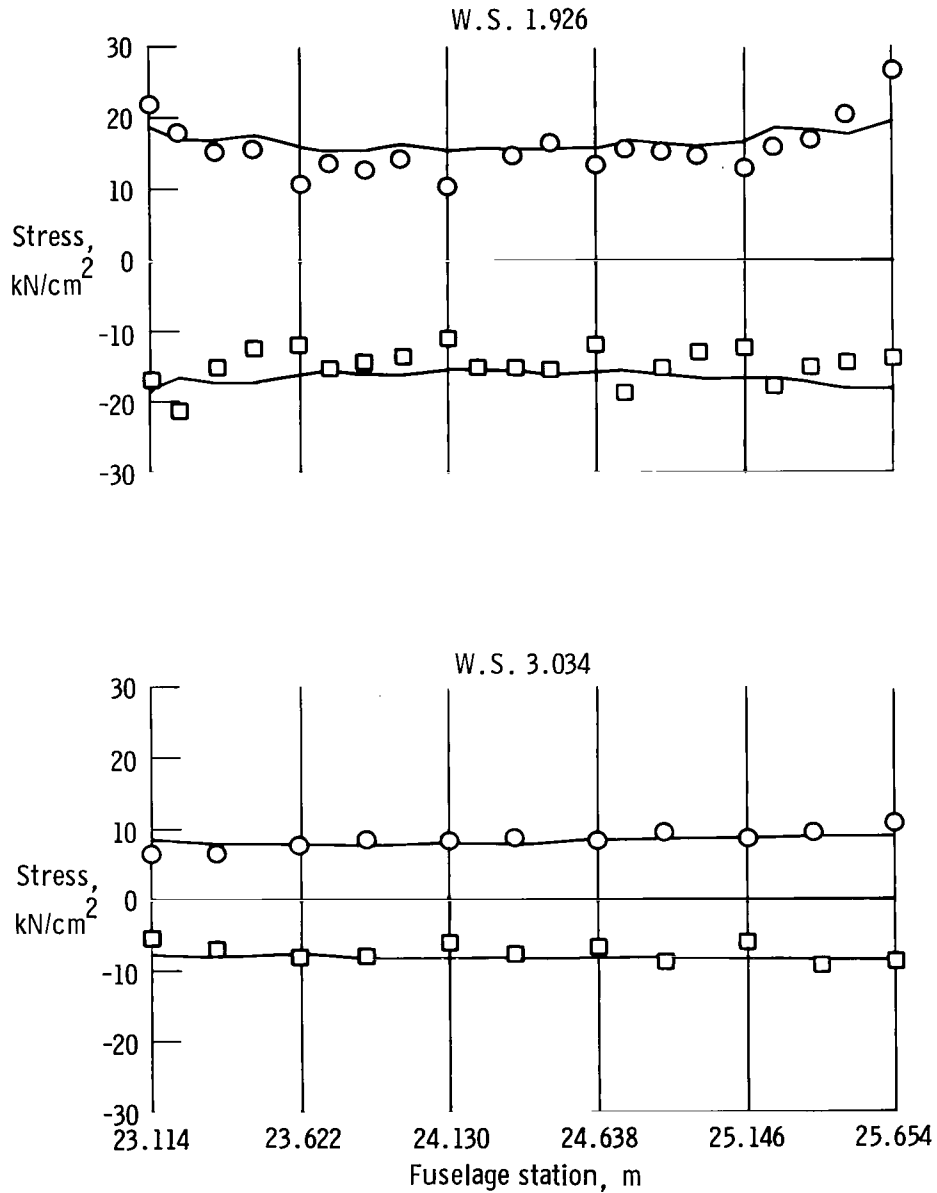
(d) Test 4.

Figure 22. Continued.

O   Measured (upper wing surface)
□   Measured (lower wing surface)
───── Analytical

W.S. 1.926

W.S. 3.034
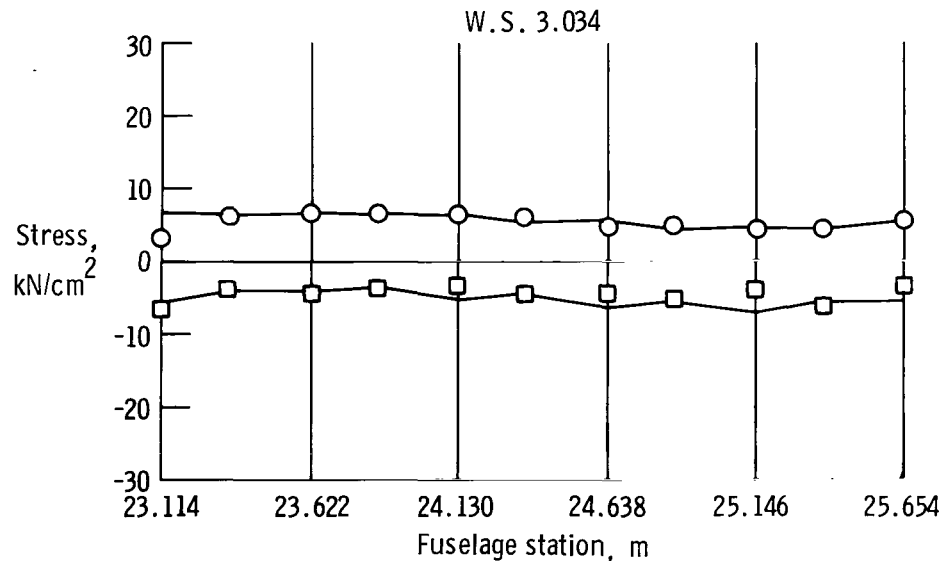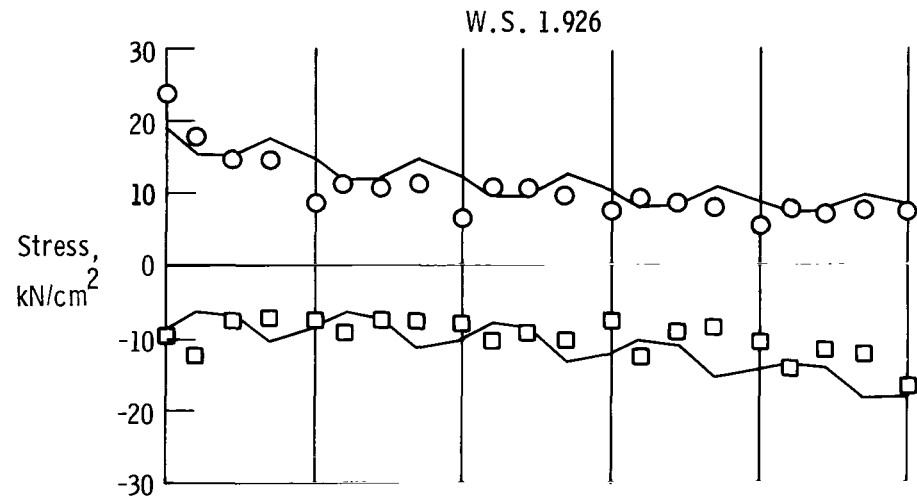
(e) Test 5.

Figure 22. Continued.

Figure legend:
O Measured (upper wing surface)
□ Measured (lower wing surface)
—— Analytical

W.S. 1.926

W.S. 3.034

Fuselage station, m
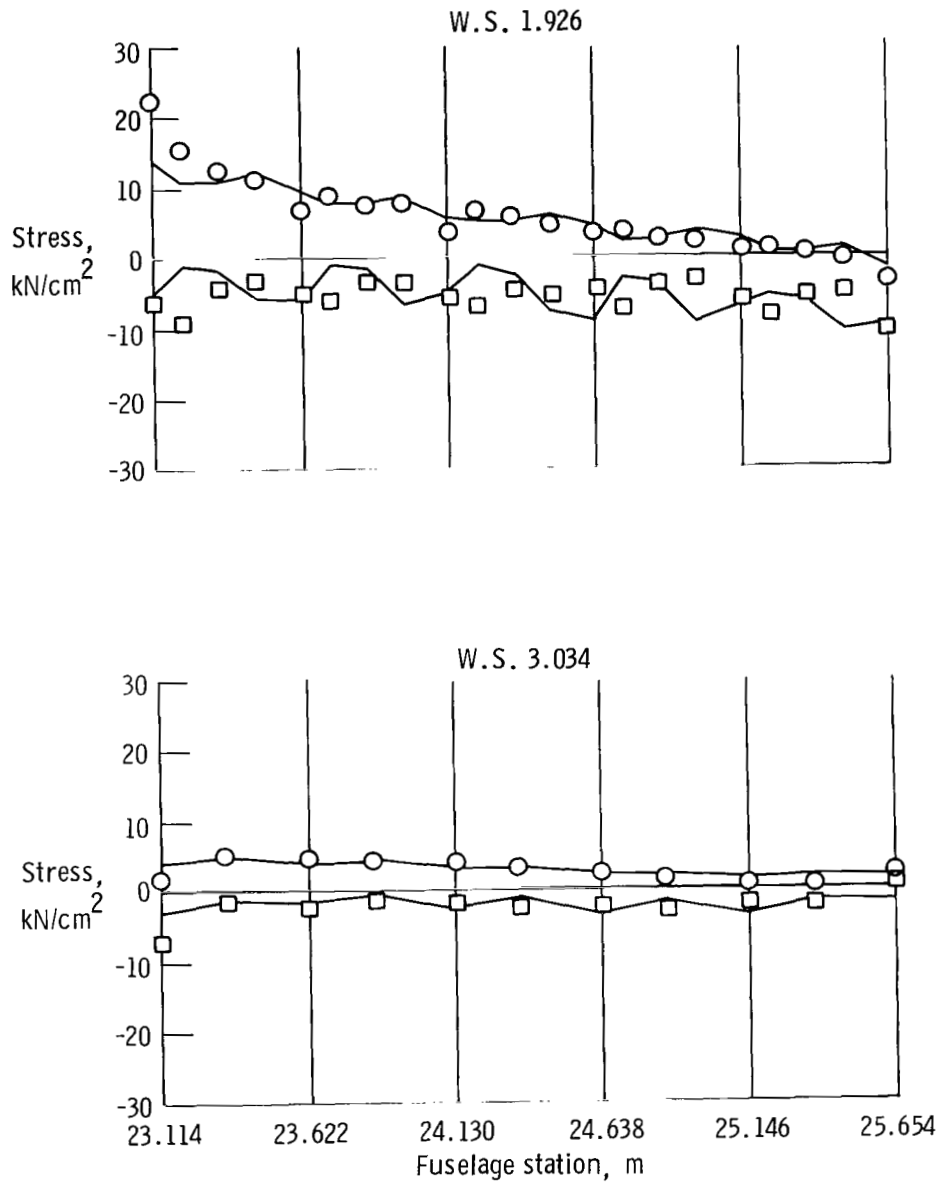
(f) Test 6.

Figure 22. Concluded.
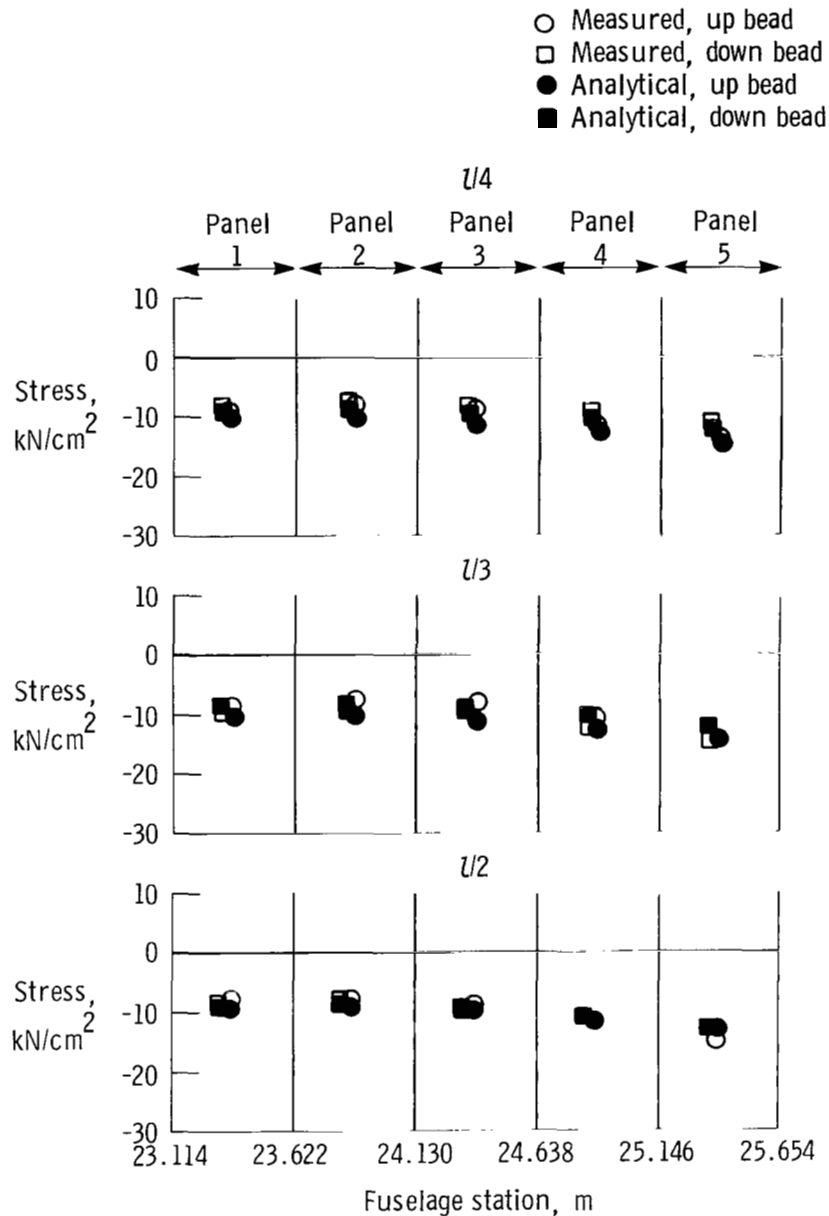
(a) Test 1.

Figure 23. Measured and analytical stresses on beads of lower surface root panels; all vertical lines (including Y-axis) denote spar locations.

Legend:
- O Measured, up bead
- □ Measured, down bead
- ● Analytical, up bead
- ◖ Analytical, down bead
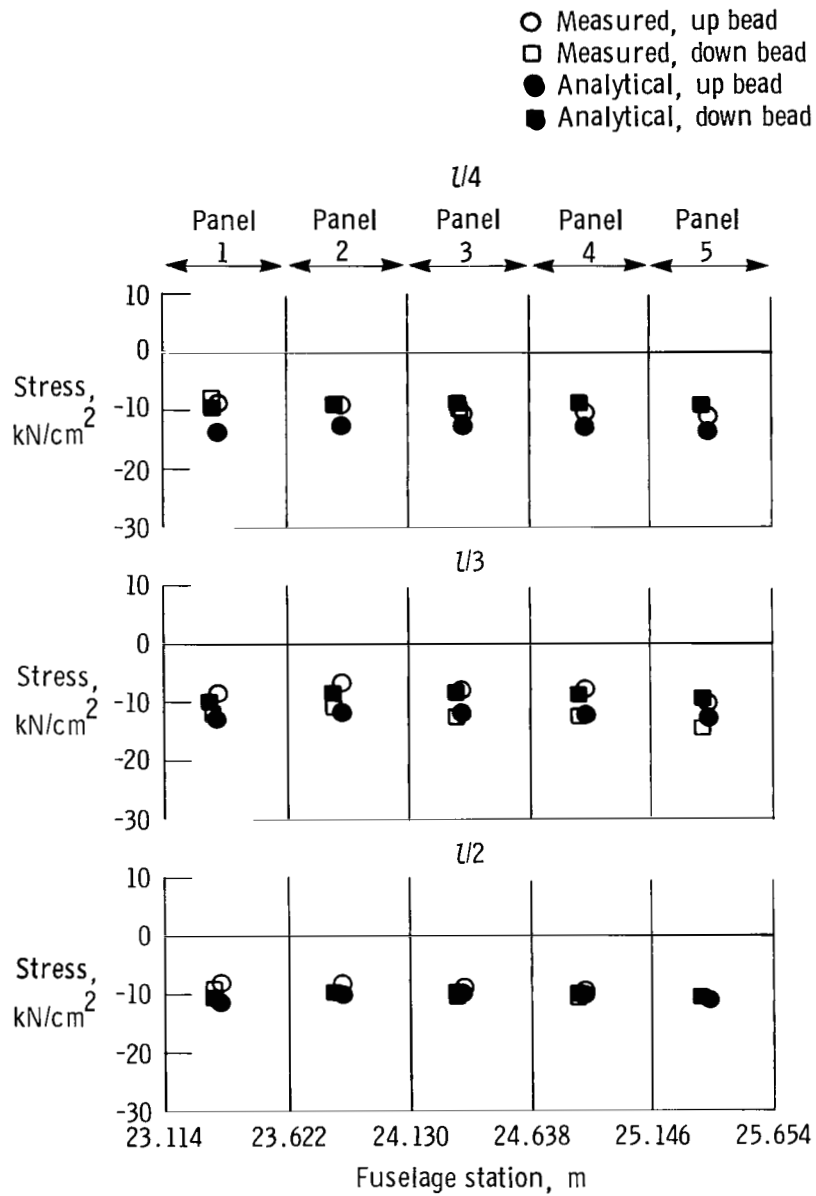
(b) Test 2.

Figure 23. Continued.
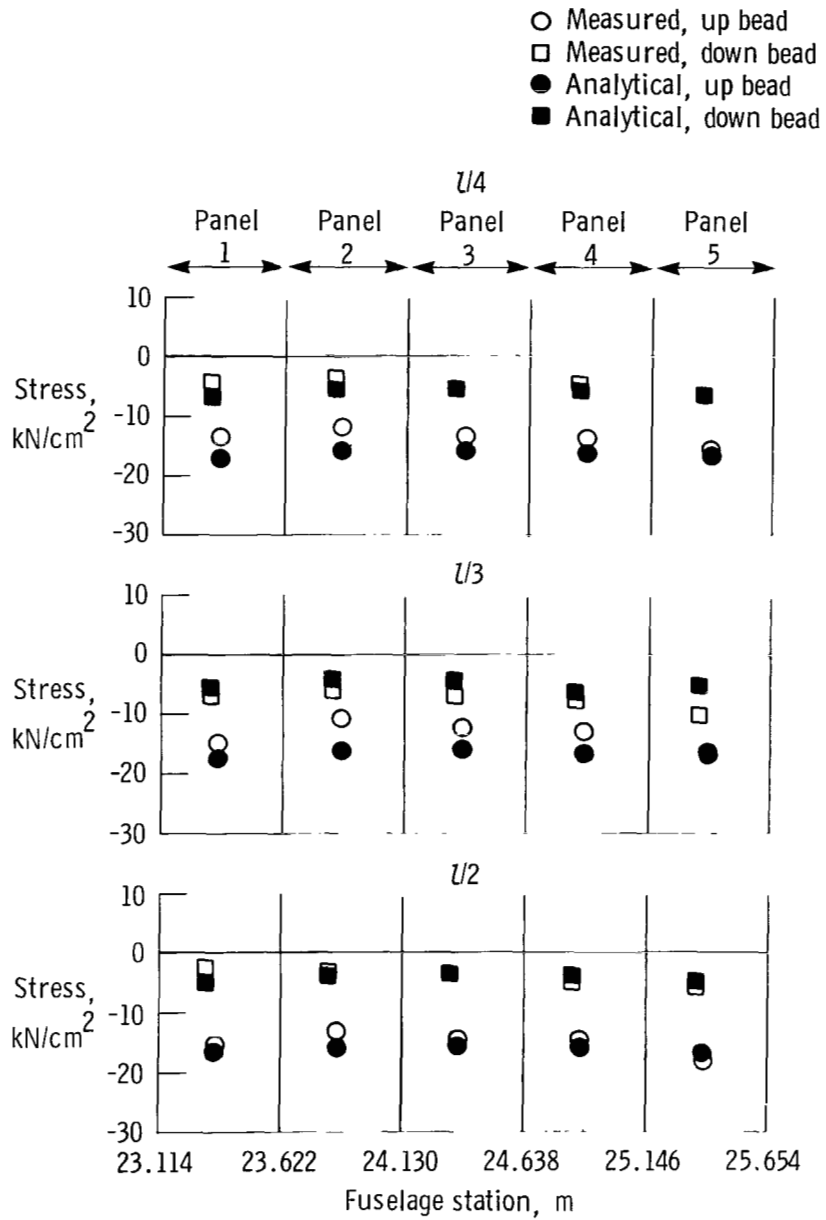
(c) Test 3.

Figure 23. Continued.
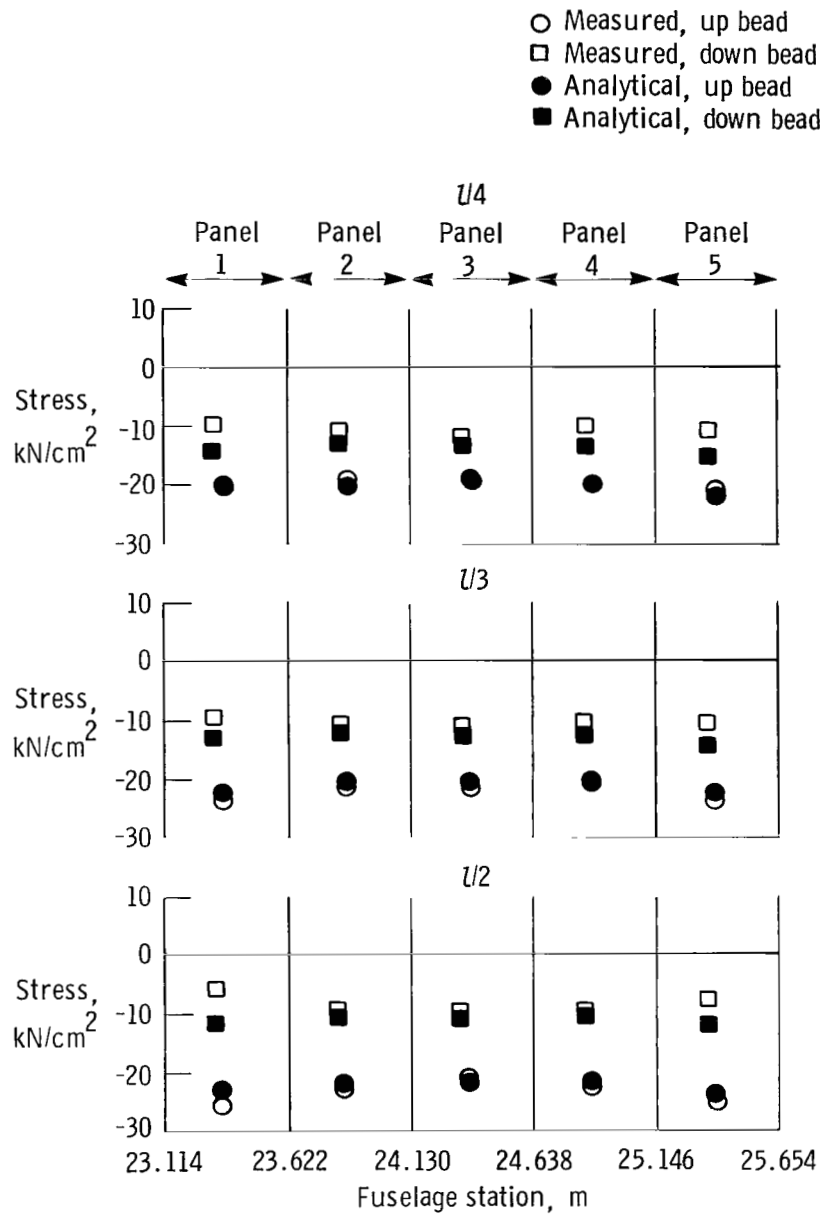
(d) Test 4.

Figure 23. Continued.
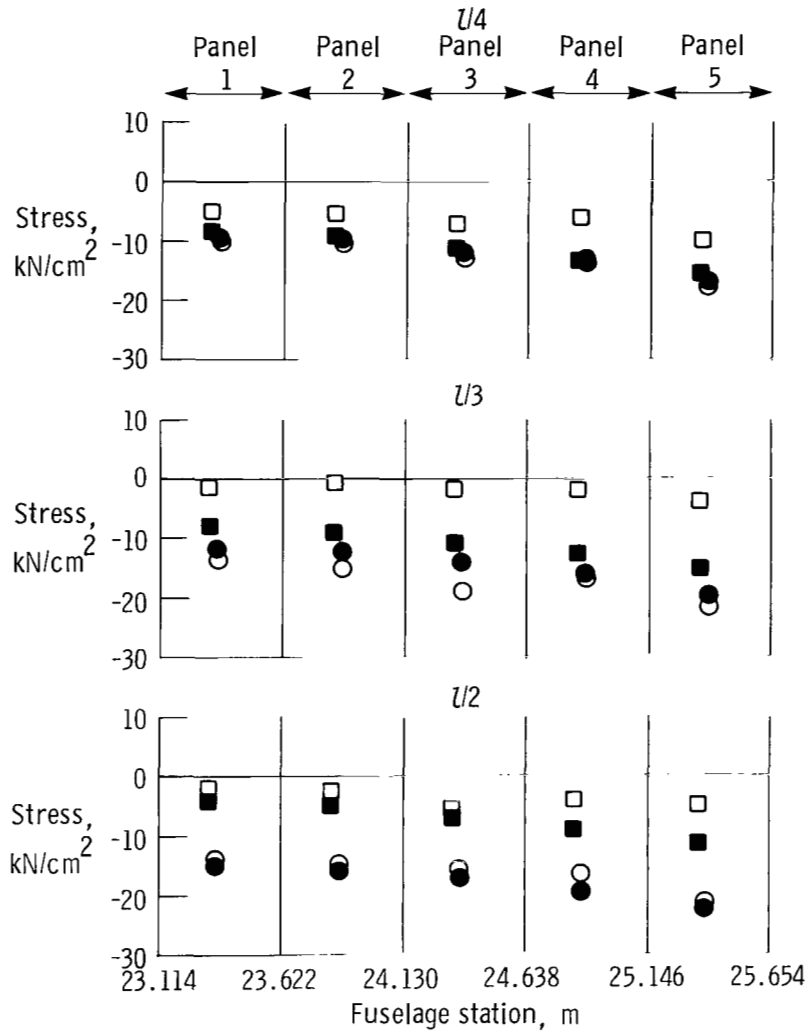
(e) Test 5.

Figure 23. Continued.
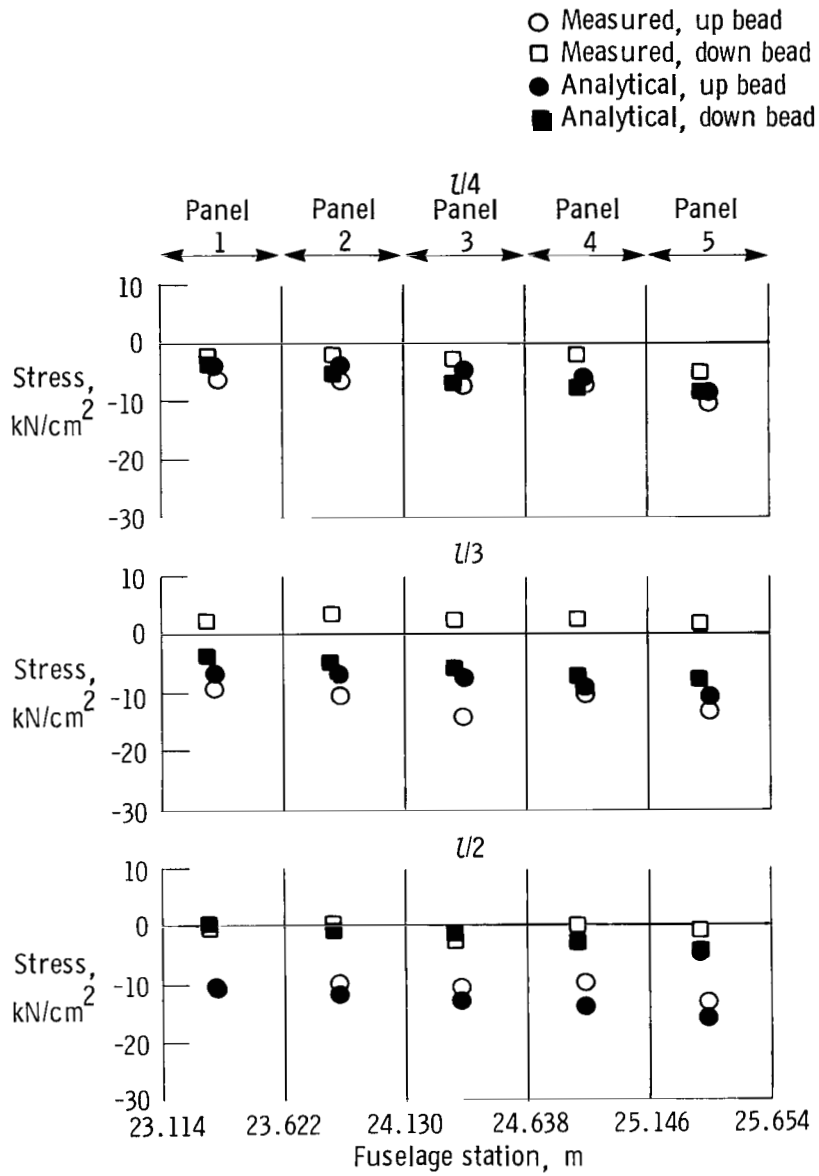
(f) Test 6.

Figure 23. Concluded.
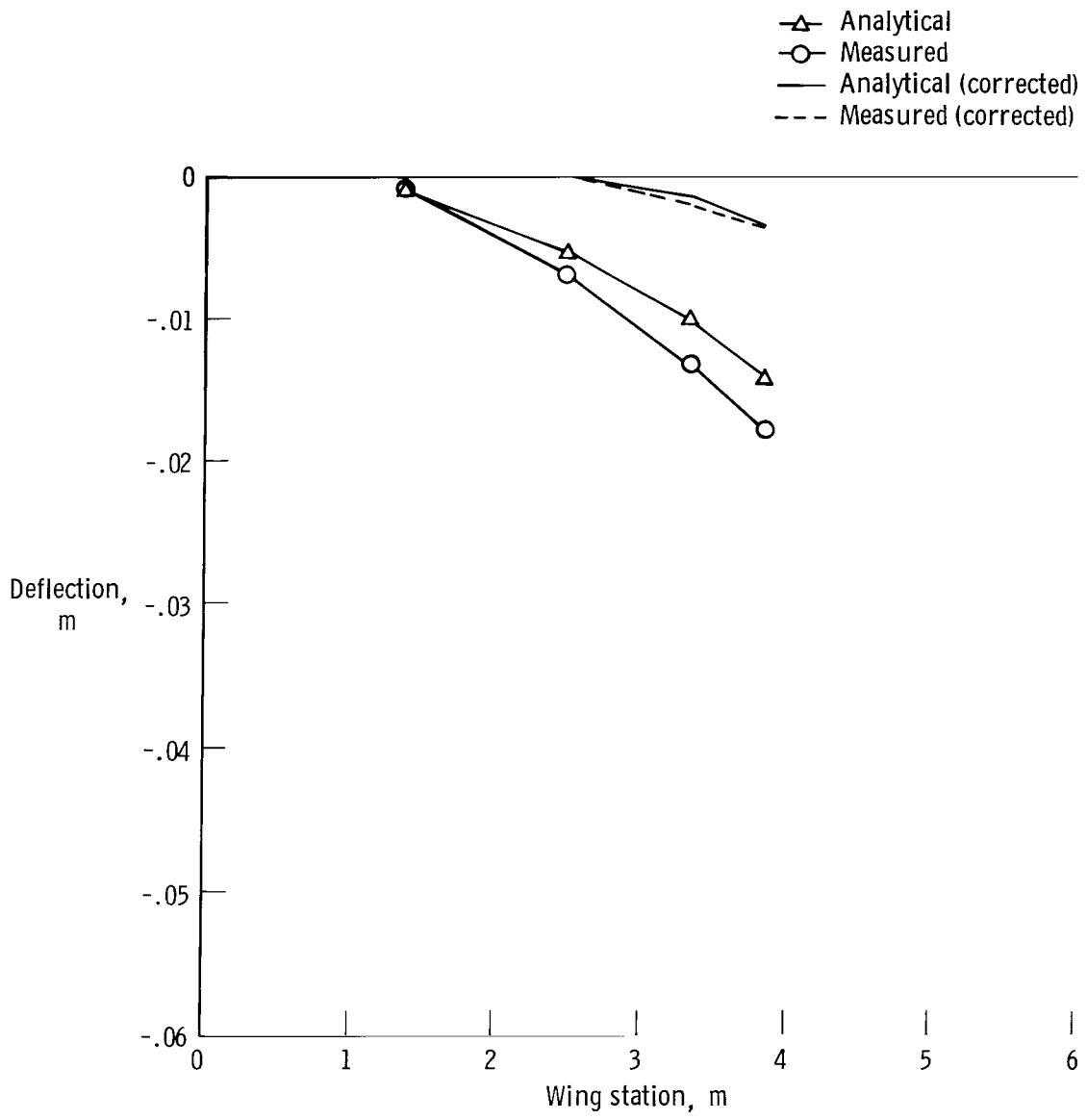
(a) F.S. 23.114.

Figure 24. Vertical deflections of hypersonic wing
test structure during test 3. All dimensions in meters.
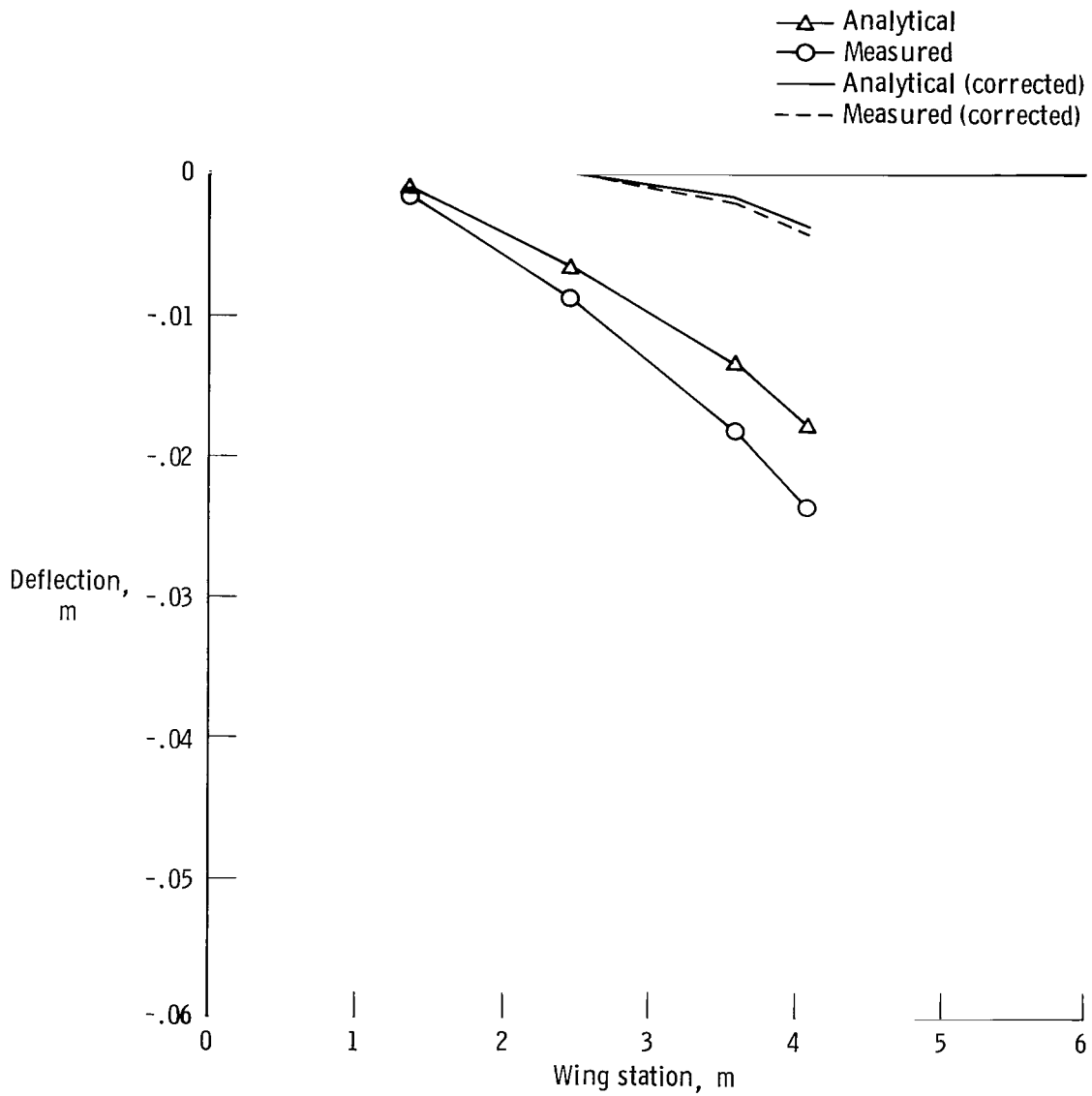
(b) F.S. 23.622.

Figure 24. Continued.
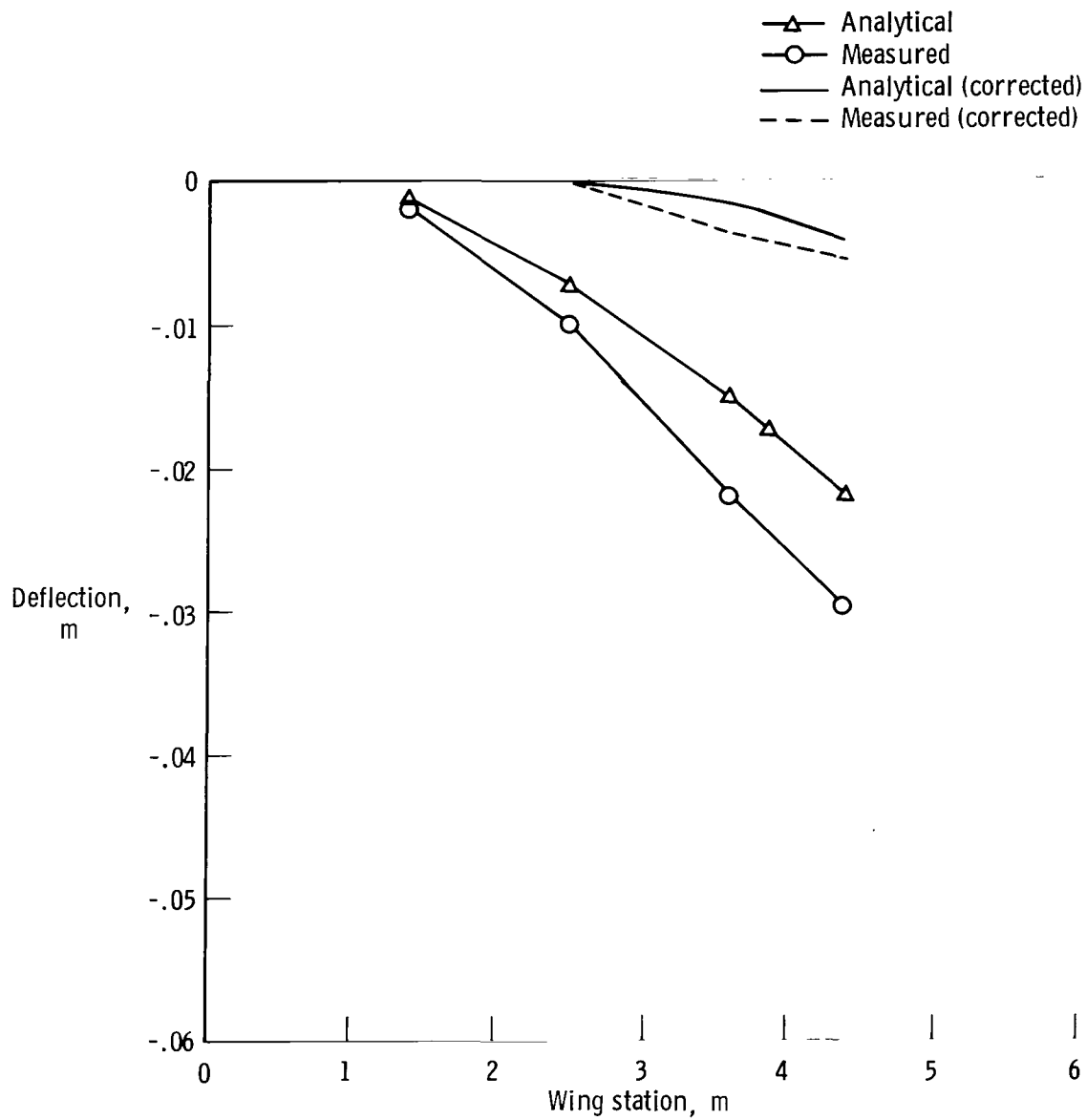
(c) F.S. 24.130.

Figure 24. Continued
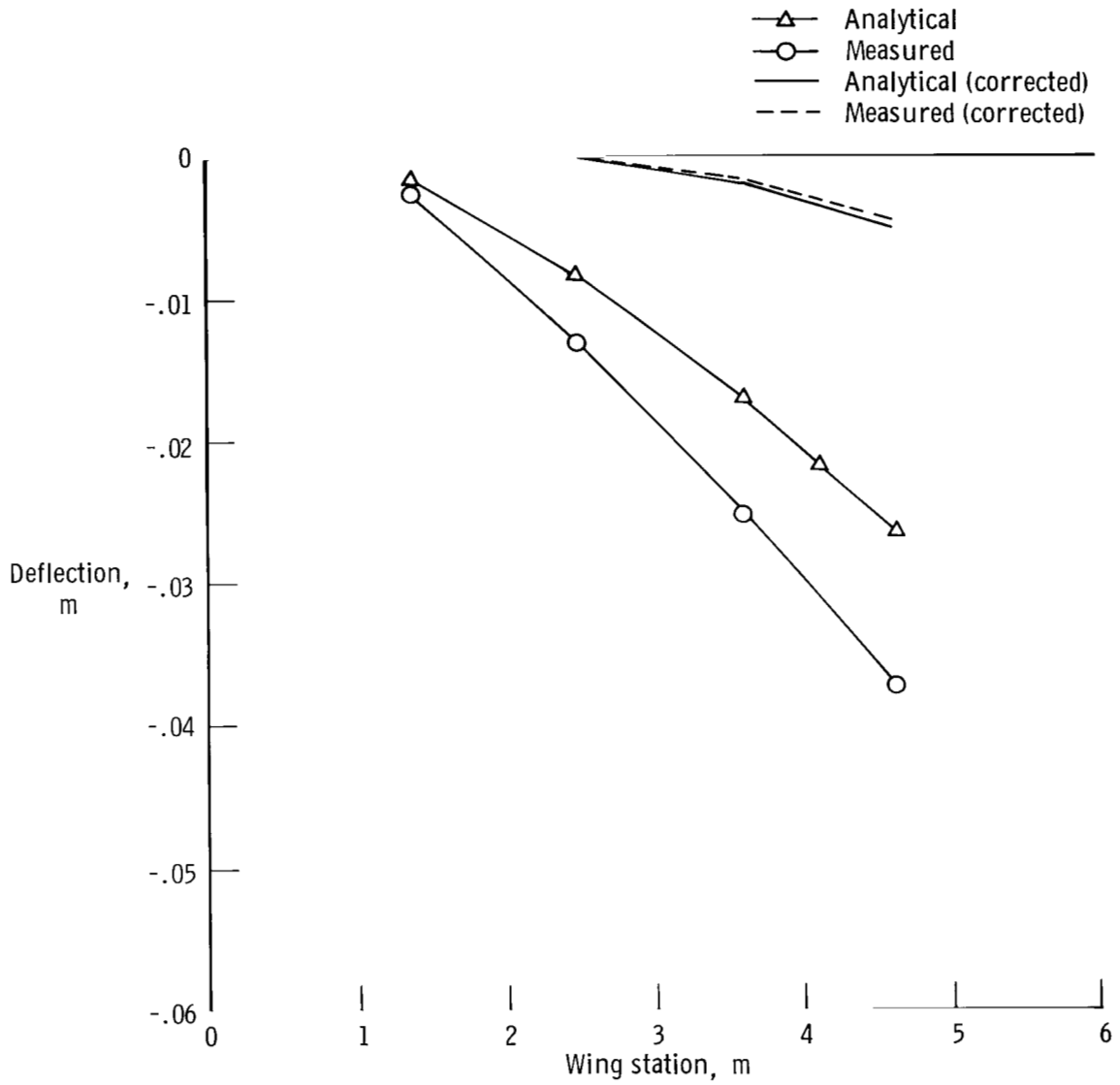
(d) F.S. 24.638.

Figure 24. Continued.
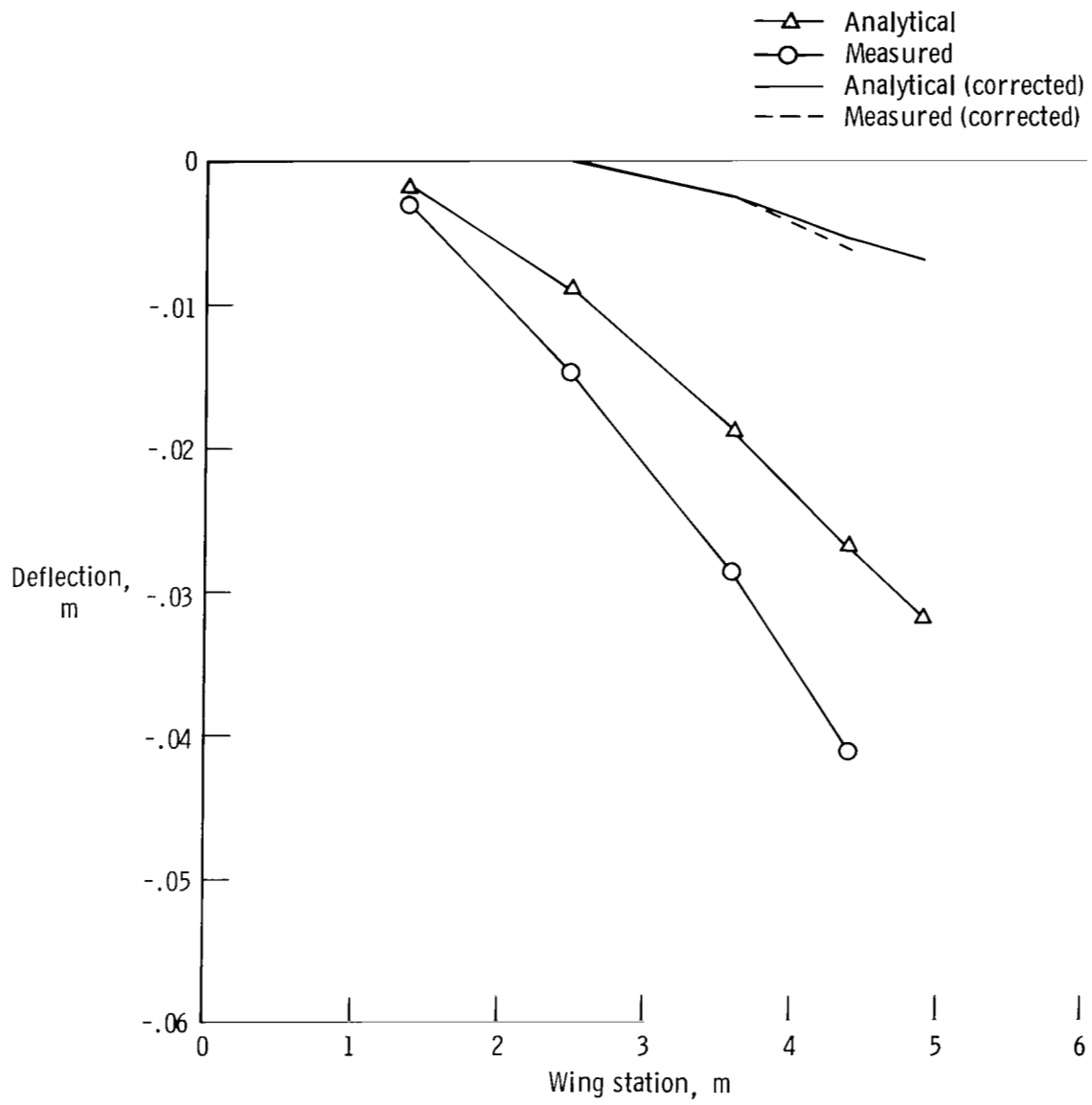
(e) F.S. 25.146.

Figure 24. Continued.
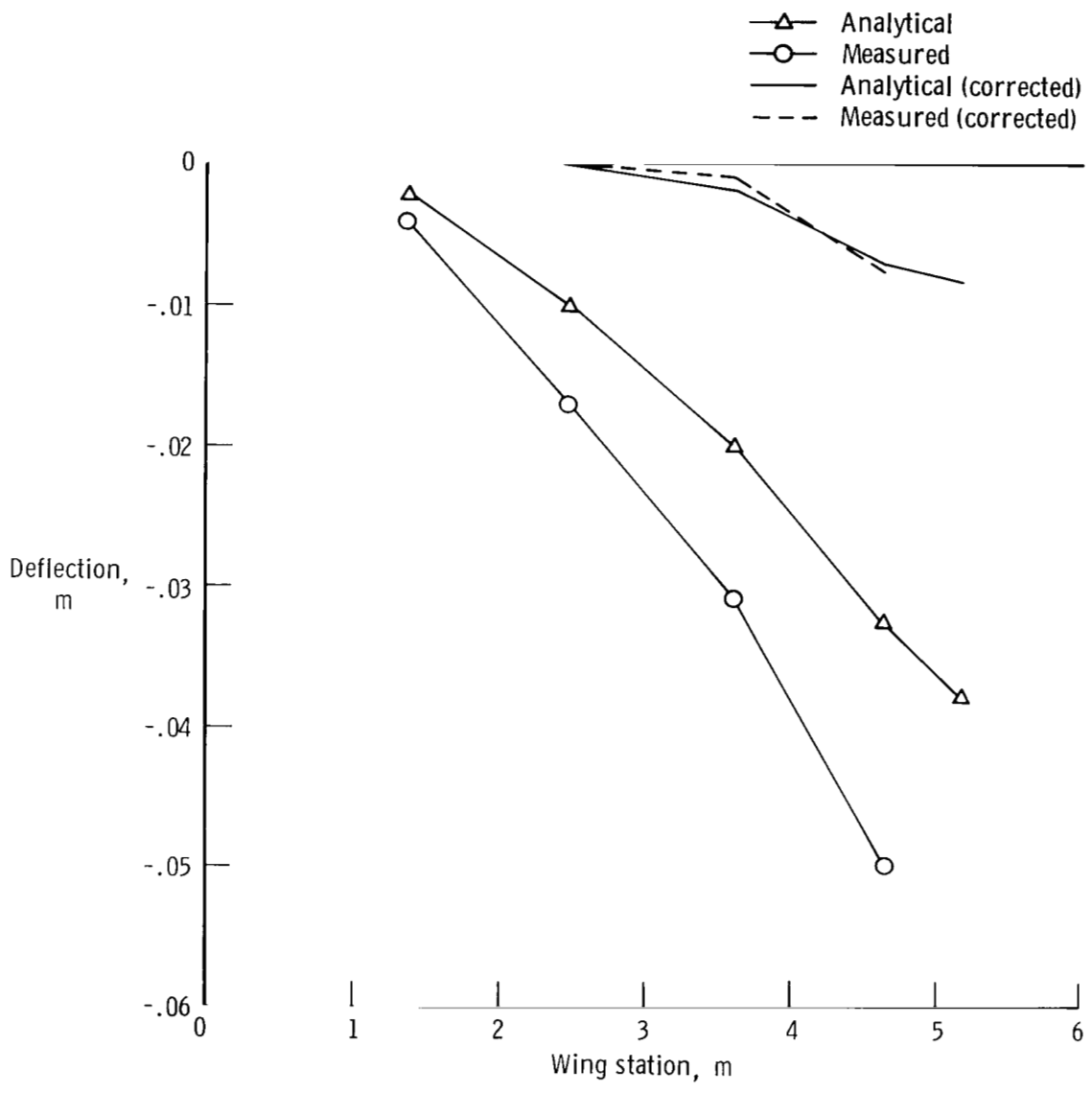
(f) F.S. 25.654.

Figure 24. Concluded.

16. Abstract

Room-temperature loading tests were conducted on a wing structure designed with a beaded panel concept for a Mach 8 hypersonic research airplane. Strain, stress, and deflection data were compared with the results of three finite-element structural analysis computer programs and with design data. The test program data were used to evaluate the structural concept and the methods of analysis used in the design.

A force-stiffness technique was utilized in conjunction with load conditions which produced various combinations of panel shear and compression loading to determine the failure envelope of the buckling critical beaded panels. The force-stiffness data did not result in any predictions of buckling failure. It was, therefore, concluded that the panels were conservatively designed as a result of design constraints and assumptions of panel eccentricities.

The analysis programs calculated strains and stresses competently. Comparisons between calculated and measured structural deflections showed good agreement. The test program offered a positive demonstration of the beaded panel concept subjected to room-temperature load conditions.

National Aeronautics and
Space Administration

Washington, D.C.
20546

Official Business
Penalty for Private Use, $300

THIRD-CLASS BULK RATE

U.S.MAIL

3   1 1U, A,   122179 S00903DS
DEPT OF THE AIR FORCE
AF WEAPONS LABORATORY
ATTN: TECHNICAL LIBRARY (SUL)
KIRTLAND AFB NM 87117

NASA

POSTMASTER: If Undeliverable (Section 158
Postal Manual) Do Not Return